PHOTOCATALYTIC TREATMENT OF INDUSTRIAL WASTEWATER CONTAINING CITRIC ACID AND TOXIC HEAVY METALS

Dissertation submitted in fulfillment of the requirements for the Degree of Magister Technologiae in the Department of Chemical Engineering, Faculty of Engineering and Technology, Vaal University of Technology.

Siwela Jeffrey Baloyi

Vaal University of Technology

Supervisor: Prof Ochieng Aoyi

Vanderbijlpark, 2014

Declaration

I declare that this thesis is my own, unaided work. It is being submitted for the degree of Magister Technologiae: Chemical Engineering at the Vaal University of Technology, Vanderbijlpark. This is not a reproduced copy nor has it been previously submitted before for any degree or examination in any other body or organisation or person outside the Vaal University of Technology, Vanderbjlipark. I further declare that all sources cited or quoted are indicated and acknowledged by means of a comprehensive list of references.

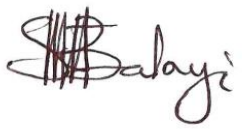

(signed) Siwela Jeffrey Baloyi

18th December 2014

Acknowledgements

I would like to express my appreciation to the following people for assisting me professionally and making this thesis possible.

The All Mighty GOD for his protection, love, giving me strength and more importantly without whom I would not be in existence.

Prof. Ochieng Aoyi, my supervisor, for believing in me by accepting me as his student, for his guidance, immeasurable contribution to this work and investing knowledge in me.

Dr. Mpfunzeni Raphulu, for simplifying all the 'horrible' aspects, the scientific input, all the bright ideas, teaching, and for believing in me by recruiting me as a student to the Advanced Material Division-Catalysis group, Mintek Research and Development. Most importantly, I would like to thank you for your hospitality, support and caring, which was made available to me since I joined Mintek. I especially enjoyed the fieldwork in different provinces and the tone of our meetings which allowed me to express my views openly.

Dr. Richard Moutloali, for allowing me to share ideas with his research students at the Advanced Material Division-DST/Mintek Nanotechnology Innovation Centre (NIC) Randburg, RSA and his knowledge in the field of wastewater treatment using polymer composites is priceless.

Mr. Tumelo Seadira and Ms. Lufuno Nemadodzi, for helping me with some technical laboratory work where extra hands were needed.

Mr. Richard Couperthwaite, Mr. James Aluha and Mr. Siyasanga Mpelane for their assistance with TEM, BET, EDX, SEM and XRD techniques at Mintek.

Dr. Lay Shoko, the laboratory manager at VUT Chemical Engineering Department for his endless support and words of encouragement.

The Mintek Catalysis and VUT Center for Renewable Energy and Water (CREW) groups for their assistance in various ways, sharing ideas and for creating a conducive environment for doing my research.

Thanks to the Mintek and DST/NRF for project funding and financial assistance.

Finally, and most importantly, I would like to thank my wonderful family. You have always been my greatest strength and support throughout this journey, you have given me your full support and above all you have always put your trust in me. *Xikwembu a xi mikatekisi!!!!!!*

Dedication

This thesis is dedicated to my special late mother, Mphephu Baloyi, the late Tiyiselani Glen Maswanganyi (nephew), my wonderful sister Sesi Rose Amukelani Baloyi and my father Papa Sikheto Phillemon Baloyi.

Scientific activity arising from this work

List of publications

1. **Jeffrey Baloyi,** Tumelo Seadira, Mpfunzeni Raphulu and Aoyi Ochieng, "Simultaneous photocatalytic reduction of Cr(VI) and oxidation of citric acid in aqueous solutions." Paper presented and published at International Conference on Chemical, Integrated Waste Management & Environmental Engineering (ICCIWEE'2014), 15th - 16th, April 2014, Johannesburg, South Africa. ISBN 978-82242-71-0.

2. **Jeffrey Baloyi,** Tumelo Seadira, Mpfunzeni Raphulu and Aoyi Ochieng, "Synthesis of dandelion-like TiO_2 structure as a photocatalyst for industrial wastewater treatment containing toxic heavy metals." Paper presented and published at International Conference on Chemical, Integrated Waste Management & Environmental Engineering (ICCIWEE'2014), 15th -16th April 2014, Johannesburg, South Africa. ISBN 978-82242-71-0.

3. **Jeffrey Baloyi**, Tumelo Seadira, Mpfunzeni Raphulu and Aoyi Ochieng, "Co-treatment of toxic heavy metals and citric acid in aqueous solution by UV/TiO_2 photocatalytic process." Paper presented at WISA 2014 Biennial Conference, 25th – 29th, May 2014, Mbombela, South Africa. ISBN 987-0-802623-9-1. *Submitted for publication in WaterSA Special Edition*

4. **Jeffrey Baloyi,** Tumelo Seadira, Richard Moutloali, Mpfunzeni Raphulu and Aoyi Ochieng, "Kinetic investigation of photocatalytic reduction of Hg(II) using TiO_2-immobilized on calcium alginate beads: Effect of ferric ion and organic compound." Paper presented and published at International Institute of Engineer's (IIE) International Conference on Chemical Engineering and Advanced Computational Technologies (ICCEACT'2014), 24th - 25th, November 2014, Pretoria, South Africa. ISBN 978-93-84422-00-4.

5. **Jeffrey Baloyi**, Tumelo Seadira, Mpfunzeni Raphulu and Aoyi Ochieng, "Preparation, characterization and growth mechanism of dandelion-like TiO_2 nanostructures and their application in photocatalysis towards reduction of Cr(VI)." Paper presented at 7th International Symposium on Macro and Supramolecular Architectures and Materials (MAM-14), 23rd - 27th, November 2014, Johannesburg, South Africa. *Submitted for publication in Materials Today Proceeding*

6. **Jeffrey Baloyi,** Tumelo Seadira, Richard Moutloali, Mpfunzeni Raphulu and Aoyi Ochieng, "Synthesis and characterisation of dandelion-like TiO_2/calcium alginate composite for photocatalytic reduction of Cr(VI)." *Submitted to Chinese journal of chemical engineering*

Abstract

The co-existence of organic acids and toxic heavy metals in natural water creates harmful effects on human, plants and animals. Therefore, it is necessary to treat organic acids and toxic heavy metal contaminated wastewater prior to its discharge to the environment. The aim of this study was to apply co-treatment of industrial wastewater containing citric acid and toxic heavy metals in single and binary systems using photocatalysis process. The hydrothermal method was used to synthesise dandelion-like TiO_2 structures. Modifications of the dandelion-like TiO_2 by deposition of gold nanoparticles and immobilisation on calcium alginate were done using deposition precipitation and one-step encapsulation methods, respectively. Dandelion-like TiO_2 and dandelion-like TiO_2 immobilised on calcium alginate (Alg/TiO_2) were used as photocatalysts for Cr(VI), Hg(II) and citric acid removal from water.

The results showed that the production of dandelion-like TiO_2 structures strongly depends on the reaction time and synthesis temperature as key process parameters. The characterisation of the dandelion-like TiO_2 by X-ray diffraction (XRD), transmission electron microscope (TEM), scanning electron microscopy (SEM), energy-dispersive X-ray (EDX) and Brunauer-Emmett-Teller (BET) revealed the crystal structure, morphology, chemical composition and surface area. It was found that the efficiency of photocatalytic process depends on the type of pollutants, initial pH of the solution, photocatalyst dosage, contact time, substrate initial concentration, UV wavelength and light intensity. The reduction efficiency of Cr(VI) ion and citric acid increased with decreasing the initial pH values and initial concentration. On the other hand, Hg(II) reduction efficiency increased with increasing the initial pH values and initial concentration. In a binary system, the reduction of Cr(VI) and Hg(II) was found to be faster than in the single and ternary systems. The relationship of the chemical reaction rate of Cr(VI), Hg(II) and citric acid were expressed by the pseudo-first-order kinetic equation. Addition of ferric ions to Cr(VI)-citric acid complex and Hg(II)-citric acid complex enhanced the reduction of Cr(VI) and Hg(II), a complete reduction was accomplished within 30 and 60 minutes (min) of irradiation time, respectively. The reduction efficiency of both Cr(VI) and Hg(II) in the presence of citric acid in a solution was still significant after four times of Alg/TiO_2 reuse. These results indicated that the UV/TiO_2 photocatalysis process can be considered as a suitable method to reach a complete reduction of Cr(VI) and Hg(II) in the presence of citric acid in a solution.

Table of Contents

List of Figures

List of Tables

Nomenclature

e^-	Electron
Eg	Band gap energy eV
h^+	Hole
k	Pseudo-first-order rate constant (min^{-1})
$^{\bullet}OH$	Hydroxyl radical
e-	Photogenerated Electron
vb	Valence Band
cb	Conductance Band
λ	Wavelength
r	Rate of reaction
R^2	Correlation coefficient
Å	Angstrom
k_{app}	Apparent rate constant (min^{-1})
θ	Bragg's angle

Acronyms

AOP	Advanced oxidation process
AMD	Acid mine drainage
PZC	Point of zero charge
HRT	Hydraulic retention time
SC	Semiconductor
UV	Ultra violet
UV-Vis	Ultraviolet-visible
SEM	Scanning electron micrograph
TEM	Transmission electron microscope
BET	Brunauer, Emmett and Teller
TiO_2	Titanium dioxide
LED	Light-emitting diode
Cit	Citric acid
Alg/TiO_2	Titanium dioxide immobilised on calcium alginate beads
Au/TiO_2	Gold nanoparticles deposited on titanium
FMD	Ferrochrome mine discharge
WB	Western basin

CHAPTER 1: INTRODUCTION

1.1 General background

The increase in global industrialisation and urbanisation has led to the transport and introduction of various contaminants in the aquatic environment. Water pollution caused by organic pollutants and heavy metal ions presents an important ecological and health hazard and has gradually gained great scientific interest. Heavy metals such as chromium hexavalent, Cr(VI); methyl mercury, Hg(II); cadmium, Cd(II); copper, Cu(II); and lead, Pb(II) enter the aquatic environment through the discharge of treated or untreated industrial wastewater and municipal sewage, storm water runoff, acid mine drainage (AMD), and other diffuse sources (Barakat et al., 2011).

Organic pollutants, like citric acid, dye, phenol, humic acid and 4-chlorophenol along with heavy metals, such as Hg(II), Pb(II), Cd(II), Ag(I), Ni(II) and Cr(VI) are very toxic among the metal ions present in the environment and are present in various industrial effluents that pose serious health hazards to humans. The industrial wastewater such as AMD contains heavy metal ions that are generated by acidity of the water from the rocks with which it interacts. Thus, toxic heavy metals are generally non-degradable, have infinite lifetimes, and build up their concentrations in food chains to toxic levels (Dozzi et al., 2012).

Heavy metal pollutants such as Cr(VI) and Hg(II) are of great concern because their toxicity threatens human life and the environment. Chromium (Cr) is a multivalent ion, among which Cr(VI) and Cr(III) states form stable compounds. Cr(VI) compounds (as in chromates, CrO_4^- , and dichromates, $Cr_2O_7^{-2}$) (Popuri et al., 2007) are mostly water soluble and are extremely toxic to humans, with toxicity levels 500 times higher than that of Cr(III). On the other hand, Cr(III) is only slightly toxic to humans and assists different enzymatic reactions in the human body such as regulating functioning glucose, lipid, and protein metabolism. However, long-term exposure to a high concentration of Cr(III) may cause poisoning symptoms such as allergic skin reactions (Kalidhasan et al., 2009).

Mercury (Hg), on the other hand is a highly volatile and highly toxic heavy metal present in the environment. The oxidation states of Hg in water are 0, +1 and +2, however, Hg(II) is most stable. For this reason, many of Hg removal studies in wastewater have focused on Hg(II) compared to more reduced oxidation states. Inorganic Hg in water is mainly seen in

the +2 oxidation state. Mercury-chloride ($HgCl_2$) salts are present in the environment from the microbial breakdown of inorganic Hg^{2+} salts and from organomercurials used as bactericides, fungicides and insecticides. $HgCl_2$ is the most toxic form that causes irreversible damage to the central nervous system, circulatory system, rheumatoid arthritis and diseases of the kidneys (Manohar et al., 2002).

Cr(VI) and Hg(II) cannot be degraded biologically, but their compounds may be transformed chemically to more toxic species (Dou et al.,. 2001). Therefore, due to the high toxicity of Cr(VI) and Hg(II), it is of great importance that effluents from industries such as mining, metallurgical, tannery, chemical manufacturing and battery manufacturing must be free from these compounds and/or their salts without creating more toxic products before being discharged into the environment

Many methods that have been actively investigated to remove heavy metal ions from wastewater are chemical precipitation, ion exchange, adsorption, membrane filtration, electrochemical treatment technologies and liquid extraction (Gherbi et al., 2011). However, these methods have certain disadvantages such as higher operational cost, requiring additional chemical, high energy consumption, residual metal sludge disposable and are often ineffective at low concentrations. Therefore, it is clear that the prospect of developing a more efficient and durable system became necessary (Gherbi et al., 2011). Compared with the conventional chemical reduction methods, the photocatalytic reduction of toxic heavy metals has some advantages, such as simple operation, ambient conditions, low cost, high efficiency, reusability, direct use of infinite, clean and safe natural solar energy, and no use and no release of sludge (Ibhadon et al., 2013). As a friendly environmental treatment process, heterogeneous photocatalysis has proved to be quite interesting in the elimination of Cr(VI) and Hg(II), which can comply with the World Health Organization (WHO) guidelines to decrease the maximum concentration less than 5 and 0.005 mg/L (Fu et al., 2010). Furthermore, photocatalysis was proven to be efficient in degrading citric and other acids in relatively high concentrations, as representatives of wastewaters coming from cleaning of boilers in power plants and the oxidative destruction of citric acid in conjunction with the reductive removal of heavy metals (Ag(I), Cr(VI), Hg(II) and Pt(IV)) via titanium dioxide (TiO_2) photocatalysis, pointing out the synergy between reduction and oxidation processes (Colon et al., 2001).

The photochemical degradation of pollutants using semiconducting powders as catalysts is a subject of current interest. Heterogeneous photocatalysis in the presence of a semiconductor photocatalyst has been studied for the co-treatment of toxic heavy metals and organic compounds in wastewater (Chen and Ray, 2001; Colo'n et al., 2001; Bussi et al., 2002; Testa et al., 2004; Shao et al., 2009; Yang et al., 2010; Dozzi et al., 2012 & Xu et al., 2013). The photocatalytic method is based on the activation of a semiconductor photocatalyst under the irradiation of light to enable redox reactions. When a semiconductor is irradiated with light, it adsorbs energy greater than its band gap energy and transfers an electron from its valence band to its conduction band. The generation of electron-hole pairs will then take part in either reduction or oxidation reactions. In the process of co-treatment of toxic heavy metal and organic compound, both metal reduction and organic species oxidation are of great importance. Compared to the conventional wastewater treatment processes mentioned above, photocatalysis enables simultaneous reduction of metal ions to their elemental state and oxidation of organic compounds to CO_2 and H_2O.

Different semiconductors such as TiO_2, ZnO, CeO_2, CdS and ZnS, have been intensively studied as the photocatalysts for photocatalytic reactions (Dozzi et al., 2012). Among these semiconductors, TiO_2 is the most widely used photocatalyst because of its favourable chemical property, physical sunblock in sunscreens, high degree of photocatalytic activity, non-toxicity, high stability, and low cost (Tryk et al., 2000). The band-gap energy of TiO_2 is 3.2 eV, equivalent to UV light of 380 nm, and, therefore, is photo-excited by near-UV irradiation (Ibhadon et al., 2013). The holes that are generated on TiO_2 are highly oxidising and these result in the oxidising of organic matter into carbon dioxide (oxidation path). On the other hand, electrons reduce the heavy metals (reduction path), and there has been abundant literature on the utilisation of TiO_2 in the oxidative degradation of organics. In addition to organics, the inorganic species with a reduction potential more positive than that of the conduction band of the semiconductor can consume the electrons and complete the redox reaction cycle. The one limitation of TiO_2 as a photocatalyst is its poor efficiency in the visible region of the solar spectrum due to its wide band gap (3.2 eV for anatase). Also, the use of free-suspended TiO_2 is impractical due to the difficulty in separation of TiO_2 particles in water after use. Therefore, this work focused on the co-treatment of citric acid and toxic heavy metals in single and binary photocatalytic systems using synthesised rutile dandelion-like TiO_2; modified dandelion-like TiO_2 by gold deposition; and immobilisation on Ca-alginate.

1.2 Problem statement

AMD emanating from gold and ferrochrome mining, contaminated by toxic heavy metals such as Cr(VI) and Hg(II) contains some of the most complex, troublesome pollutants as it exhibits high amounts of heavy loads of high toxic metal. Removal of Cr(VI) and Hg(II) in aqueous solutions is difficult because they are hard to biodegrade. At high concentrations, Cr(VI) and Hg(II) can be removed from a solution by membrane filtration, chemical precipitation, ion exchange, adsorption and electrochemical treatment. However, these methods are much less efficient and very expensive for concentrations lower than 100 mg/l (Manohar et al., 2002).

Adequate treatment with the use of robust methods such as UV/TiO_2 photocatalysis process, therefore, is imperative before the effluent is discharged, as it has been demonstrated (Ibhadon et al., 2013) as a low cost process by taking advantage of using an inexpensive photocatalyst (TiO_2). Moreover, UV/TiO_2 photocatalysis process can simultaneously remove toxic heavy metals ions along with citric acid in wastewater. However, some of the significant problems for practical application that still need to be addressed are its poor efficiency in the visible region of the solar spectrum and difficulty to be separated from water after being used.

To overcome the above problems, synthesis of 3D dandelion-like TiO_2 nanostructures and its modification by deposition of gold nanoparticles and immobilisation over calcium alginate beads were taken into consideration during this study. The aim of this study is to apply co-treatment of industrial wastewater containing citric acid and toxic heavy metals in single and binary systems using the photocatalysis process.

1.3 Justification/significance

The co-existence of toxic heavy metals such as Hg(II), Cr(VI), Pb(II) and others along with oligocarboxylic acids such as citric acid are considered to be creating hazardous effects on humans, plants and animals. Since toxic heavy metals do not degrade easily, they accumulate over time, posing a greater danger to living organisms. Therefore, removal of these toxic heavy metals is essentially important for human health and water quality.

The UV/TiO_2 photocatalysis process using semiconducting powders shows the potential to become a preferred future treatment technology. This can be attributed to their capability of simultaneously converting toxic heavy metals and organic pollutants into less-toxic products. As a method for removal of contaminants in water and air, UV/TiO_2 photocatalysis process using semiconductors such as TiO_2 is more efficient than conventional methods (Ibhadon et al., 2013). This is because, as the UV/TiO_2 photocatalysis process gradually breaks down the contaminant molecules, no residue of the original material remains and, therefore, no sludge, requiring disposal to landfill, is produced. The catalyst itself is unchanged during the process and no consumable chemicals are required. These results in considerable savings and a simpler operation of the equipment involved, in comparison with the conventional methods. Moreover, because the contaminant is attracted strongly to the surface of the catalyst, the process will continue to work at very low concentrations. Taken together, these advantages mean that the UV/TiO_2 photocatalysis process results in considerable savings in water production cost and keeping the environment clean.

In this study, UV/TiO_2 photocatalysis process has been proposed as a promising cost-cutting, effective and robust treatment method. This method can not only reduce the toxic heavy metals to their less-toxic form, but can also simultaneously treat inorganic compounds and transform non-biodegradable to biodegradable organic compounds.

1.4 Objectives

The purpose of this study is to apply co-treatment of citric acid and toxic heavy metals in single and binary photocatalytic systems.

In order to achieve the research objective, the study sought to:

a. Synthesise a pure rutile phase crystalline dandelion-like TiO_2 powder and investigate the parameters affecting its production and photocatalytic activity.

b. Characterise the pure rutile phase crystalline dandelion-like TiO_2 powder using a range of techniques (XRD, SEM, TEM, EDX and BET).

c. Deposit the gold nanoparticles on a pure rutile phase crystalline dandelion-like TiO_2 powder and immobilisation over calcium alginate.

d. Determine the effect of process parameters such as initial pH, photocatalyst dosage, contact time and initial concentration of toxic heavy metals [Cr(VI) and Hg(II)] and citric acid.

e. Analyse the effect of citric acid on the Cr(VI) and Hg(II) removal.

f. Determine/ analyse the reusability of TiO_2 immobilized on calcium alginate.

g. Analyse the effect of UV irradiation wavelength and light intensity on the photocatalytic treatment.

1.5 Scope of the thesis

In this study, batch reactor and recycle photocatalytic reactor were used to investigate the kinetics of UV/TiO_2 photocatalytic photo reduction of selected toxic heavy metals [Cr(VI) and Hg(II)] and oxidation of citric acid. Dandelion-like TiO_2 nanostructures were synthesised using the hydrothermal method and further modified by deposition of Au nanoparticles, and immobilised on calcium alginate using deposition-precipitation and one-step encapsulation methods, respectively. As-prepared dandelion-like TiO_2 and in its modified form was used as photocatalysts for Cr(VI), Hg(II) and citric acid removal from wastewater.

1.6 Thesis layout

The thesis has five chapters. Following the introduction in Chapter 1, detailed literature review about water pollution by toxic heavy metals along with organic compounds and photocatalysis process is provided in Chapter 2. In Chapter 3, experiment details are illustrated, including the materials, equipment, experimental set-up, experimental procedure, experimental design and experimental analysis. Chapter 4 presents the experimental results and discussions section, which is divided into two parts. Part I presents the synthesis and characterisation of dandelion-like TiO_2 photocatalysts. Furthermore, the photocatalytic activity of as-prepared and calcined dandelion-like TiO_2 and P25 TiO_2 reducing Cr(VI) and Hg(II). Part II investigated the technical feasibility of UV/TiO_2 photocatalytic process for the removal of Cr(VI), Hg(II) and citric acid using dandelion-like TiO_2 photocatalyst immobilised on calcium alginate beads (Alg/TiO_2). Finally, Chapter 5 summarises conclusions reached as a result of this study and some recommendations for further studies.

CHAPTER 2: LITERATURE REVIEW

2.1 Water pollution by heavy metals and organic compounds

The growth in civilisation and industrial activities has caused a number of environmental problems such as water pollution worldwide. The quality of water resources is declining every day due to advanced industrialisation in different fields such as metal plating facilities, mining operations, fertiliser industries, tanneries, paper industries, batteries and pesticides (Litter et al., 1999; Chen and Ray, 2001 & Pelaez et al., 2012). The continuous release of various pollutants such as heavy metals and organic compounds into the environment is causing growing concern to the whole world (Munoz et al., 1990; Yang et al., 2010 & Shaban et al., 2013). Unlike most organic contaminants, heavy metals are particularly problematic because, they are not biodegradable and tend to accumulate in living organisms, posing great threat to both human health and ecological environment (Dozzi et al., 2012). Heavy metals wastewaters are discharged directly or indirectly into the environment increasingly, especially in developing countries like South Africa.

The most common toxic heavy metals of particular concern in treatment of industrial wastewaters include zinc, mercury, cadmium, lead, chromium, arsenic, copper, nickel and cobalt. Living organisms can absorb these toxic heavy metals due to their high solubility in the aquatic environments. Once they enter the food chain, large concentrations of heavy metals may accumulate in the human body. If the metals are ingested beyond the permitted concentration, they can cause serious health disorders (Wang et al., 2004).

Chromium has both beneficial and detrimental properties. Chromium exits in the aquatic environment mainly in two states, Cr(III) and Cr(VI), which have contrasting toxicities, mobilities and bio availabilities. Cr(III) is essential in human nutrition it assists different enzymatic reaction the in human body to regulate functioning glucose, lipid, and protein metabolism. On other hand, Cr(VI) is 500 times more toxic than Cr(III) and the toxicity of Cr(VI) affects human physiology, accumulates in the food chain and causes severe health problems such as skin irritation, kidney, liver, gastric damage and lung carcinoma cancer (Wang et al., 2004; Wang et al., 2009; Yang et al., 2010; Barakat et al., 2011 & Xu et al., 2013). Furthermore Cr (III) is relatively innocuous and immobile; Cr (VI) moves readily through soils and aquatic environments and is a strong oxidising agent capable of being absorbed through the skin (Nilisha and Yogesh, 2014). Chromium, especially in a hexavalent

oxidation state, is used commonly in the mining, leather tanning, electroplating and production of steel and other metal alloys. In this study Cr(VI) was chosen as a model compound, therefore, it could be a good choice to show the benefits of the recent develop of technologies for the removal of Cr(VI) from wastewater.

Mercury in water is mainly seen in the +2 oxidation state. Hg(II) has universally been considered to be very toxic at low and high concentrations and causes rheumatoid arthritis, diseases of the kidneys, circulatory system, and nervous system in humans (Serpone et al., 1987; Wang et al., 1993; Khalil et al., 2002; Zhang et al., 2004 & Deng et al., 2010). The major sources of mercury pollution in the aquatic environment are industries, such as chloralkali, paint, electrical, rubber processing, oil refining, mining, and fertiliser industry. Nowadays, most of these industries are facing the difficult problem of disposal of Hg(II) in wastewater produced in large quantities. Therefore, it is essential to develop the effective and robust wastewater treatment technology to treat Hg(II) prior to its discharge into the environment. On this basis, Hg(II) was also chosen as a model compound in this study.

Quici et al. (2007) claimed that wastewaters from the cleaning process of boilers in power plants composed of a mixture of oligocarboxylic acids, such as citric acid and oxalic acid. These oligocarboxylic acids cause serious problems to the environment. The discharge of waste containing oligocarboxylic acids is reported by Meichtry et al. (2010) to be toxic to microorganisms, aquatic life and humans. Oligocarboxylic acids such as citric acid ($C(OH)(COOH)(CH_2COOH)_2$, 2-hydroxy-propane-1, 2, 3-tricarboxylic acid, Cit), is a model compound of several natural systems due to its presence in plants and soils. It is a heavy metals transport agent in biological systems, a frequent domestic and industrial chelating agent used in the nuclear power plants, food industry and in detergents (Quici et al., 2007), and it is often used as a reducing agent in photolytic and photocatalytic systems. Moreover, new technology was recently developed to use citric acid as a more environmental friendly alternative to nitric acid in the passivation process of stainless steel surfaces. In natural water systems and industrial effluents toxic heavy metals often co exist with citric acid wastewater and they may affect each other's behaviour (Khalil et al., 2002; Yang et al., 2010 & Xu et al., 2013). Therefore, the removal of citric acid in industrial wastewaters has received increasing attention and traditional methods of wastewater treatment have been widely used. However, this is limited in the removal of heavy metals and persistent organic compounds, which can create secondary pollution, even at low concentrations (Yang et al., 2010). On this basis,

citric acid was introduced and investigated as the organic model compound in this study by evaluating its effect on the removal of Cr(VI) and Hg(II).

2.2 Technologies for treatment of heavy metals and organic compounds wastewater

It is in the global situation described in Section 2.1 that the recently developed robust technologies or green technologies become highly relevant to the complex wastewater systems. A wide range of physical and chemical processes that are being used to remove toxic heavy metal ions include chemical precipitation (Kurniawan et al., 2006), ion exchange (Eccles, 1999), adsorption (Aklil et al., 2004), membrane filtration (Trivunac and Stevanovic, 2006) and electrochemical treatment technologies (Mohammadi et al., 2005). These processes have significant disadvantages, which are, for instance, chemical precipitation results in sludge production. Ion exchange is considered as a better alternative technique for such purposes. However, it is non-economical because of high operational cost. Adsorption is often ineffective at low concentrations, less than 100 mg/L and incomplete removal of toxic heavy metals. Membrane filtration and electrochemical treatment are not economically appealing because of high energy requirements, (Kurniawan et al., 2006). Recently, numerous approaches have been studied for the development of inexpensive and more effective technologies, to improve the quality of the treated effluent. Heterogeneous photocatalysis has become one of the alternative treatments in recent years, as it is an environmentally friendly treatment process and uses less expensive photocatalysts (Ibhadon et al., 2013).

On the other hand, removal of citric acid in industrial wastewaters has received increasing attention due to its frequent use in various processes as mentioned earlier and a method such as biological treatment has been widely used. However, a major factor complicating the removal of polluted sites is the co-existence of citric acid and heavy metals. This limits the biological process for the removal of citric acid along with heavy metals in natural wastewater systems. Therefore, traditional physicochemical methods, such as coagulation by chemical agents, ion-exchange, ultrafiltration and adsorption, have been suggested and used for removal of citric acid along with heavy metals (Fu et al., 2010). However, these methods also have problems, such as requiring a high capital cost and the formation of secondary pollutants. As a response, the development of environmentally friendly treatment methods for co-treatment of toxic heavy metals and citric acid pollutants became an imperative task. The semiconductor photocatalysis process is considered a promising technology in addressing

these requirements. This is because the semiconductor photocatalysis process showed the potential in removal of metals ions and organic pollutant simultaneously and produces less harmful by-products.

2.3 Basic principles of heterogonous photocatalysis

The acceleration of a chemical transformation by the presence of a catalyst with light is called photocatalysis. It is a discipline which includes a large variety of reactions such as organic synthesis, water splitting, photoreduction, photooxidation, hydrogen transfer, O_2^{18}-O_2^{16} and deuterium-alkane isotopic exchange, metal deposition, disinfection and anti-cancer therapy, water detoxification, and gaseous pollutant removal (Fujishima et al., 2000 & Ibhadon et al., 2013). Among these reactions UV/TiO_2 photoreduction-photooxidation has received more attention for many years as an alternative method for purification of both air and water streams. The catalyst may accelerate the photoreaction by interaction with the substrate in its ground or excited state and/or with a primary photoproduct, depending upon the mechanism of the photoreaction and itself remaining unaltered at the end of each catalytic cycle.

The basic principles of heterogeneous photocatalysis underlying photocatalysis are already established and have been reported in many literatures (Pelizzetti et al., 1993; Hoffmann et al., 1995; Fujishima et al., 2000 & Ibhadon et al., 2013). Xu et al. (2013) reported the dependence of the rate of toxic heavy metals along with citric acid photodegradation on the surface coverage. In other words, only the molecules that are in direct contact with the semiconductor photocatalyst surface undergo photocatalytic degradation. A semiconductor (SC) is characterised by an electronic band structure in which the highest occupied energy band, called valence band (VB), and the lowest empty band, called conduction band (CB), are separated by a band gap, *inter alia* a region of forbidden energies in a perfect crystal. When a photon of energy higher or equal to the band gap energy is absorbed by a semiconductor particle, an electron from the VB is promoted to the CB with simultaneous generation of a hole (h+) in the VB. The e^-_{cb} and h^+_{vb} can recombine on the surface of the particle in a few nanoseconds (and the energy dissipated as heat) or can be trapped in surface states where they can react with donor or acceptor species adsorbed or close to the surface of the particle. Thereby, subsequent anodic and cathodic redox reactions can be initiated. The energy level at the bottom of the CB is actually the reduction potential of photoelectrons and the energy level

at the top of the VB determines the oxidising ability of photoholes, each value reflecting the ability of the system to promote reductions and oxidations. The efficiency of a photocatalyst depends on the competition of different interface transfer processes involving electrons and holes, and their deactivation by recombination. A semiconductor band gap structure is shown in Figure 2.1.

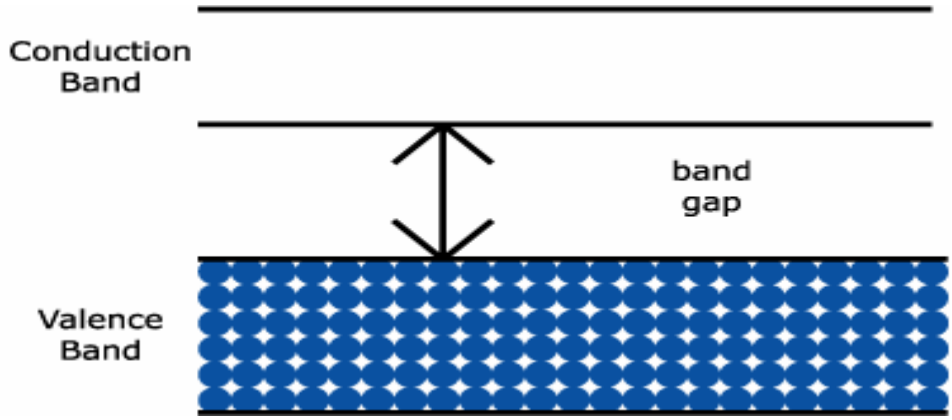

Figure 2.1: Semiconductor band gap structure (Algarin et al., 2008).

2.4 Mechanism of heterogonous photocatalysis

Heterogeneous photocatalysis is a process in which two active phases, solid and liquid, are present. The solid phase is a catalyst, usually a semiconductor. The molecular orbital of semiconductors has a band structure. The bands of interest in photocatalysis are the populated valence band (VB) and it's largely vacant conduction band, which is commonly characterised by band gap energy (Eg). The semiconductors may be photoexcited to form electron-donor sites (reducing sites) and electron-acceptor sites (oxidising sites), providing great scope for redox reaction. When a semiconductor catalyst of the chalcogenide type oxides (TiO_2, ZnO, ZrO_2, CeO_2) or sulfides (CdS, ZnS) is irradiated with photons whose energy is equal to or greater than their band-gap energy e.g. ($h\nu \geq$ Eg), there is absorption of these photons and creation within the bulk of electron-hole pairs, which dissociates into free photoelectrons (e^-) in the conduction band and photoholes (h^+) in the valence band. Simultaneously, in the presence of a fluid phase (gas or liquid), a spontaneous adsorption occurs and according to the redox potential (or energy level) of each adsorbate, an electron transfer proceeds towards acceptor molecules where they, as positive photoholes, are transferred to donor molecules.

The hydroperoxyl radical formed also has scavenging property as O_2 thus doubly prolonging the lifetime of photohole. Both the oxidation and reduction can take place at the surface of the photoexcited semiconductor photocatalyst. These hydroxyl radicals oxidise dissolved organic compounds and convert them to carbon dioxide (CO_2), water (H_2O) and other inorganic products. The electrons on the other hand, combine with dissolved oxygen to form superoxide anions and H_2O_2, which after further reactions also forms hydroxyl radicals. In addition to the formation of superoxide, dissolved metal ions are reduced by the electrons.

In addition, the recombination of the photoelectron-photohole pair is also possible if no electron acceptor or an electron donor (oxygen) is present in the solution to scavenge the electrons to form superoxides ($O_2^{\bullet-}$), its protonated form, the hydroperoxyl radical ($HO_2^{\bullet}$) and subsequently H_2O_2 (Pelizzetti et al., 1993 & Xu et al., 2000). This recombination prevents the oxidation and reduction reactions required for the degradation of pollutants. Therefore, the electron-hole pair must be prevented from recombining. This is obtained by trapping either the photogenerated electrons or the photo-generated holes (Fujishima et al., 2000).

The reduction of toxic heavy metal ions such as Cr(VI) and Hg(II) to their valence state in the presence of oligocarboxylic acids such as citric acid is the primary focus of this research. In order for the redox reaction between metal ions, (Cr(VI) and Hg(II) in this case), and electrons to occur it is important to prevent the electron-hole recombination by scavenging the holes that are generated. As a response, citric acid acted as a hole scavenger. The photocatalysis mechanism is illustrated in Figure 2.2.

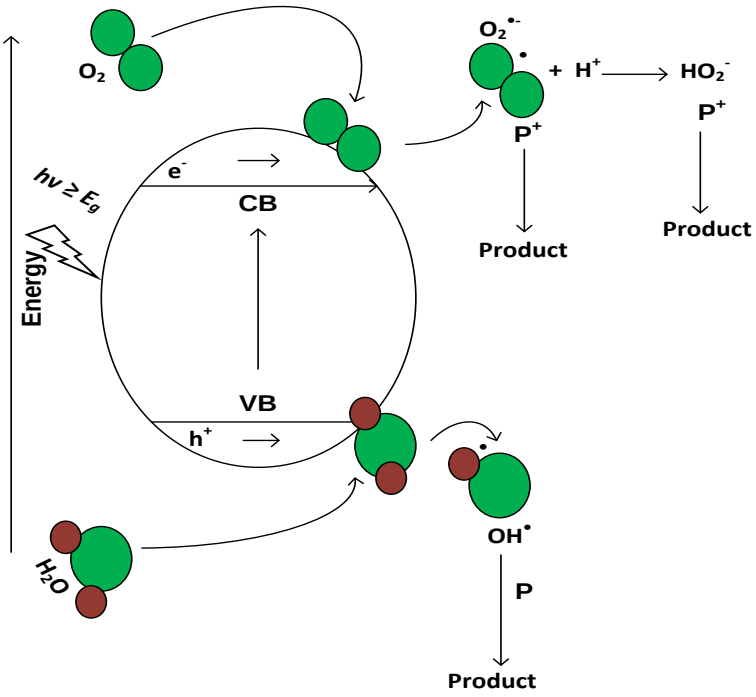

Figure 2.2: Schematic diagram of photocatalytic process for formation mechanism of electron-hole pair in a semiconductor particle with the presence of water pollutant (P).

2.5 Heterogeneous TiO_2 photocatalysis reactions involved

The reactions involved during the photocatalytic degradation of organic contaminants over TiO_2 are already established and have been reported in many literatures (Pelizzetti et al., 1993; Muneer et al., 1997; Fujishima et al., 2000; Augugliaroa, 2012 & Manojar et al., 2012). However, little has been reported on the photocatalytic reactions involved during the removal of toxic heavy metals from water in the presence of organic compounds (Gkika et al., 2005 & Fu et al., 2010). The removal of toxic heavy metals from water occurs in two main steps. First, it is the physical adsorption of metal ions onto the photocatalyst surface by Van der Waal forces. Next, it is the photo-reduction of toxic heavy metal ions from a higher oxidation state to a lower oxidation state due to the activation of the semiconductor photocatalyst. The reactions involved in semiconductor photocatalysis (Wang et al., 2009) are illustrated below.

Charge carrier generation:

$$TiO_2 + hv \rightarrow TiO_2\ (e^- + h^+) \qquad (2.1)$$

Generation of hydroxyl radicals:

$$h^+ + OH^- \rightarrow {}^{\bullet}OH \qquad (2.2)$$

Photooxidation of citric acid

$^{\bullet}OH + Cit \rightarrow CO_2 + H_2O + H^+$ (2.3)

Photoreduction of Cr(VI):

$Cr_2O_7^{2-} + 14H^+ + 6e^- \rightarrow 2Cr\ (III) + 7H_2O$ (2.4)

Photoreduction of Hg(II):

$Hg^{2+}_{(ads)} + 2e- \rightarrow Hg^0_{(ads)}$ (2.5)

Reaction 2.1, illustrates the generation of electron-hole pairs induced by the irradiation of TiO_2 in UV light. After the electron-hole pair separation, the combination of holes with water to generate hydroxyl radicals is shown by reaction 2.2. The formation of carbon dioxide, water, and organic acids when the hydroxyl radicals react with the citric acid in the solution is shown by reaction of 2.3. Reactions 2.4 and 2.5 shows photo-generated electrons in the conduction band that are used by the toxic heavy metal ions (Cr^{6+} and Hg^{2+}), which are subsequently reduced to non-toxic Cr^{3+} and Hg^0, respectively.

2.6 Titania as a photocatalyst

TiO_2 has attracted considerable attention for various applications such as pigments, photocatalysis, dye-sensitised solar cells, sensor devices, cosmetics and protective coatings (Malato et al., 2009; Chong et al., 2010; Khin et al., 2012 & Pelaez et al., 2012). Apart from TiO_2, different semiconductors such as ZnO, α-Fe_2O_3, ZnS, CdS and WO_3, have enough band-gap energies for the effective catalysis of many chemical reactions. Though it is well known that metal oxides are usually less active catalysts than noble metals in the majority of applications, metal oxides are more suitable since they are more resistant to poisoning and deactivation. In addition, combining two or more metal oxide catalysts, addition of metals and dopants, could improve or enhance catalytic activity. In particular, TiO_2 is the most studied photocatalyst because of its photo stability and low cost, combined with its biological and chemical inertness and resistance to photo and chemical corrosion (Malato et al., 2009). Also because of its higher photocatalytic activity compared to other common semiconductors used in photocatalysis. For example, Okamoto et al. (1985a, 1985b) observed the greater photocatalytic activity for TiO_2 compared to CdS catalyst for the decomposition of phenol as the target organic species. Sakthivel et al. (2000) showed that under similar study conditions, TiO_2 had greater photocatalytic efficiency than α-Fe_2O_3, ZrO_2, CdS, WO_3 and SnO_2. Wu et al. (2004) also observed higher photocatalytic activity for TiO_2 compared to SnO_2 and ZnO.

On the other hand, studies by Hsu et al. (2005); Shao et al. (2009); Kamat et al. (2010); Teoh et al. (2012) & Pingfan et al. (2013) show that ZnO has attracted considerable interest in photocatalysis because of its similar energy characteristic to TiO_2. For instance, ZnO performed better than TiO_2 in some other studies (Degen and Kosec, 2000 & Catano et al., 2012). However, Catano et al. (2012) indicated that, although ZnO had a higher activity (although the surface area is less) than TiO_2, the latter was photochemically more stable in aqueous media. They further report that ZnO suffers from photo-corrosion problems upon excitation in solution and is unstable because it readily dissolves in water (Degen and Kosec, 2000) to yield $Zn(OH)_2$ on the ZnO particle surface, which inactivates the catalyst over time. Binary metal sulphide semiconductors such as ZnS and CdS are reported to be insufficiently stable for catalysis and suffer from photoanodic corrosion (Nguyen et al., 2006), while iron oxides such as Fe_2O_3 are reported to be prone to photocathodic corrosion (Mekatel et al., 2012). WO_3 has also been investigated as a potential photocatalyst, but it is generally less active catalytically than TiO_2 (Wang et al., 1993 & Wang et al., 2010). As shown in Table 2.1 WSe_2, V_2O_5, WO_3, CdS and α-Fe_2O_3 possess a narrow bandgap for harnessing solar energy; however, all of them have drawbacks compared to TiO_2 such as low electron conduction band. The band structure of the substrate is vital since a change in surface or bulk electronic structure can affect the chemical events (Nguyen et al., 2006).

As already explained, one of the limitations of TiO_2 as photocatalyst is its large band gap (3.2 eV for anatase) and thus resulting in poor efficiency in the visible region of the solar spectrum (Linic et al., 2011& Wang et al., 2012). Furthermore because of the wide band gap of TiO_2 only a small UV fraction of solar light (3–5%) can be utilised (Chen and Mao, 2007; Fujishima et al., 2008 & Tong et al., 2012). To overcome the above inconvenience, many attempts have been made to effectively synthesise pure rutile TiO_2 (3.0 eV rutile) photocatalysts (Jia et al., 2006). On the other hand, rutile TiO_2 crystal possesses some advantages among the three common polymorphs (anatase, rutile, and brookite) of TiO_2 such as a high UV ray absorption rate and high chemical stability (Yin et al., 2001) and in some cases rutile TiO_2 is reported to achieve higher photocatalytic activities than anatase (Tsai et al., 1997; Watson et al., 2003 & Habibi and Vosooghian, 2005). Modification of TiO_2 by deposition of noble metal nanoparticles is proved to be effective to narrow the band gap and increase photocatalytic activity of TiO_2 (Tada et al., 2009; Primo et al., 2011 & Kubacka et al., 2012). As response, in this study pure rutile TiO_2 was synthesised, modified by metal

deposition and immobilised on calcium alginate thus making the environmental application of TiO_2 photocatalysis technology easier for implementation.

Table 2.1: Bandgap energies for some common semiconductor materials used for photocatalytic processes at 273 ºC (Serpone et al., 1989; Sakthivel et al., 2000; Bhatkhande et al., 2001 & Nguyen et al., 2006).

Semiconductors	Band energy (eV)	Semiconductors	Band energy (eV)
TiO_2 rutile	3.02	WSe_2	1.2
TiO_2 anatase	3.23	α-Fe_2O_3	2.3
ZnO	3.2	V_2O_5	2.7
ZnS	3.7	WO_3	2.8
CdS	2.4	SnO_2	3.5

2.6.1 Synthesis and morphologies

Fujishima and Honda discovered the photocatalytic splitting of water on TiO_2 electrodes in 1972 (Fujishima and Honda, 1972). Since then, TiO_2 has been the subject of intensive investigation as a semiconductor photocatalyst owing to its high level of photo-activity, photodurability, chemical and biological inertness, mechanical robustness as well as low cost (Anpo et al., 1987; Hoffman et al., 1995; Linsebigler et al., 1995 & Sriwong et al., 2012). Usually, the photocatalytic performance of TiO_2 depends strongly on its morphological, structural and textural properties. Therefore, much work has been devoted to the synthesis of TiO_2 with different structures and morphologies.

Numerous efforts have been made to enhance the activity of rutile TiO_2 and it is found that the morphology is one of the important factors influencing the activity, which may lead to interesting shape-dependent properties (Li et al., 2007). In various morphologies, the hierarchical 3D nanostructures have been regarded as the more attention-grabbing structures due to their dimensions and the greater number of active sites than other 2D or 1D nanostructures (Hu et al., 2007 & Sarkar et al., 2012). Thus makes it promising for potential applications in photocatalysis. For instance, when used as a photocatalyst, the nanometer-scale unit in the 3D TiO_2 geometric architecture could be responsible for the high level of photocatalytic ability; meanwhile, the micrometer-scale structure favours light-harvesting and separation of the powders from the solution compared to nanometer-scale powders (Dong et

al., 2009). Therefore preparation of high-quality hierarchical 3D TiO_2 nanostructure of desired morphology is of great fundamental and technological interest.

A variety of techniques such as chemical vapour decomposition (Qian et al., 1993), sol-gel (Samuneva et al., 1993), reversed micelle (Kielbassa et al., 2006), Ostwald ripening (Kielbassa et al., 2006), Kirkendall effect (Mazdiyasni et al., 1965) and hydrothermal reactions (Bai et al., 2008) are used to produce TiO_2 nanostructures. For the preparation of different inorganic materials in a nanocrystalline state, hydrothermal synthesis is a widely used method (Zhu et al., 2004). Since the reactions are carried out in an enclosed system, the method using an aqueous solvent as reaction medium can be classified as environmentally friendly. The products, during hydrothermal reactions, can be well controlled by the temperature, reaction time and concentration of the chemical species (Bai et al., 2008 & Yu et al., 2008). This method provides the advantages of controlling the stoichiometry, homogeneous products and allowing the formation of complex shapes and preparation of composite materials (Yu et al., 2008). Moreover, the hydrothermal method provides excellent homogeneity and the possibility of deriving unique stable structures at low reaction temperatures (Bao et al., 2005). Particles and rod-like TiO_2 structures are easy to synthesise by this method, while the flower-like TiO_2 prepared by this method is hardly ever reported in the literature. In addition, a systematic study on the synthesis of TiO_2 by the hydrothermal method has not been reported.

Recent efforts have made this technique a new platform for synthesising flower-like TiO_2 nanostructures having controllable hierarchical features. For example, Jin et al. (2012) synthesised dandelion-like rutile TiO_2 microspheres using rutile hollow SnO_2 spheres as templates. Bai et al. (2008), synthesised pure rutile phase TiO_2 powder with novel 3D dandelion-like structures by facile hydrothermal method with $TiCl_3$ as the main starting material. Zhou et al. (2013) synthesised a novel 3D sea-urchin-like hierarchical TiO_2 microsphere with 1D nanostructure by the hydrothermal method using Ti plate in a mixture of H_2O_2 and NaOH aqueous solution, and investigated the influence of reaction time, reaction temperature and calcinations temperature. However, these studies were based mainly on the growth mechanisms of the 3D TiO_2 structures and none of them considered the optical property of the catalysts, especially photocatalytic activity in the removal of inorganic pollutants. In this study, the hydrothermal method has been used to synthesise 3D dandelions-like TiO_2 photocatalysts.

2.6.2 Enhancement of the activity of titania

As mentioned previously, modifications of semiconductor surfaces by the addition of metals, dopants, or combining two or more metal oxide catalysts can play an important role in science and technology. The modified materials with their unique optical, electrical, magnetic, catalytic, and chemical properties are widely used in fields such as photoluminescence, photocatalysis, and nano electronics (Primo et al., 2011). During photocatalysis, the main reason for the surface modification of TiO_2 is to inhibit recombination of photogenerated electrons and holes by increasing the charge separation and, therefore, enhancing the efficiency of the photocatalytic process. Recently, many researchers have focused on enhancing the photocatalytic activity of TiO_2 photocatalyst in the whole spectrum through a number of modification methods, such as coupling of two semiconductor particles with different electronic energy levels and deposition of noble metals. The coupling of different semiconductors has led to the discovery of photoinduced vectorial electron transfer from one semiconductor to another semiconductor (Yang et al., 2010 & Gherbi et al., 2011). However, the charge carrier recombination occurs within nanoseconds and hence low photocatalytic activity is usually observed (Gherbi et al., 2011). Among the most widely used modification methods, deposition of noble metals has aroused great interest since this method can enhance the activities of a TiO_2 photocatalyst in many types of photocatalytic reactions (Tada et al., 2009). Noble metals such as Pt, Au, Pd, Rh, Ni, Cu and Ag are deposited on the semiconductor surface to solve this problem. It has been reported by (Tada et al., 2009; Primo et al., 2011 & Silva et al., 2011) that the photocatalytic activity may be enhanced by impregnating the surface of TiO_2 with noble metals.

A similar approach has been adopted to increase the catalytic activity of TiO_2 by depositing metals as heterojunction; thus, enhancing the quantum yield of the electron transfer processes through improvement in charge separation in the semiconductor, discharging photogenerated electrons across the interface and providing a redox pathway with low over-potential. The interfacial charge transfer processes are influenced by the presence of a noble metal co-catalyst. If noble metal nanoparticles are coupled to the semiconductor nanoparticle, they readily accept and shuttle electrons to an acceptor molecule at the interface easily. Because the Fermi levels of these noble metals nanoparticles are lower than that of TiO_2, the discharge capacity of noble metal nanoparticles plays an important role in dictating Fermi level equilibration between semiconductors and metal nanoparticles (Subramanian et al., 2004).

It follows from these studies, that in order to enhance the photocatalytic activity of TiO_2 particles, interfacial charge-transfer reactions need to be enhanced. Improved charge separation and inhibition of charge carrier recombination is essential to improving the overall quantum efficiency for interfacial charge transfer. In this study, TiO_2 has been modified by Au deposition to improve the visible-light absorption, prevent charge carrier recombination and lengthen the carrier lifetime characteristics of TiO_2.

2.6.3 Modification of titania by metal deposition

Noble metals addition to TiO_2 is another approach for modifying TiO_2 photocatalyst. Noble metals, such as Pt, Au, Pd and Ag, have been reported to be very effective for enhancement of TiO_2 photocatalysis (Chen et al., 2007). As the Fermi levels of these noble metals are lower than that of TiO_2, photo-excited electrons can be transferred from CB to metal particles deposited on the surface of TiO_2, while photo-generated VB holes remain on the TiO_2. This greatly reduces the possibility of electron-hole recombination, resulting in efficient separation and higher photocatalytic activity.

Numerous studies have found that the Au noble metal deposited on TiO_2 has a higher photocatalytic compared to other noble metals. For example, Rupa et al. (2009) deposited approximately 1 wt% noble metal (Au/TiO_2, Ag/TiO_2 and Pt/TiO_2) into synthesised TiO_2 nanoparticles. Noble metal/TiO_2 photocatalysts showed remarkable photocatalytic activity towards the decolorisation of tartrazine even under visible irradiation. The order of the photocatalytic activity of the different catalysts was Au/TiO_2 > Ag/TiO_2 > Pt/TiO_2 > Synthesised TiO_2 > TiO_2 (P-25 Degussa). Sakthivel et al. (2004) reported that the addition of 1 wt% of Pt, Au and Pd increased the photocatalytic activity towards the degradation of leather dye, acid green 16 in aqueous solution. The order of the photocatalytic activity of the different photocatalysts was: Au/TiO_2 > Pt/TiO_2 > Ag/TiO_2 > TiO_2 (P-25 Degussa). The use of noble metals such as Au can therefore improve the photocatalytic activity and feasibility of TiO_2 photocatalysts for application in wastewater treatment. However, further research efforts may be needed to get a better understanding of the costs involved in comparison with the photocatalytic activities reported by different authors. In this study, Au loading was chosen to modify TiO_2.

2.6.4 Immobilisation of titania

In the past years, much research has been carried out into a slurry system (suspension of fine powdered TiO_2). However, the suspended particles contaminate the yield and need to be removed after treatment. This is more difficult for smaller particles as they stay suspended in water easily, clog filter membranes and penetrate filter materials (Ibhadon et al., 2013). The filtering of the slurry is not practical, and can be a time-consuming and costly process. As a result, filtration and resuspension of photocatalyst powder should, if possible, be avoided in any wastewater treatment processes.

Since 1993, the idea of an immobilised photocatalyst on an inert support has begun to be widely accepted because it could help to eliminate the costly post-separation processes (Tuprakay and Liengcharensit, 2005 & Harikumar et al., 2013). This could provide advantages such as easier solid-liquid separation, easier regeneration and reuse of the TiO_2 and minimal blockage in continuous flow system, thus making the environmental application of TiO_2 photocatalysis technology easier for implementation. To this end, many studies have been published on the anchoring of the photocatalyst particles onto supports that are readily removable.

As a response, numerous researchers undertook many efforts to immobilise TiO_2 particles into different supports for the degradation of organic compounds and reduction of toxic heavy metal ions, such as silica (Vohra et al., 2003), zeolite (Anandan et al., 2003), activated carbon (Shaban, 2013) and chitosan (Zulkarnain et al., 2009). However, the problem of detachment of the deposited catalyst particles was reported in earlier studies with films comprising immobilised powders of TiO_2 (Mills et al., 2002). Moreover, during the heating process, which is used for fixing the photocatalyst, a part of the porous structure gets lost through a sintering process. These reduce the surface area-to-volume ratio of the photocatalyst, which causes mass transfer limitations. On the other hand, bio-polymer supports are a good adhesion of the TiO_2 particles, no sintering temperatures, a high specific surface area and strong absorbance affinity towards the pollutants (Idris et al., 2010).

Bio-polymers such as alginate is a mechanically and biocompatible stable gel, nontoxic, biodegradable, non-immunogenic, produces thermally irreversible and water insoluble gels (Harikumar et al., 2011). Alginate, in the presence of divalent cations such as Ca^{2+}, Cu^{2+} and Ba^{2+} can form stable hydrogels with the formation of a 3D network (Papageorgiou et al.,

2012). Based on these properties, alginate is considered a promising support for TiO_2 and has continuously been studied in recent years (Liu et al., 2013). Ca-alginate support, as the biodegradable polymer material, reduces the need for synthetic polymer and results in production at low cost, thereby producing a positive effect both environmentally and economically. Therefore, Ca-alginate can be used as a green support for TiO_2 immobilisation that can be used for developing a new environmentally friendly immobilisation system for wastewater treatment by heterogeneous photocatalysis. The application of immobilised TiO_2 nanoparticles on Ca-alginate (Alg/TiO_2) is still scarce, especially in the co-treatment of toxic heavy metals and organic acids. This study reports on the utilisation of TiO_2 immobilised on calcium alginate for the co-treatment of Cr(VI), Hg(II) metals and citric acids.

2.7 Co-treatment of toxic heavy metals and organic compounds by UV/TiO_2 photocatalysis

Citric acid is a strong chelating agent, and has been widely used in processed foods and beverages, pharmaceutical preparations and for the chemical cleaning of the steam generator internals in nuclear power plants. (Quici et al., 2007 & Meichtry et al., 2010). In South Africa, Koeberg nuclear power plant has been generating large volumes of radioactive wastewater containing citric acid complexes with toxic heavy metal ions such as iron, copper, cobalt, chromium, and mercury as part of their normal operations since 1987.

As explained before in Section 2.1, different technologies have been studied for the treatment of citric acid-heavy metal ions complexes. In particular, UV/TiO_2 photocatalysis was regarded as promising technology applicable for efficient and simultaneous treatment of Cr(VI) or Hg(II) and citric acid. Photocatalysis has been known to treat both organic pollutants and toxic heavy metal ions simultaneously (Litter, 1999 & Chen and Ray, 2001). The rate of photocatalytic reduction was reported to be dependent on the reductant that is used. As mentioned in Section 2.4, in a system without citric acid, the toxic heavy metal ion reduction is the electrochemical oxidation of water. It is reported that this is a kinetically slow process, and the competing recombination of the photogenerated holes and electrons plays an active inhibiting role for such a process. Hence, the co-treament of Cr(VI) or Hg(II) with citric acid may accelerate the photocatalytic reduction of Cr(VI) or Hg(II). The presence of citric acid results in the accelerating effect of photocatalytic reduction of Cr(VI) or Hg(II) more efficiently on the toxic heavy metal-TiO_2-citric acid systems than a toxic heavy metal-TiO_2 system.

Several research groups (Chen and Ray, 2001; Bussi et al., 2002; Khalil et al., 2002; Deng et al., 2010 & Zhou et al., 2013) studied the effects of organic compounds on the photocatalytic reduction of Hg(II) and found that the presence of organic species accelerated the photocatalytic reduction of Hg(II). On the other hand , Colo´n et al. (2001); Testa et al. (2004); Shao et al. (2009); Yang et al. (2010); Chaudhary et al. (2012); Dozzi et al. (2012) & Xu et al. (2013), have investigated the effects of organic compounds on the photocatalytic reduction of Cr(VI). The above studies reported that the reduction of Cr(VI) proceeded more quickly in the presence of organic compounds than that observed in the Cr(VI) alone. Most of these studies further compared the various organic compounds such as citric acid, salicylic acid, acetic acid, ethanol and methanol. They have found a reduction rate of Hg(II) and Cr(VI) to follow the order of citric acid > salicylic acid > acetic acid > ethanol > methanol. They suggested chelating and adsorption may contribute to the observed results. They have also suggested that conduction band reduction reactions were faster for organics that were more easily oxidised. Although there are several reports mentioned above that have investigated the reduction of Cr(VI) or Hg(II) in the presence of citric acid using UV/TiO_2 photocatalysis, the reduction of Cr(VI) or Hg(II)–citric acid complexes, especially in ternary (mixed Cr(VI) and Hg(II)-citric acid) systems, has not been previously reported. Therefore, simultaneous photocatalytic reduction of Cr(VI) and Hg(II) in a mixed system and the oxidation of citric acid is a technically challenging environmental remediation problem. Furthermore, great attention is paid to the addition of Fe(III) to citric acid solution, to enhance the reduction of metal ions. This enhanced behavior is hypothesised to be due to some unknown reductant in the citric acid phase and light irradiation that is able to reduce Fe(III) to Fe(II). The present study is focused on the co-treatment of Cr(VI) and Hg(II) and citric acid in single, binary and ternary photocatalytic systems.

2.8 Fe(III) photocatalytic reduction of toxic heavy metals by citric acid

Recent efforts have focused on the photocatalytic influence of Fe(III) on the reduction of toxic heavy metals by organic acids such as citric acid. The rate of toxic heavy metals photoreduction in sunny natural waters is related to the amount of Fe(III) present and the nature of the dissolved organic substance substrate and the organic acid type (classified as low Fe(III) photoreductivity acetate, and high Fe(III) photoreductivity citrate) (Sun et al., 2009). The fast reaction between toxic heavy metals and organic acids in the presence of Fe(III) is mainly due to the photoreaction products generated when the solution is exposed to

UV light irradiation. These products such as Fe(II), $HO_2/O_2^{\bullet-}$ or $CO_2^{\bullet-}$, are reported to catalyse the reduction of toxic heavy metals (Sun et al., 2009). Fe(II)/Fe(III) acts as a photocatalyst by shuttling electrons from the organic acid to toxic heavy metals. The photocatalytic cycle consists of (1) Fe(III)-citric acid absorbance of UV light to produce Fe(II) and radicals; (2) oxidation of Fe(II) to Fe(III) by toxic heavy metals, accompanied by the intermediated production of toxic heavy metal (in case of Cr(VI) intermediate such as Cr(V) and Cr(VI) will be formed as shown in Eq.(2.11a); (3) reformation of Fe(III)-organic acid as follows (Eqs. (2.7) ‑ (2.13)) (Gaberell et al., 2003).

$$\text{Fe(III)-Cit} + hv \rightarrow \text{Fe(II)} + \text{Cit}^{\bullet} + hv + CO_2 \rightarrow R^{\bullet} \quad (2.6)$$

$$R^{\bullet} \rightarrow ROO^{\bullet} \rightarrow O_2^{-} \quad (2.7)$$

$$R^{\bullet} + \text{Fe(III)} \rightarrow \text{Fe(II)} \quad (2.8)$$

$$H^{+} + O_2 - \rightarrow HO_2^{\bullet} \quad (2.9)$$

$$HO_2^{\bullet} + {}^{\bullet}HO_2 \rightarrow H_2O_2 \quad (2.10)$$

$$\text{Cr(VI)} + \text{Fe(II)} + \text{Cr(V)} + \text{Fe(II)} + \text{Cr(VI)} + \text{Fe(II)} + \text{Cr(III)} \quad (2.11a)$$

$$3\text{Fe(II)} + HCrO_4^{-} + 7H^{+} \rightarrow 3\text{Fe(III)} + \text{Cr(III)} + 4H_2O \quad (2.11b)$$

$$O_2^{-}/HO_2^{\bullet} + \text{Fe(II)} + H^{+} \rightarrow \text{Fe(III)} + H_2O_2 \quad (2.12)$$

$$H_2O_2 + \text{Fe(II)} \rightarrow \text{Fe(III)} + {\bullet}OH + OH^{-} \quad (2.13)$$

In this reaction cycle, the complex formation between Fe(III) and the citric acid is a key step for the reduction of toxic heavy metals.

2.9 Effects of operating parameters

The reduction rate of Cr(VI) or Hg(II) and oxidation of citric acid by photocatalysis depends mainly on the initial pH, initial concentration and the contact time, photocatalyst dosage, wavelength, light intensity and substrate adsorption. Thus, the efficiency of the co-treatment of Cr(VI) or Hg(II) with citric acid by photocatalysis is a function of all the above-mentioned parameters. Each of the parameters will be discussed individually in the following sections as they influence the UV/TiO_2 photocatalytic process in wastewaters.

2.9.1 Effect of initial pH

In heterogeneous UV/TiO_2 photocatalytic process, pH is one of the most important operating parameters that affect the surface charge properties of the photocatalyst, size of catalyst

aggregates it forms (Hoffmann et al., 1995). The change in pH also affects the positions of conductance and valence bands (band edge) of the photocatalyst. Due to the nature of TiO_2 catalyst used, any variation in the operating pH is known to affect the isoelectric point or the surface charge of the photocatalyst used. The point of zero charge (pzc) of TiO_2 is reported by Kosmulski (2006) to be 6.8. Under acidic or alkaline conditions, the ionisation state of TiO_2 surface can be protonated or deprotonated respectively according to the following reactions:

At pH < PZC: $TiOH + H^+ \rightarrow TiOH_2^+$ (2.14)

At pH > PZC: $TiOH + OH^- \rightarrow TiO^- + H_2O$ (2.15)

Thus, the TiO_2 surface will remain positively charged in acidic medium (pH < 6.8) and negatively charged in alkaline medium (pH > 6.8). While under acidic conditions the positive charge of the TiO_2 surface increases as the pH decreases (Eq.2.6); above pH 6.8 the negative charge at the surface of the TiO_2 increases with increasing pH (Eq.2.7). Moreover, the pH of the solution affects the formation of hydroxyl radicals by the reaction between hydroxide ions and photo-induced holes on the TiO_2 surface. The degree of electrostatic attraction or repulsion between the photocatalyst's surface and the ionic forms of toxic heavy metals and citric acid molecule can vary with the change in solution pH, which can result in enhancement or inhibition on the photocatalytic reduction-oxidation of toxic heavy metals and citric acid pollutants in the presence of TiO_2.

At optimised conditions, better photocatalytic degradation has been reported by various researchers (Tuprakay and Liengcharernsit, 2005; Arthi and Madres, 2008; Shao et al., 2009 & Wang et al., 2010) who studied the effect of pH on the photoreduction rate of Cr(VI) at different pH range. They reported that the photoreduction rate of Cr(VI) increases as the pH decreases from 2 to 12 in the presence of TiO_2. However, at higher pH (pH $\geq$ 6) values Cr(VI) was reported to be reduced to Cr(III), then followed by precipitation of Cr(III) to form metal hydroxide such as soluble $Cr(OH)_3$.

On the other hand, Serpone et al., 1987; Xu et al., 2002 & Cristante et al., 2006, suggested that the photoreduction rate of Hg(II) increases as the pH increases from 2 to 8 in the presence of TiO_2. However, at high pH above pH 9, Kannan and Malar (2005) observed the precipitation of Hg(II) ions in the solution to $Hg(OH)_2$. Moreover, Meltzer et al. (2007)

observed the precipitation of Fe(III) ions to $Fe(OH)_3$ over the pH range of 3.5 to 7 and Fe(II) to $Fe(OH)_2$ at pH ≥ 8.5. Therefore, in this study the optimum pH values were found at the pH values where the metals ions do not get reduced from the solution due to formation of colloidal precipitates such as $Hg(OH)_2$, $Fe(OH)_2$ and $Fe(OH)_3$ and not due to photocatalysis. Quici et al. (2007) & Meichtry et al. (2010) observed that the photocatalytic degradation of citric acid was efficient in acidic pH in comparison to alkaline pH range in the presence of TiO_2. In all these studies, particle agglomeration was reported to reduce the substrate adsorption as well as photon absorption, thus reducing the photocatalytic efficiencies of Cr(VI), Hg(II) and citric acid.

2.9.2 Effect of initial concentration and contact time

It is imperative both from a mechanistic and application point of view to study the dependence of the photocatalytic reaction rate on the substrate initial concentration. It is noted generally that the removal rate increases with the decrease of toxic heavy metal and citric acid initial concentrations to a certain level and a further increase in toxic heavy metal and organic compounds initial concentration leads to a decrease in the photocatalytic removal. However, not all toxic heavy metals and organic compounds will have such a profound effect, and this also depends on the corresponding chemical nature of the targeted compounds for TiO_2 photocatalysis reaction.

For example, previous investigations have reported the dependency of the Cr(VI), Hg(II) and citric acid photocatalytic reaction rate on the initial concentration of Cr(VI), Hg(II) and citric acid contaminants (Saquib and Muneer, 2003; Deng et al., 2010 & Mekatel et al., 2012). Mekatel et al. (2012), reported that the Cr(VI) photoreduction rate increases with the decrease in initial Cr(VI) concentration. Quici et al. (2007) also found that the photocatalytic degradation rate of citric acid increases with a decrease in initial citric acid concentration. In contrast, Deng et al. (2010) reported that the Hg(II) photoreduction increases with an increase in Hg(II) initial concentration to a certain level. However, a further decrease in the Hg(II) initial concentration leads to a decrease in Hg(II) photoreduction rate. Chen et al. (2011) reported that under similar operating conditions, a variation in the initial concentration of the wastewater contaminants would result in different contact time necessary to achieve complete photoreduction-oxidation of toxic heavy metals and citric acid.

2.9.3 Effect of photocatalyst dosage

In heterogeneous photocatalytic process, the optimum catalyst concentration must be determined, in order to avoid excess catalysts and ensure total absorption of efficient photons. This is because excess TiO_2 particles can create an unfavourable light-scattering light that reduces the surface area of TiO_2 being exposed to light irradiation and the photocatalytic efficiency (Fujishima et al., 2008). Therefore, any chosen photo reactor should be operated below the saturation level of TiO_2 photocatalyst used to avoid excess catalyst and ensure efficient photons absorption.

Numerous studies (Wang et al., 2004; Nezamzadeh-Ejhrehet et al., 2010 & Ma et al., 2012) have shown that the photocatalytic reaction rate initially increases with catalyst dosage and then decreases at high dosage because of light scattering of TiO_2 particles. The tendency towards agglomeration (particle-particle interaction) also increases at high solids concentration, resulting in a reduction in surface area available for light absorption and hence a drop in photocatalytic degradation rate. Although the number of active sites in solution will increase with catalyst dosage, a point will be reached where light penetration is to be compromised because of excessive particle concentration. The interchange between these two opposing phenomena results in an optimum photocatalyst dosage for the photocatalytic reaction (Ma et al., 2012). A further increase in catalyst loading beyond the optimum will result in decreased passage of irradiation through the sample, so that the reaction rate would indeed be lower with increased catalyst dosage. Therefore, it is important to obtain the optimum catalyst concentration for a photocatalytic reaction to avoid excess catalysts. Furthermore, it ensures that the maximum amount of TiO_2 is irradiated as a higher concentration of catalyst could result in light scattering, resulting in low photon efficiency.

2.9.4 Effect of UV irradiation wavelength

The photochemical effects of light sources with different wavelength-emitting ranges will have a profound consequence on the photocatalytic reaction rate, depending on the types of photocatalysts used, crystalline phase and any state of photocatalyst modifications. For example, using commercial Degussa P-25 TiO_2, which has a crystalline ratio of anatase 70/80: 20/30, a light wavelength at $\lambda < 380$ nm is sufficient for photonic activation (Herrmann, 1999 & Bahnemann, 2004). The crystalline phase of rutile TiO_2 has smaller bandgap energy of $E_B \sim 3.02$ eV, compared to the anatase TiO_2 of 3.2 eV (Xu et al., 2000).

This dictates that rutile TiO_2 can be activated with light wavelength of up to 400 nm, depending on the bandgap edge for the type of rutile TiO_2 used.

For UV irradiation, its corresponding electromagnetic spectrum can be classified as UV-A, UV-B and UV-C, according to its emitting wavelength. The UV-A range has its light wavelength spans from 315 to 400 nm (3.10-3.94 eV), while UV-B has wavelength ranges of 280 to 315 nm (3.94-4.43 eV) and the germicidal UV-C ranges from 100 to 280 nm (4.43-12.4 eV) (Rinco´n and Pulgarin, 2005). In a photocatalytic reactor, fluorescent low-pressure mercury lamps emitting low-intensity provide UV-A radiation. Medium pressure mercury lamps have also been used, which emit high intensity UV light in the short, medium and long UV spectrums. However, short (UV-C) and medium (UV-B) UV radiation, emitted by the mercury, usually is cut off by the photoreactor material, unless it is made of quartz.

2.9.5 Effects of light intensity and irradiation time

The light intensity of the irradiation source is one of the few parameters that affect the photocatalytic processes. Fujishima et al. (2000) indicated the initiation of TiO_2 photocatalysis reaction rates is not highly dependent on light intensity, where a few photons of energy (i.e. as low as 1 μW cm^{-1}) can sufficiently induce the surface reaction. In order to achieve a high photocatalytic reaction rate, particularly in water treatment, a relatively high light intensity is required to provide each TiO_2 surface active sites with sufficient photons energy adequately. However, when using the as-prepared TiO_2 particles without modifications, the surface reaction is restricted to photons with wavelengths shorter than the absorption edge of approximately 400 nm.

The application of photocatalytic process in the presence of UV wavelength ($l < 400$ nm) in many studies obeyed the linear proportionality correlation to the incident radiant flux. Glatzmaier et al. (1990); Magrini and Webb. (1990) & Glatzmaier et al. (1991), reported that the photocatalytic reaction rate increased with the radiation intensity. The reaction rate decreased with irradiation time since it followed apparent first-order kinetics and additionally a competition for degradation might occur between the reactant and the intermediate products.

2.9.6 Effect of substrate adsorption

As heterogeneous photocatalysis occurs at the surface of the semiconductor photocatalyst, it is of great importance to study the ability of the substrate to adsorb or be adsorbed onto the TiO_2 photocatalyst surface (Kormann et al., 1991). If the substrate is incapable of being adsorbed onto the surface, the photocatalysis process will be inefficient. Similarly, if the substrate is readily adsorbed onto the surface of the photocatalyst, more substrate will be oxidised/reduced by the electron/hole at the catalyst surface resulting in a more efficient photocatalytic process.

2.9.7 Effect of temperature

During photocatalytic processes, excitation and activation through irradiation is done at an ambient temperature (25ºC). The true activation energy is very small or even zero as the band gap energy to be exceeded is too high to be overcome by thermal activation, therefore, the effect of temperature should be quite weak. All the experiments in this study were carried out at ambient temperature with no heating involved.

2.10 Reusability of immobilised TiO_2 photocatalyst

The catalyst's lifetime is an essential parameter of the photocatalytic process, because its use for a longer period of time leads to a significant cost reduction of the treatment. A photocatalyst should be resistive to photo corrosion, stable under different reaction conditions, and able to promote reactions efficiently upon repetitive use. TiO_2 is one catalyst that has been found to meet the above criteria, and so it has been widely used in photocatalysis. Liu et al. (2013) evaluated the activity of a pure recycled TiO_2-impregnated glutaraldehyde crossslinked alginate beads in the reduction of toxic heavy metals and observed that the reduction ratio kept 100% after three times of reuse. There was no loss in the activity of the TiO_2 catalyst for 6 h run. Therefore, the reuse of catalysts is a critical criterion for commercialisation of this technology, as this is a major factor contributing to the operating costs of the system.

CHAPTER 3: METHODOLOGY

3. 1 Materials

Degussa P25 TiO_2 powder and the synthesised pure rutile dandelion like-TiO_2 were used as photocatalysts. Degussa P25 (anatase: rutile 80:20, BET surface area of 49 m^2/g, particle size 21 nm) sourced from Merck Chemicals (Pty) Ltd. South Africa, catalyst was used without further treatment in all experiments. Nitric acid (99.99% HNO_3) and sodium hydroxide (99% NaOH) were bought from Merck. R.S.A and used to adjust the pH of the solution. Tetrachloride (99% $TiCl_4$) that was used to synthesise dandelion like-TiO_2 nanostructures (anatase: rutile 0:100, BET surface area of 81 m^2/g, particle size 17 nm) was sourced from Merck Chemicals. An aqueous solution of tetrachloroauric acid ($HAuCl_4$ as 1 wt% Au) sourced from AngloGold Ashanti was used to prepare gold nanoparticles–titania photocatalyst (Au/TiO_2) (anatase: rutile 0:100, BET surface area of 103 m^2/g, particle size 18 nm). Potassium dichromate (99.99% $K_2Cr_2O_7$), mercury-chloride (99.5% $HgCl_2$), iron(III) chloride hexahydrate (99.99% $FeCl_3.6H_2O$) and citric acid (99.5% $HOC(COOH)(CH_2COOH)_2$) and also sourced from Merck, were used to prepare wastewater containing Cr(VI), Hg(II), Fe(III) metal ions and citric acid, respectively. Sodium alginate (99% $NaC_6H_7O_6$) and calcium chloride (99.99% $CaCl_2$), purchased from Sigma Aldrich South Africa, were used to prepare immobilised TiO_2-alginate beads (amorphous, BET surface area of 62 m^2/g, particle size 1 - 2 mm). All of the chemicals were analytical grade and employed as received. High purity water (resistivity 18.2 MΩcm) purified by a Milli-Q water system (millipore) was used throughout.

3.2 Equipment

The main equipment, which was used includes batch and recycled photocatalytic reactors. The batch reactor was used for the synthesis and photocatalytic activity of as-prepared, calcined and immobilised dandelion- like TiO_2 beads under different experimental conditions. An oven (Thermo Scientific (R), PR305220M) was used to dry the prepared catalyst and a muffle furnace (Thermo Scientific (R), Lindberg/Blue M(R), BF51634C) was used to calcine the dried prepared catalyst, while the magnetic stirrer (Heidolph MR Hei-end 1000) was used for stirring. Centrifuge (5810-R Eppendorf centrifuge) was used to separate the catalyst from the suspension. Heating mantle (Bibby scientific, EMA0500/CEB) was used to heat and stirring the reaction mixture during catalyst preparation. Overhead stirrer (United scientific,

RW 20) using R 1342 propeller stirrer, 4-bladed and magnetic stirrer (Heidolph MR Hei-end 1000) with magnetic stir bar (VP 772BK-S29-11-23.1) was used to stir the reaction mixture during the immobilisation of TiO_2 catalyst and photocatalytic experimental runs. The pH meter (Jenway 3510) was used to adjust the pH condition of the wastewater.

3.3 Experimental set-ups

The schematic diagram of the experimental set-up used for the synthesis of the dandelion-like TiO_2 is shown in Figure 3.1. The experimental set-up is composed of the heating mantle, magnetic bar, reaction flask (batch reactor) and refluxing tube. Figure 3.2 shows the schematic set-up for the preparation of Alg/TiO_2 composite. The set-up comprised an overhead magnetic stirrer, beakers (batch reactor), magnetic stirrer, magnetic bar and needle. The experimental set-up for the optimisation of experimental parameters influencing UV/TiO_2 photocatalytic process is presented in Figure 3.3. The experimental set-up consists of a magnetic stirrer, magnetic bar, batch reactor, UV lamp, and reactor box. A pure polyvinyl chloride (PVC) box with an interior structure covered with aluminium foil and a cylindrical glass transparent window was used as a batch reactor. In this design, the photocatalyst particles were suspended and immobilised on calcium alginate, and fixed inside the reactor. The solutions were filled up to the desired volume through the top opening of the cylindrical glass and stirred continuously for enough contact time between the photocatalyst surface and the solutions. Aluminum foil inside the interior of a box allowed UV light irradiation of the photocatalyst surface in all directions.

Figure 3.4 shows the experimental set-up of the recycle photocatalytic reactor system. The set-up is composed of an irradiation UV lamps source, UV lamps controller, reactor tube, magnetic stirrer, magnetic bar, reactor box, and circulation tank. The real effluent wastewater and optimum parameters obtained in the batch experiments were used for further studies, which were carried out using recycled photo reactor. A PVC box with inserted UV tubes on a special interior structure and quartz reactor tube was used as the recycle photo reactor. In this design, a quartz cylindrical tube with internal and external diameters of 4 cm and 4.2 cm, respectively, was placed and fixed vertically inside the reactor box with an internal diameter of 18 cm and external diameter of 19 cm. In order to investigate the effect of light intensity, 12 UV tubes of different intensities were placed 4 cm away from the reactor tube along the side of the reactor in all four sides of the photocatalytic reactor box. Two membrane caps (0.5 – 0.9 mm) at the bottom and top of the reactor tube were used to close the system to allow

only solution to circulate. TiO_2 particles immobilised on calcium alginate were suspended on the solution in the inner side of the reactor tube. The UV light lamps were located outside the inner tube, thus uniformly irradiating all surfaces of the tube around the source.

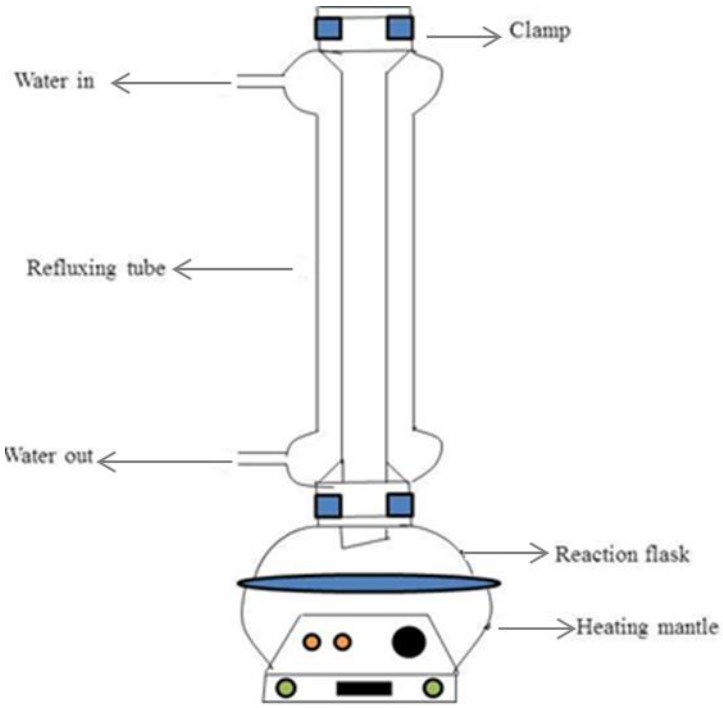

Figure 3.1: Experimental set up for synthesis of the dandelions-like TiO_2.

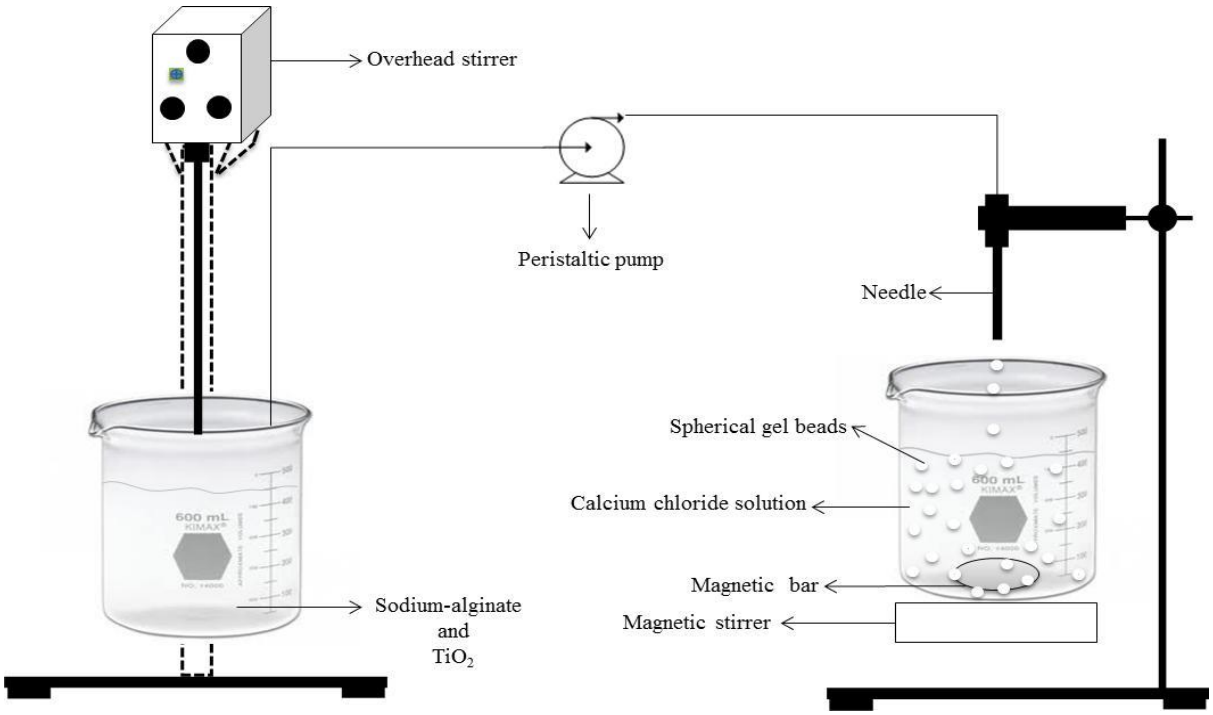

Figure 3.2: Schematic diagram of experimental setup for preparation of Alg/TiO_2.

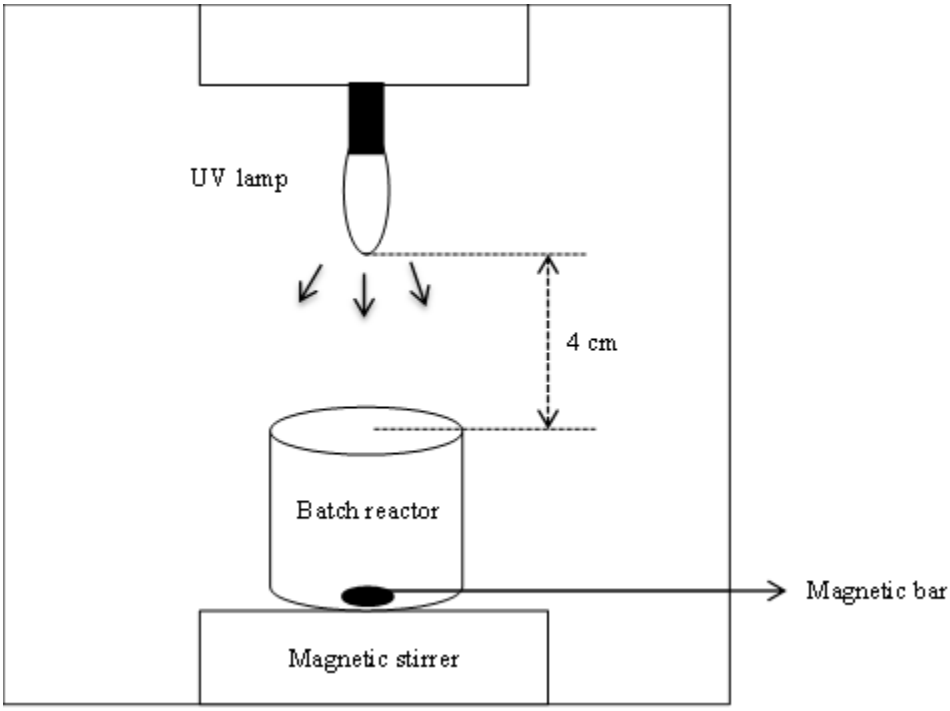

Figure 3.3: Experimental set up of batch photocatalytic reactor system.

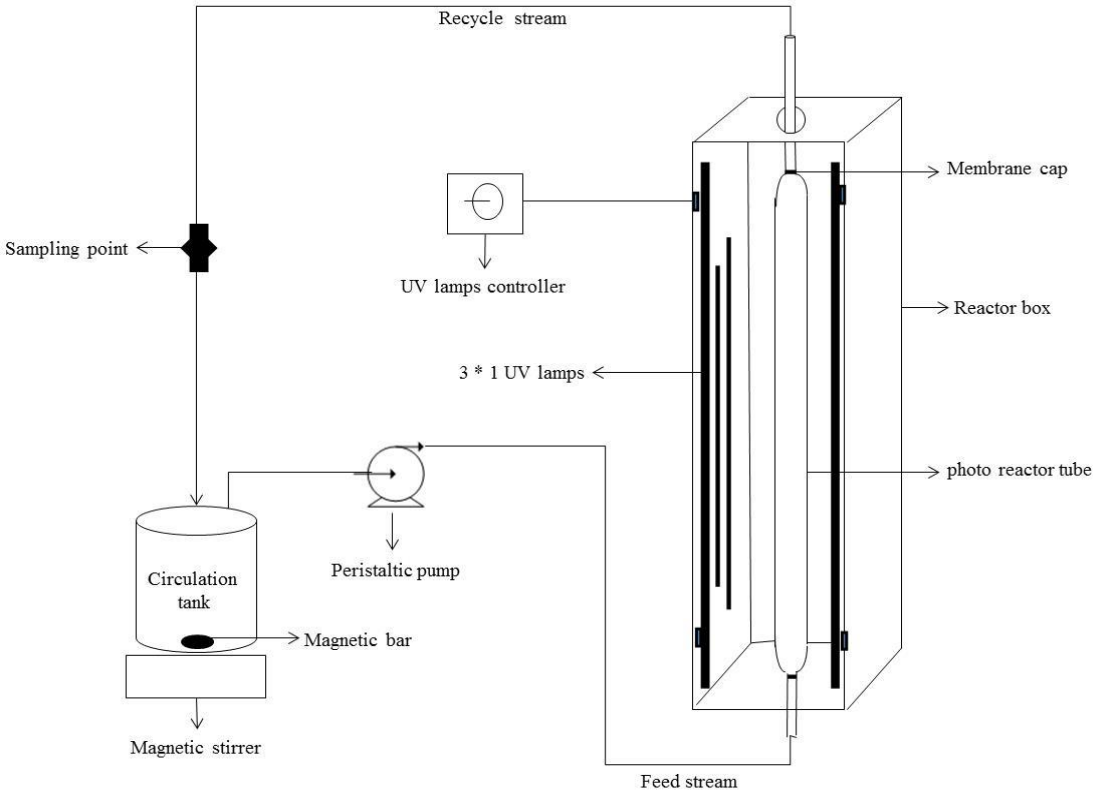

Figure 3.4: Experimental set up of the recycle photocatalytic reactor.

3.4 Experimental procedure

3.4.1 Dandelion-like rutile TiO_2 photocatalyst synthesis

Dandelion-like rutile TiO_2 structures were prepared using the hydrothermal method. Super cooled high purity water (160 mL) at a temperature close to 0°C was added to a 2000 mL reaction flask. The flask was placed on a magnetic stirrer with a 2 cm magnetic stir bar inside. A desired amount (60 mL) of $TiCl_4$ was added to the super cooled high purity water drop wise using separatory funnel while vigorously stirring at 500 rpm. High purity water was super cooled to suppress vigorous reaction. After all the $TiCl_4$ had been dropped into 160 mL of high purity water and the two substances had completely mixed and reacted, the heating mantle was turned on and the temperature was gradually increased to 100^oC, the contents of the flask were then refluxed for the next 24 h, while stirring at 100 rpm. After 24 hours (h), a 5810-R Eppendorf centrifuge centrifuged the suspension obtained at 3000 rpm at

21˚C for a period of 99 minutes (min). The washing of the solids with high purity water was done five times for five minutes per wash in order to remove any chloride ions from the solid TiO_2. The solids were extracted then from the tube into petri-dish and oven-dried using an oven for approximately 16 h overnight at 120˚C. Samples were calcined in air for 120 min using a muffle furnace at different temperatures (200˚C, 350˚C, 450˚C and 550˚C).
The balanced reaction equation for the formation of TiO_2 is as follows:

$$TiCl_4\ (aq) + 2H_2O\ (aq) \leftrightarrow TiO_2(s) + 4HCl\ (g) \qquad (3.1)$$

3.4.2 Au/TiO_2 photocatalyst preparation

Catalysts were prepared by deposition-precipitation method in an automatic laboratory reactor known as Labmx^{TM}. Where 2 mL of 50 g Au/L $HAuCl_4$ solution and 130 mL of high purity water were reacted together, later on 10 g of TiO_2 support was added to the reaction mixture. This was then heated up to 70˚C while stirring. The pH of the reactor contents was maintained at 7 by a solution of 0.5 M Na_2CO_3 and 2 M HNO_3 and aged for 60 min at 70˚C with Au loading target of 1 wt.%. The Labmax^{TM} was used to prepare the reaction solution and maintain control of the following operating variables; pH, temperature, stirring rate, acid and base addition. The liquid to solid ratio of the TiO_2 support material, auric acid solution and high purity water were kept at 10 g, 2 mL and 130 mL respectively. After 60 min, the reactor was stopped and the content was drained through the bottom of the reactor then filtered and washed five times with 360 mL of high purity water, with each washing being stirred at a speed of 150 rpm for 5 min. The catalyst sample obtained was oven-dried at 120˚C for 16 h and stored in a refrigerator to prevent deactivation.

3.4.3 Immobilisation of rutile dandelion-like TiO_2 on biopolymer Ca-Alginate (Alg/TiO_2)

In order to avoid separation problems, which have already been mentioned for slurry applications, TiO_2 nanoparticles were used as immobilised photocatalyst. The rutile dandelion-like TiO_2 was immobilised on calcium alginate ($CaC_{12}H_{14}O_{12}$).

The immobilisation of photocatalyst was carried out according to the procedures described by Harikumar et al. (2013). One-step encapsulation method for immobilisation of nanoparticles in semi permeable alginate beads was used. A solution containing TiO_2 nanoparticles (40 g) and sodium alginate (40 g) was prepared with high purity water, and stirred for 30 min at 23 ± 2^{o}C using overhead stirrer. After thoroughly mixing, the calcium alginate beads were

prepared by dropping the suspension in an aqueous solution of $CaCl_2$ (8 wt. %) with the aid of a peristaltic pump, where spherical gel beads were formed with a size of 1-2 mm. The gel beads were retained in the $CaCl_2$ solution for 12 h for hardening and then washed with high purity water. The excess water in the beads was removed by filtering with filter paper and air-dried at ambient temperature (23 ± 2^oC) for 10 h (Lyn et al., 2010). To prepare alginate blank beads, (beads without TiO_2) similar procedures were employed except that instead of the addition of TiO_2 suspension only sodium alginate was used.

3.4.4 Wastewater sampling and preparation

The wastewater containing Cr(VI), Hg(II) and citric acid were synthesised at Mintek catalysis laboratory. However, for comparison purposes some acid mine drainage effluent was obtained from South African gold and ferrochrome mines. Samples were collected from three different points at a collection site, and at each point, samples were drawn from three different fluid depths. These samples were mixed to produce a representative sample for subsequent use. Thus, effluent water samples were collected from the Witwatersrand goldfields (Western basin) and Mogale alloys ferrochrome mines, in order to investigate the impact and the removal of Cr(VI) and Hg(II) via UV/TiO_2 photocatalysis. Actual Cr(VI) and Hg(II) concentrations in the effluent were not detectable on the AAS using standard methods described by APHA (1995), so the water was spiked with a $K_2Cr_2O_7$ and $HgCl_2$. This was done in order to achieve a total Cr(VI) and Hg(II) desired concentration of 20 and 100 mg/L.

The $K_2Cr_2O_7$ and $HgCl_2$ were used as the sources of Cr(VI) and Hg(II) stock solutions, respectively. All the required solutions were prepared with analytical reagents and high purity water. The Cr(VI) and Hg(II) stock solutions (1000 mg/L) were prepared by dissolving 2.835 g of $K_2Cr_2O_7$ and 1.351 g of $HgCl_2$ in 1L high purity water, while citric acid solution was prepared by dissolving 20, 60, 80, 100 and 120 mg of citric acid in 1 L high purity water (Meichtry et al., 2007). Synthetic samples of different concentrations of Cr(VI) and Hg(II) were prepared from this stock solution by appropriate dilutions of the above stock standard solution (Krishna et al., 2013).

3.4.5 Photocatalysis experiments

In this study Cr(VI) and Hg(II) were chosen as model pollutants, as they are listed as priority and hazardous pollutants (WHO, 2008) which are very harmful to the environment and humans. While citric acid was chosen/acted as the hole scavenger due to its strong chelating

action that forms stable complex with Cr(VI) or Hg(II) and its molecules are complex with various metals, based on the literature review (Chen and Ray 2001; Colon et al., 2001; Bussi et al., 2002; Testa et al., 2004; Shao et al.,. 2009; Yang et al., 2010; Dozzi et al., 2012 & Xu et al., 2013). The effects of the following parameters were studied; initial pH, photocatalyst dosage, contact time, initial concentration, UV irradiation wavelength and light intensity. The photocatalytic activity of the dandelion-like TiO_2 powder was examined by the reduction of Cr(VI) and Hg(II) in aqueous solution under UV irradiation and sunlight. Followed by optimisation of the above-mentioned parameters affecting UV/TiO_2 photocatalysis process of Cr(VI), Hg(II) and citric acid in single and binary systems using immobilised dandelion-like TiO_2 on calcium alginate. Lastly, photocatalytic removal of real acid mine drainage wastewater contaminated by/ spiked with Hg(II) and Cr(VI) in recycle photocatalytic reactor under UV irradiation in presence of immobilised dandelion-like TiO_2 photocatalyst. The catalyst was suspended in the solution and stirred using magnetic stirrer with a stir bar at 650 rpm in the dark for 60 min to attain the adsorption equilibrium of the substrates on the photocatalyst surface prior to the photoreduction experiment under UV irradiation. Stirring was continued during the experimental runs.

3.4.5.1 Photocatalytic activity of the dandelion-like TiO_2 powder experiments

Photocatalytic experiments with UV lights were carried out using a cylindrical glass batch reactor, 6 cm in diameter and 8 cm in working height. Various lamps were tested, including UV-C (HPR 125 W) and UV-LED (80 mW) which were placed inside a box about 4 cm above the cylindrical glass batch reactor (Figure 3.3) containing 250 mL of $K_2Cr_2O_7$ and $HgCl_2$. The UV-C lamp generated 100–280 nm wavelengths, and illumination was carried out with UV light intensities of 171 W/m^2. The UV-LED lamp generated 385 nm wavelengths, and light intensities of 80 mW and solar photoreduction experiments were carried out from 10.30 am to 13.30 pm during summer (October–February) under clear sky. Similar experimental procedures as photocatalytic experiments with UV lights were used except the use of UV lights as light source. At different time intervals during the runs, 5 mL samples of the suspension were withdrawn from the batch reactors and centrifuged employing a 5810-R Eppendorf centrifuge before the absorption spectrum was taken. The absorbance of Cr(VI) and Hg(II) was measured spectrophotometrically at 360 and 478.4 nm, respectively, using UV-vis spectrophotometer by using APHA, standard methods for examination of water and

wastewater (APHA, 1995). The photocatalytic activity was evaluated by analysing the Cr(VI) and Hg(II) reduction after a fixed contact time.

3.4.5.2 Photocatalytic activity of Alg/TiO_2 composite experiments

Experiments were carried out in a batch type photoreactor at room temperature (23 ± 2^{o}C). The pH of solutions was adjusted by 1M HNO_3 or NaOH aqueous solution. Prior to photocatalytic experiments, the UV-C lamp was preheated for 30 min to obtain a constant light intensity. As the reaction progressed, 5 mL samples of solution were withdrawn from the batch reactors at specific time intervals for analysis. The absorbances of Cr(VI), Hg(II) and citric acid were measured spectrophotometrically at 360, 478.4 and 340 nm, respectively, using UV-vis spectrophotometer. Performance of the processes was evaluated by analysing the reduction of Cr(VI), Hg(II) and citric acid. Control experiments were conducted under three different conditions namely: (i) under UV light without Alg/TiO_2; (ii) with blank beads under UV light irradiation and (iii) with Alg/TiO_2 in the dark.

3.4.5.3 Evaluation of recycle photocatalytic reactor system using Alg/TiO_2 composite photocatalyst

The reaction mixture consisted of two phases, which are liquid and solid, where the feed was in a liquid form and catalyst in a solid form. The reactor also consists of three main parts: UV-C lamps, circulating tank and reaction tube (Figure 3.4). The UV sources were high pressure mercury lamp, containing 16 integrally fitted UV tubes (4×4 W, 4×6 W and 4×8 W), with a maximum emission at approximately 280 nm. The intensity of UV light was changed by decreasing or increasing the number of UV lamps. The circulation tank was able to contain a maximum volume of 600 mL solution. The wastewater was recycled through the reactor system, using a peristaltic pump, at 400 mL/min.

In order to investigate the substrate reduction, the photoreduction reaction was conducted under ambient conditions in a lamp-housing box as shown in Figure 3.4. The photo reactor and the UV lamps were enclosed in a black box to ensure safe operation and preventing the entrance of extraneous light. The optimum operating conditions obtained from batch experiments were used to evaluate the performance of recycle photocatalytic reactor.

3.5 Experimental design

A one factor at a time experimental design was used to investigate the optimum operating parameters for the synthesis of dandelion-like TiO_2 and photocatalytic removal of toxic heavy metals and citric acid in a single and binary photocatalytic system.

Table 3.1: Experimental design for synthesis of dandelion-like TiO_2 photocatalyst.

Parameter	Variations
Reaction time (h)	12 - 48
Synthesis temperature (˚C)	80 – 100
TiO_2 preparation quantity (g)	10 - 100
Calcination temperature (˚C)	200 - 550

Table 3.2: Experimental design for photocatalytic reduction of Cr(VI), Hg(II) and citric acid.

Parameter	Variations
Initial pH	2 - 12
Catalyst dosage (g/L)	0.5 - 2.5
Initial Cr(VI) concentration (mg/L)	10 - 50
Initial Hg(II) concentration (mg/L)	20 - 100
Initial citric acid concentration (mg/L)	20 - 120
Citric acid dosage (mg/L)	20 - 80
Light intensity (W)	16 - 32
Calcination temperature (˚C)	200 - 550

3.6 Experimental and data analysis

3.6.1 Catalyst characterisation

Catalyst characterisation is an essential part of all investigations in surface chemistry and a number of characterisation techniques are required to complement each other with information on the surface structure of the catalyst. There are many techniques available for this purpose and the choice depends on the information required. Techniques that have been used in the present work are as follows.

3.6.1.1 Porosity and the Brunauer-Emmett-Teller (BET) surface area analysis

The porosity and surface area of the catalysts were measured by the BET method, using the Micromeritics ASAP 2020 unit, which operates with physical adsorption of a monolayer of nitrogen gas (area = 0.162 nm^2) at –196˚ and at a pressure of about 2 μmHg for porosity measurement. The catalyst, approximately 1 g, was placed in the sample holder and first degassed by passing a mixture of N_2 and He at 90˚C for 30 min. The temperature was then raised at a ramp rate of 10˚C.min^{-1} to 150˚C and held there for 3 while evacuation was carried out until a pressure of less than 10 μmHg was obtained in the sample holder prior to analysing. After degassing, the sample was re-weighed and analysed under liquid nitrogen. Adsorption and desorption of nitrogen was repeated until two consistent values for desorption were obtained. By using the adsorption-desorption isotherm at 77K, surface areas were calculated by the BET method. Pore distribution, pore area and pore volume were obtained by the Barret-Joiner-Halenda (BJH) adsorption curves.

3.6.1.2 X-ray diffraction (XRD)

The powder X-ray diffraction (p-XRD) analysis was conducted on the high resolution Bruker AXS D8 X-ray advanced powder diffractometer. The powder X-ray diffraction was fitted with a LinxEye detector, nickel filter and Co Kα-radiation operated at 40 kV and 35 mA with wavelength alpha as 1.78897 Å. The XRD patterns were recorded with a step size of 0.02˚ in the 2θ range of 20 to 80˚ diffraction angle and using a standard speed with an equivalent counting time of 1 second per step. Samples were run as powders and deposited on the flat-plate glass sample holder (in the hollow space) mounted on an aluminium sample holder. The collected data was used qualitatively and semi-quantitavely to analyse various phases in the samples by comparing with the data base Powder Diffraction Files, an invaluable source of information from the Joint Committee on Powder Diffraction Standards (JCPDS) Swarthmore (USA), published by the International Centre for Diffraction Studies (ICDS).

3.6.1.3 Scanning electron microscopy (SEM)

SEM imaging and analysis was carried out using a FEI Nova NanoSem 200 scanning electron microscope from FEI Company, equipped with the Energy-Dispersive X-ray (EDX) spectrometer and X-ray mapping for the determination of structural composition of the samples. Samples were prepared by hand grinding in agate mortar and coated with carbon

grid. Then the coatings were completely dehydrated and fixed on the sample holder. Subsequently, the samples were sputtered with a thin layer of gold or carbon to avoid the static electricity effect for increasing the image quality.

3.6.1.4 Transmission electron microscopy (TEM)

TEM analysis was conducted using a JEM2100F electron microscope from JEOL, Ltd. fitted with an EDX, wavelength dispersive spectroscopy (WDS) and electron beam back scattered diffraction (EBSD) operating on Oxford Instruments software. The instrument was operated at an accelerating electron beam of 120 kV. The images were photographed using a Proscan CCD camera and image analysis was done using the Soft Image System (SIS) software. Samples were prepared by suspending the powder in methanol and applying the suspension to a carbon coated copper grid. The samples were then allowed to dry at 25ºC (by evaporation) and the grid viewed under the microscope.

3.6.1.5 Energy-dispersive X-ray (EDX)

SEM was coupled with EDX analysis to obtain information about the chemical nature and composition of the samples. This was achieved by bombarding a region in the sample with an electron beam, which leads to the emission of a characteristic scanning electron and subsequently gives information about the spatial distribution and concentration of elements in the sample. The samples were prepared as described in 3.6.1.3.

3.6.2 Synthetic and real wastewater analysis

Analyses of synthetic and real wastewater samples were done using UV-Vis-IR spectrophotometer, Direct Reading Spectrophotometer and atomic absorption spectrometer (AAS), according to standard methods for examination of water and wastewater (APHA 1995). For the UV-Vis-IR spectrophotometer analysis, samples were analysed at 360, 478.4 and 340 nm for removal of Cr(VI), Hg(II) and citric acid respectively. For AAS the samples were prepared by pipetting 1.25, 2.5, 5 and 7.5 mL of the 1 mg/L standard solution into 25 mL volumetric flasks and a blank sample as well. Dextrose (2.5 g) was added to each flask. A sample of 2.5 mL of lanthanum chloride solution was added to each flask to be analysed for calcium and magnesium, while 1.25 mL of cesium chloride solution was added to each flask for aluminium analysis. The total concentration of heavy metals were analysed on a 210VGP

AAS. Sulphate concentration was determined using the (HACH DR/2000) Direct Reading Spectrophotometer at 450 nm.

The calculations that were used to determine the amount of toxic heavy metals adsorbed per unit mass of the adsorbent and removal of the samples are similar to those used by Assadi *et al*. (2012) and Karthika and Sekar, (2013). The removal percentage (Ø) and adsorption capacity values at equilibrium q_e (mg/g) were calculated using the following equations:

$$Ø = \frac{(C_o - C_e)}{C_o} \times 100 \quad (3.2)$$

$$q_e = \frac{(C_o - C_e)V}{W} \quad (3.3)$$

where C_o is the initial concentration and Ce is the equilibrium concentration, mg/L, V (mL) is the volume of the solution and W (g) is the weight of the adsorbent.

3.6.3 Error analysis

All the experiments were performed at least three times to ascertain reproducibility and average values were determined. The results presented in Chapter 4 showed a standard deviation of about 5% total analytical error.

3.7 Reaction kinetics

The data necessary for fitting the kinetic model were obtained in the photoreduction batch experiments as described earlier. Many researchers (Chen et al., 1999 & Guettai et al., 2005) have observed that the reduction rates of photocatalytic reduction and degradation of various metal ions and organic compounds over irradiated TiO_2 follows the Langmuir – Hinshelwood (L-H) kinetics model. The Langmuir–Hinshelwood kinetic relates the rate of surface catalysed reactions to the surface covered by the substrate, being the kinetic equation expressed as

$$r = \frac{-d[C]}{dt} = \frac{K_{ads} \,.k_{\mathrm{H-L}}.C}{1+ K_{ads}\,.\ C}, \quad (3.4)$$

where r is the reduction rate, C is the reactant concentration, t is the time, $k_{\text{H-L}}$ is the rate constant, and K_{ad} is the adsorption equilibrium constant.

This model assumes that, if the adsorption of Cr(VI), Hg(II) and citric acid onto the surface of the photocatalysts is very low, $K_{\text{ads}} \cdot C$ can be neglected in the denominator simplifying the equation to a pseudo-first-order equation as given by (Song et al., 2013).

$$r = \frac{-d[C]}{dt} = K_{ads} \,.k_{H-L}.C = k.C \qquad (3.5)$$

The reduction rate for the reduction of Cr(VI) and Hg(II) for the pseudo first order reaction was calculated in terms of mg. $L^{-1} \cdot min^{-1}$.

The integration of Eq. (3.5) with boundary conditions of $C = C_o$ at $t = 0$ is represented by

$$\ln\left(\frac{C_0}{C}\right) = k_{app}.t \qquad (3.6)$$

where C_0 is the initial pollutant concentration and k_{app} is the apparent pseudo-first-order reaction rate constant.

3.8 Adsorption isotherms

Adsorption isotherm models are used to describe experimental adsorption data. The data necessary for fitting the adsorption isotherms were obtained in the adsorption batch experiments as described earlier. Langmuir and Freundlich equations are commonly used for describing adsorption equilibrium for water and wastewater treatment applications. In this study, the isotherm data was analysed using the Langmuir and Freundlich equations.

The Langmuir model (Langmuir, 1918) could be described as:

$$q_e = \frac{q_m k_L C_e}{1 + k_L C_e} \qquad (3.7)$$

The linear transformation of Eq. (4.6) can be expressed by the following Langmuir equation:

$$\frac{C_e}{q_e} = \frac{1}{q_m k_L} + \frac{C_e}{q_m} \quad (3.8)$$

where C_e (mg/L) is the equilibrium concentration of Cr(VI) or Hg(II); q_e (mg/g) and q_m (mg/g) are the equilibrium adsorption amount of Cr(VI) or Hg(II) and the saturated monolayer adsorption capacity of Cr(VI) or Hg(II) on dandelion like-TiO_2, respectively; k_L (L/mg) is an adsorption equilibrium constant depending on the affinity of binding sites. Values of q_m and k_L are determined from plots of C_e/q_e against C_e.

The essential characteristics of the Langmuir isotherm can be expressed in terms of a dimensionless constant separation factor or equilibrium parameter, R_L, which perfectly determines the favourability and shape of the isotherm of the adsorption process by applying Eq. (3.9);

$$R_L = \frac{1}{1 + K_L C_o} \quad (3.9)$$

where K_L is the Langmuir constant and C_o is the initial concentration (mg/L). The R_L value indicates the shape of the isotherm as follows: R_L>1, unfavorable adsorption; R_L=1, linear adsorption; 0<R_L<1, favorable adsorption; R_L= 0, irreversible adsorption (Ngah *et al*. 2002).

The Freundlich model (Freundlich, 1906) is an empirical equation and is based on multi-molecular layer adsorption on an energy heterogeneous adsorbent surface suggesting that binding sites are not equivalent. The experimental data on adsorption of Cr(VI) and Hg(II) were fitted to Freundlich adsorption isotherm, which is known to be the earliest relationship describing the adsorption equilibrium and is expressed as:

$$q_e = k_F C_e^{1/n} \quad (3.10)$$

The linear form is of Eq. (3.10) is expressed as:

$$\log q_e = \frac{1}{n} \log C_e + \log k_F \quad (3.11)$$

where C_e is the equilibrium concentration (mg/L), q_e is the amount adsorbed (mg/g) and k_F and n are the Freundlich constants related to adsorption capacity and intensity of adsorption, respectively. k_F and n were calculated from the slope and the intercept of the line of the Freundlich plots, respectively.

CHAPTER 4: RESULTS AND DISCUSSION

Chapter 4 covers results that were obtained after characterisation of the synthesised dandelion-like TiO_2 nanostructures, modified dandelion-like TiO_2 nanostructures and as well as the Cr(VI), Hg(II) and citric acid photocatalytic experiments. Section 4.1 outlines synthesis, characterisation and photocatalytic activity results before immobilisation of dandelion-like TiO_2 on calcium alginate (Alg/TiO_2). While Section 4.2 covers characterisation results of the Alg/TiO_2 as well as photocatalytic treatment of Cr(VI) and Hg(II) along with citric acid. Finally, results for the characterisation of real wastewater and phoreduction of Cr(VI) and Hg(II) in real wastewater systems are discussed.

4.1 Synthesis, characterisation and photocatalytic activity of a pure rutile dandelion-like TiO_2

As reported in the literature review that in various morphologies, the hierarchical 3D nanostructures have been regarded as the more attention-grabbing structures due to their dimensions and the greater number of active sites than that of 2D or 1D nanostructures. This makes it promising for potential applications in photocatalysis. In this section the results obtained in an attempt to synthesise 3D dandelions-like TiO_2 are discussed. The results for discussion purposes are subdivided into four parts, viz. optimisation of the experimental conditions for synthesis of the catalyst, discussion of the growth mechanism, characterisation of the catalyst and finally photocatalytic activity of the catalyst. The relationship between morphology, reaction time, synthesis temperature, calcination temperature and increasing preparation quantity of dandelions-like TiO_2 nanostructures was investigated using the SEM images.

4.1.1 Optimisation of the experimental conditions for synthesis of dandelion-like TiO_2

4.1.1.1 Reaction time

The SEM image presented in Figure 4.1(a) represents the initial growth stage of the dandelion-like structures at hydrothermal reaction time of 12 h. In this stage, many immature aggregated solid TiO_2 structures and irregular spheres were observed. Prolonging the reaction time to 24 h (Figure 4.1(b)), resulted in the denser nanostructure without irregular spheres. Figure 4.1(c) shows a collapsed dandelion-like TiO_2 structure, as the individual dandelions-like TiO_2 recombined to form undesirable sheet-like rutile TiO_2. It can be concluded that prolonging the reaction time makes the particles grow and agglomerate. Zhang et al. (2002)

observed the agglomeration of shuttle-like particles forming petal-like bundles of particles, with prolonged reaction time. Based on the results and analysis a complete morphology evolution process of the 3D TiO_2 nanostructures was proposed as follows: (i) nucleation and nanoparticle formation; (ii) formation of spheres through self-assembly growth; (iii) further growth and (iv) agglomeration of the dandelions to form sheet-like rutile TiO_2, with time being the most important controlling factor.

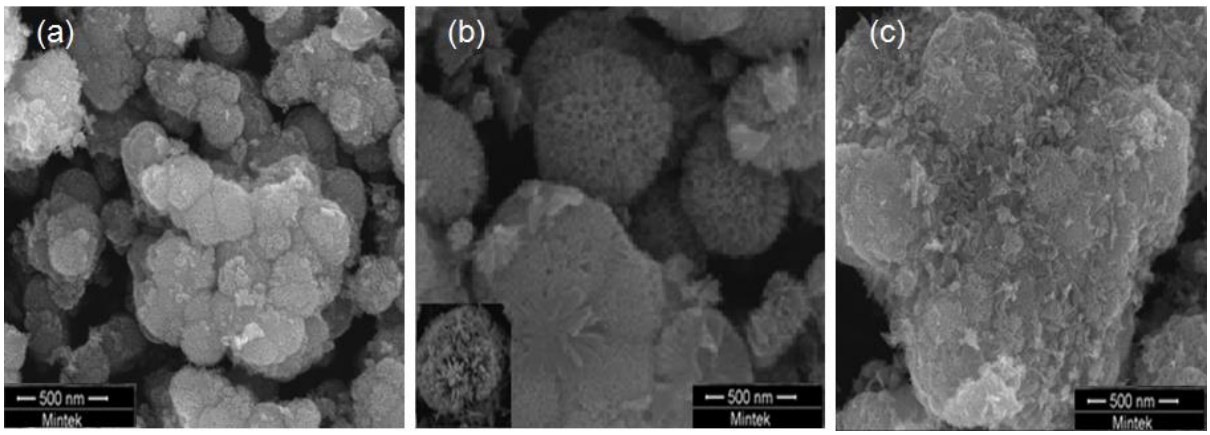

Figure 4.1: SEM images of TiO_2 samples selected at different intervals (a) 12 h; (b) 24 h; (c) 48 h.

4.1.1.2 Synthesis temperature

In the present study, it was found that the reaction temperature plays an important role in the nucleation and growth of TiO_2 crystallites, which determine the final dandelions morphology of the products. Figure 4.2 illustrates the images of TiO_2 nanocrystals prepared at various reaction temperatures. At 80˚C reaction temperature (Figure 4.2(a)), loosely packed nanorods formed the dandelion-like TiO_2 and TiO_2 dandelions or strands grow slowly and freely from the nucleus in all directions. When the reaction temperature was raised to 100˚C (Figure 4.2(b)), compact dandelions were obtained with rods originating from the centre. At a high temperature (190˚C), the dandelion-like TiO_2 structures were destroyed, resulting in sectors composed of nanorods and sheet-like TiO_2 structures (Figure 4.2(c)).

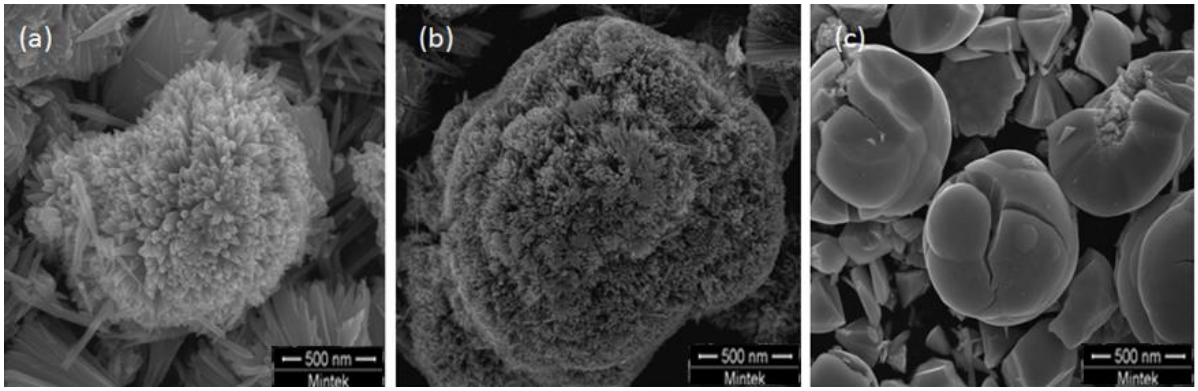

Figure 4.2: SEM images of the rutile TiO_2 synthesised for 24 h and hydrothermal treated at various temperatures; (a) 80˚C; (b) 100˚C; (c) 190˚C.

4.1.1.3 Calcinations temperature

When the as-prepared dandelion-like TiO_2 structures were calcined at 200˚C, the collapsed nanostructures were observed as in Figure 4.3(a). When the calcination temperature was increased further from 350˚C to 550˚C, there was no significant change in the morphology of the products. These results indicate that these materials are not stable at high temperatures.

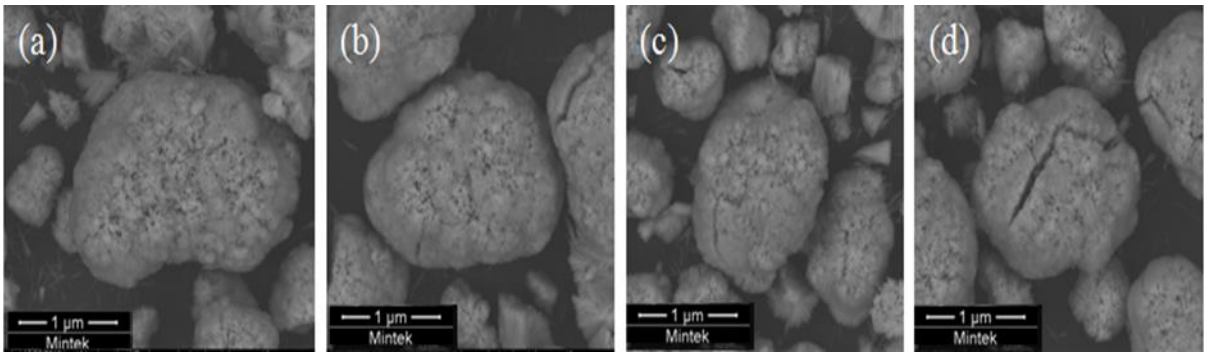

Figure 4.3(a): SEM images of the calcined dandelion-like TiO_2 synthesised for 24 h and hydrothermally treated at 100˚C; dandelions-like TiO_2 calcined at; (a) 200˚C; (b) 350˚C and (c) 450˚C.

4.1.1.4 Increasing the TiO_2 quantity

In Figures 4.4(a), 4.4(b) and 4.4(c), the overall morphology indicates the existence of many uniform, dandelion-like TiO_2 nanostructures. These results suggest that increasing the dandelion-like TiO_2 preparation quantity has no significant change on the structural and chemical characteristics of the materials. Furthermore, this is in agreement with the results

obtained from the XRD data obtained in Figure 4.7. Therefore, it is of great scientific and industrial importance to note that the dandelion-like TiO_2 nanostructures can be reproduced and scaled-up, while keeping its morphology under effective control.

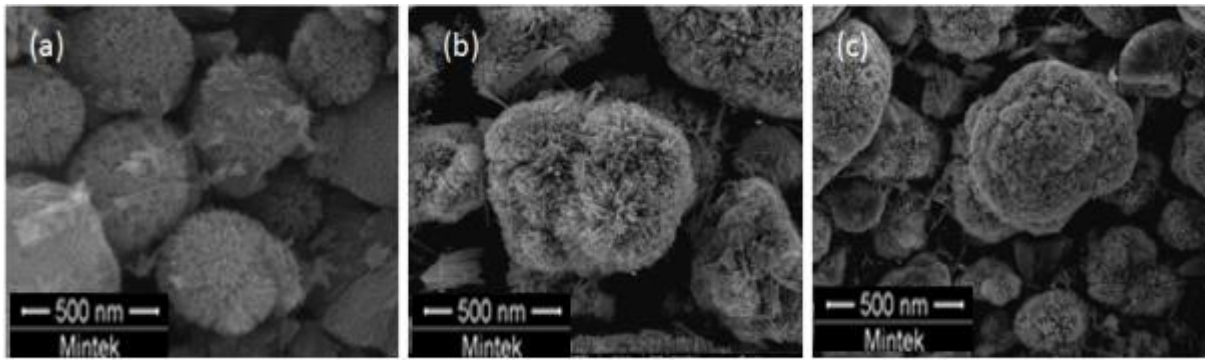

Figure 4.4: SEM images of the rutile TiO_2 synthesised for 24 h and hydrothermally treated at 100˚C; individual dandelion-like TiO_2 nanospheres of different quantities, namely ; (a) 10 g; (b) 50 g and (c) 100 g.

4.1.2 Possible formation mechanism of dandelion-like TiO_2 nanostructures

To understand the growth mechanism of dandelion-like TiO_2 nanostructures, the morphology evolution was investigated from the SEM images collected at different growth stages presented in Figure 4.1(a–c). Based on the obtained results, it is concluded that the morphology of dandelion-like TiO_2 can be controlled by using the reaction time and temperature. The effect of reaction time on the growth mechanism was studied in order to understand the formation mechanism of TiO_2 nanostructures. The mechanism adopted for the purpose of this work was similar to the one used by Ani et al. (2005), where a TiO_2 was produced by vapour phase hydrolysis of $TiCl_4$ at low temperatures. Low temperatures close to the boiling point of the precursor, in this case H_2O and $TiCl_4$. In this study, the reaction was carried out in a liquid phase at 100˚C - a temperature close to the boiling point of the precursors, and in this case, the boiling points are 136.4˚C and 100˚C for $TiCl_4$ and H_2O, respectively. From the results, a possible mechanism for the creation of TiO_2 nanosphere is illustrated in Figure 4.5. As can be seen in Figure 4.5, if there is no lattice match between the TiO_2 and the substrate, the TiO_2 is firstly nucleated as islands (i) and then nanowires grow (ii) from these islands to form dandelion-like (iii) morphologies.

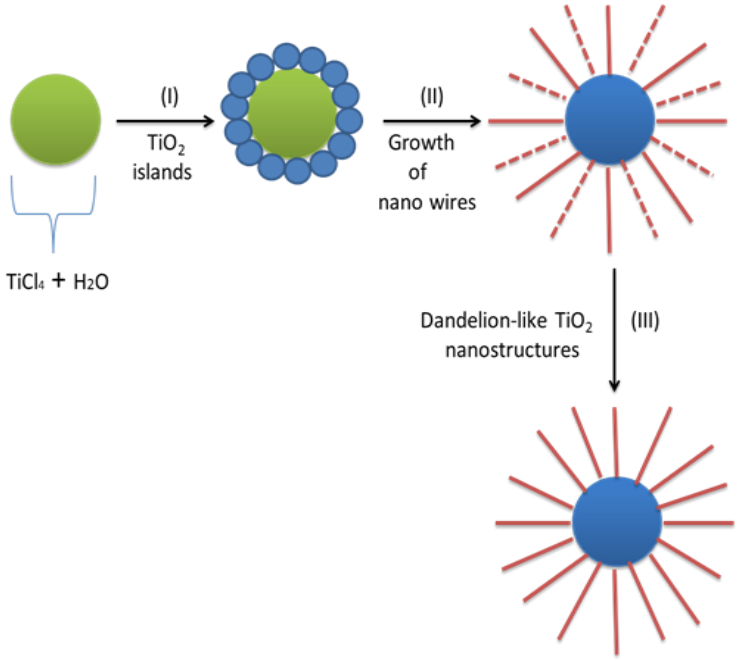

Figure 4.5: Schematic illustration of a possible growth mechanism for the dandelion-like TiO_2 nanocrystals.

In the hydrolysis method, the precursor molecules are fully hydrolysed (or undergo alcoholysis) and can then be precipitated to form nanoparticles in the water (or alcohol) solution under certain conditions. The precursors usually employed are $TiCl_4$, $TiSO_4$, and TiOR (R = alky/group). Li and Haneda. (2003); Liu et al. (2006) & Jia et al. (2006) have used the hydrolysis of $TiCl_4$ in HCl solution to synthesise rutile TiO_2 hierarchical structures with different morphologies. The average size of the flower-like TiO_2 nanorod nanostructures formed was 300 nm in diameter. In this work, $TiCl_4$ was hydrolysed in water at different experimental temperatures. The hydrolysis of $TiCl_4$ proceeds with the following steps (Jiang et al., 2012):

$$TiCl_4 + H_2O \rightarrow TiOH^{3+}_{(aq)} + H^+ + 4Cl^- \quad (4.1)$$

$$TiOH^{3+}_{\mathbf{(aq)}} \rightarrow TiO^{2+}_{(aq)} + H^+_{(aq)} \quad (4.2)$$

$$TiO^{2+} + H_2O \rightarrow TiO_{2(s)} + 2H^+ \quad (4.3)$$

At a certain high temperature (100ºC), the $TiCl_4$ began to hydrolyse and the product dispersed better. This can be attributed to the inhibition of the hydrolysis of $TiCl_4$ due to the acidity of

the aqueous solution. The solubility of TiO_2 in the HCl solution keeps a dynamic equilibrium between the immature aggregated solid TiO_2 structure and the concentration of titanium cations in the solution (Hosono et al., 2004). As a result of the mass transfer aided by the solution, the immature TiO_2 structures with high surface energies disappear while the stable mature dandelions grow. Furthermore, considering the equilibrium phenomenon of the reactions ((4.1) and (4.2)), the Cl^- ions and H^+ ions both suppress the hydrolysis reaction due to the common ion effect.

4.1.3 Characterisation of the pure rutile 3D dandelion-like TiO_2 photocatalysts

The traditional TiO_2 nanometer-scale powder has been reported by Jing *et al*. (2013) to suffer from severe agglomeration, while 3D TiO_2 nanostructures are less likely to aggregate and easier to be separated from the solution as photocatalyst. Hence, the 3D nanostructures were synthesised in this work and the results obtained using different characterisation techniques in the present work are described as follows:

4.1.3.1 Brunauer–Emmett–Teller (BET) measurement

Table 4.1 shows the properties of synthesised TiO_2 and commercially available Degussa P25. The samples calcined for 2 h in air showed a decrease in surface area as the calcinations temperature increased. In contrast to the effect on surface area, the pore size showed an increase with calcinations temperature. A mesopore range of 3.2-27 nm, as indicated in Table 4.1, was obtained. There is little information reported in the literature on the BET surface area of the dandelion-like TiO_2 structure. Jin et al. (2012) synthesised dandelion-like rutile TiO_2 microspheres using rutile hollow SnO_2 spheres as a template. They obtained the dandelion-like rutile TiO_2, which contained pores of about 4 nm, and the BET surface area was 46 $m^2.g^{-1}$. Zhou et al. (2013) synthesised dandelion-like rutile TiO_2 via a one-step solvothermal approach using titanium *n*-butoxide in a mixture of HCl and *n*-hexane, they obtained dandelion-like rutile TiO_2 with the BET surface area of 40 $m^2.g^{-1}$. As shown in Table 4.1, the prepared dandelion-like rutile kept a high surface area of 81 $m^2.g^{-1}$ with pores of about 3.2 nm, indicating the importance of this result as a positive scientific and technological contribution.

Table 4.1: Calcinations temperature, BET specific surface area, pore volume, crystalline structure, pore diameter for the samples treated hydrothermally at 100 ˚C for 24 h.

TiO_2	T (˚C)	S_{BET} (m^2g^{-1})	PV (cm^3/g)	C (anatase/rutile)	PD (nm)	References
Dandelion	0	81	0.071	(0/100)	3.2	[present]
Dandelion	200	24	0.029	(0/100)	6	[present]
Dandelion	350	7	0.022	(0/100)	13	[present]
Dandelion	450	6	0.027	(0/100)	21	[present]
Dandelion	550	5	0.029	(0/100)	27	[present]
Dandelion	0	46	-	(0/100)	4	[22]
Dandelion	0	40	-	(0/100)	4	[24]
Degussa P25	0	49	-	(80/20)	-	[present]

T, S_{BET}, PV, C, PD represent calcinations temperature, BET surface area, pore volume, crystalline structure, pore diameter, respectively.

The results supported the fact that an increase in calcination temperature results in a decrease in the catalyst surface area. Raj et al. (2004) also observed a decrease in surface area and pore volume with an increase in calcinations temperature. However, their studies were done on P25 titania samples calcined in air for 120 min. In this study, the surface area collapsed to 5 m^2/g upon calcinations at 550˚C and the pore diameter increased from 3.2 to 27 nm with increasing calcinations temperature from 200˚C to 550˚C. The results suggested that high temperature calcinations decreased the pore volume and BET surface area.

The nitrogen adsorption–desorption isotherms and Barret-Joyner-Halenda (BJH) pore size distributions derived from the desorption branch of the adsorption isotherms of the prepared and calcined dandelion-like TiO_2 samples are shown in Figure 4.6. As shown in Figure 4.6, all samples were categorised as isotherms of type IV, which is typical of mesoporous materials according to the International Union of Pure and Applied Chemistry (IUPAC) classification (Sing et al., 1985). The hysteresis loops of various samples are qualitatively different. The hysteresis loop of as-prepared and dandelion-like TiO_2 calcined at 350˚C and 450˚C fit well to type H2, which is characteristic for mesoporous materials with ink-bottle pores. However, well-defined type H3 hysteresis loops were obtained for TiO_2 calcined at 200˚C, implying the formation of slit-like pores that are associated with aggregates of nanorods (Sing et al., 1985). The result obtained is in agreement with the TEM and SEM

results. Samples containing more nanorods exhibited a hysteresis loop of type H3, whereas more nanoparticles lead to the H2-type hysteresis loop.

The pore size distribution plot calculated using the BJH equation from the adsorption branch of the isotherm is shown in Figure 4.6 (insets). The materials exhibited a narrow pore size distribution suggesting good homogeneity of the pores. It is clear that as-prepared dandelion-like TiO_2 has a higher surface area and larger pores than calcined dandelion-like TiO_2.

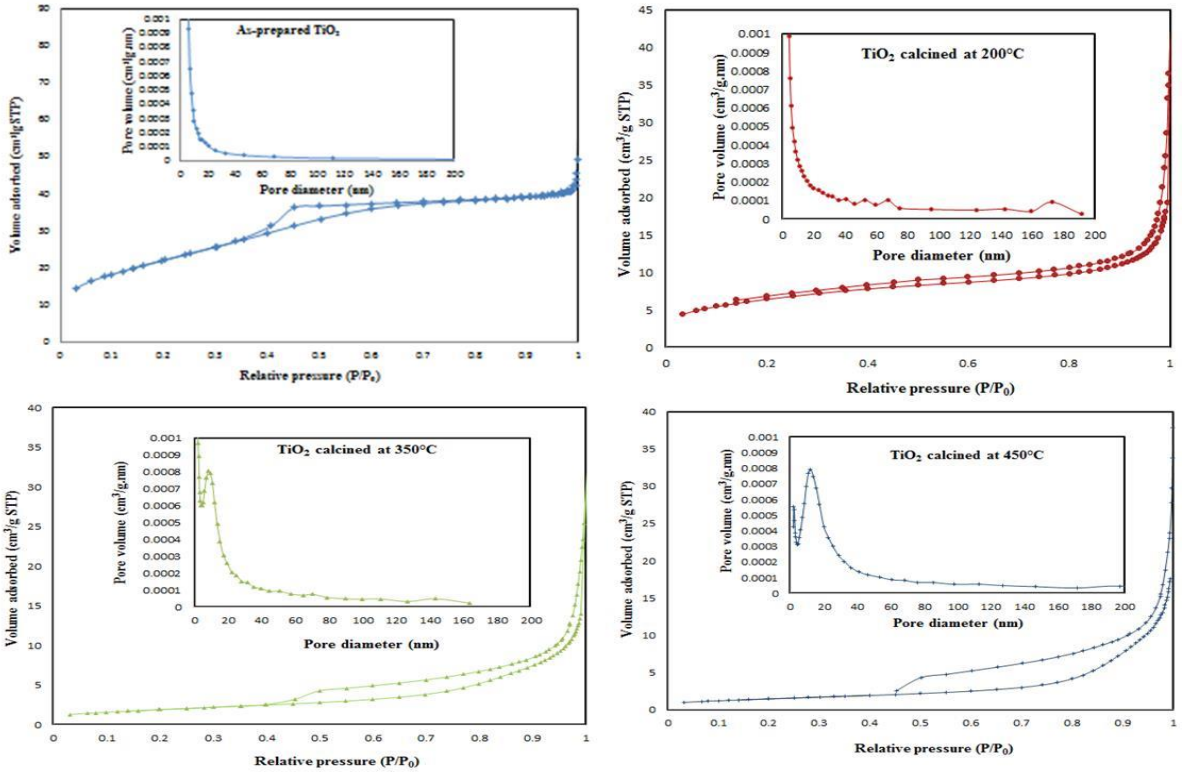

Figure 4.6: Nitrogen adsorption-desorption isotherms and BJH pore size distributions (inset) plots for as-prepared dandelion-like TiO_2 and calcined dandelion-like TiO_2 in air at different temperatures.

4.1.3.2 X-ray diffraction (XRD)

Figure 4.7 shows XRD diffraction peaks for the different quantities of rutile dandelion-like TiO_2 hydrothermally treated at 100˚C for 24 h and gold nanoparticles loaded on dandelion-like TiO_2 (Au/TiO_2). As shown in Figure 4.7A, all diffraction peaks in the XRD pattern of the nanosphere can be indexed to a pure rutile TiO_2 crystal structure (JCPDS No. 21-1276). No peaks of anatase or brookite phase are detected, indicating the high purity of the prepared samples. The Bragg diffraction peaks at 2Θ = 32˚, 42.2˚, 48.2˚ and 64˚ are the main peaks

observed in the diffraction analysis. It is well accepted that the broadening of the diffraction peaks reflects a decrease in the particle size and the intensity of the diffraction peaks reflects the crystallisation of the samples (Jin et al., 2012). The results suggest that increasing the dandelions quantity has no significant change on the crystalline phase, as the Bragg diffraction peaks and the rutile phase remained the same with an increase in the dandelions quantity.

As confirmed by XRD pattern in Figure 4.7B, the prepared catalyst is also identified with a pure rutile phase, with the same Bragg diffraction peaks as Figure 4.7A. From the XRD results, no crystalline phase attributable to gold was observed. This indicates that either the Au content is below the detection limit or the gold is highly dispersed in the dandelions-like TiO_2 network.

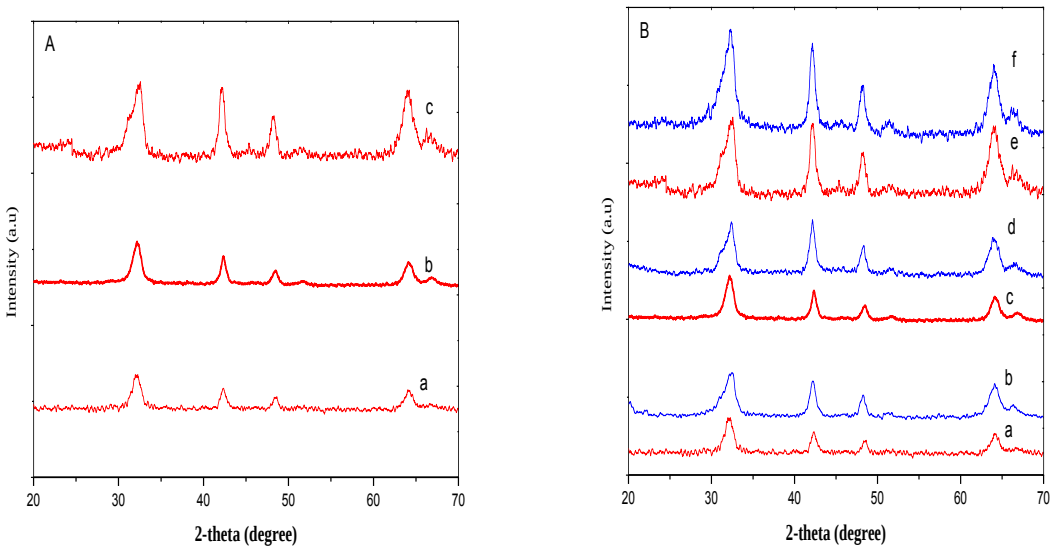

Figure 4.7: XRD diffractograms for the different quantities (a. 10 g; b. 50 g; c. 100 g) of the rutile dandelion-like TiO_2 (A) hydrothermal treated at 100˚C for 24 h and (a & b. 10 g; c & d. 50 g and e & f. 100g) of dandelion-like TiO_2 and gold nanoparticles deposited on dandelions-like TiO_2 (B).

4.1.3.3 Scanning electron microscopy (SEM)

Figures 4.8(a), 4.8(b) and 4.8(c) show the SEM images of the rutile TiO_2 synthesised for 24 h and hydrothermal treated at 100˚C. Enlarged individual 3D TiO_2 nanospheres with numerous densely packed TiO_2 nanostructures can be observed in Figure 4.8(a) and Figure 4.8(b). As it

can be seen in Figure 4.8(c), a close inspection of the top surface reveals that the sphere was composed of many loosely packed nanometer-scale crystals. Similar results were obtain by Bai *et al*. (2008), where they synthesised the dandelion-like TiO_2 structure by facile hydrothermal method using $TiCl_3$ and NaCl as the main starting materials.

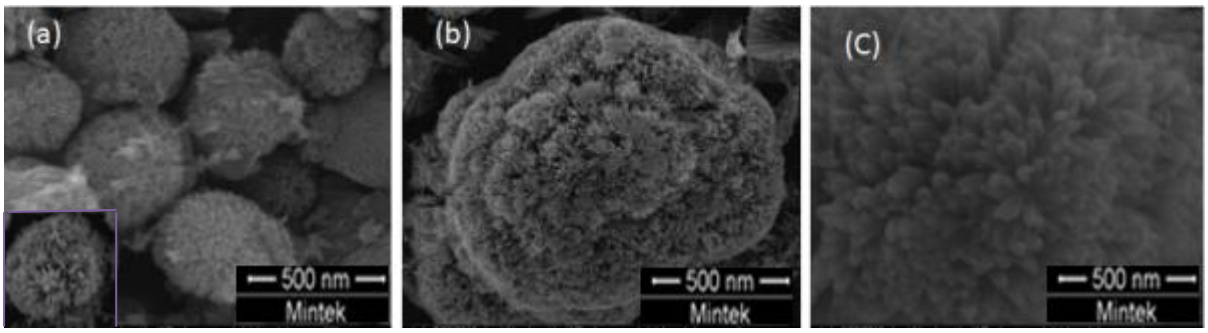

Figure 4.8(a): SEM images of the rutile TiO_2 synthesised for 24 h and hydrothermally treated at 100˚C; Inset: an enlarged individual dandelion-like TiO_2 sphere; (b) typical well-crystallised dandelion-like TiO_2 microsphere; (c) top-image of a dandelion.

4.1.3.4 Transmission electron microscopy (TEM)

Figures 4.9(a) and 4.9(b) show the TEM images of a typical well-crystallised and half dandelion-like rutile TiO_2, respectively. The TEM images show that each dandelion-like nanostructure is composed of ordered nanorods with an average diameter of 17 nm. A similar nanorods-structured TiO_2 surface has been observed by Jin et al. (2012), who synthesised dandelion-like microspheres as anode materials for lithium ion batteries with enhanced rate capacity and cycling performances. The full rutile-dandelions were formed as shown in Figure 4.9(a) and 4.9(b). This was also supported by the XRD patterns of the dandelion-like TiO_2, which is identified as pure rutile phase as shown in Figure 4.9. The resulting product contains nano rutile dandelions shaped structure, which indeed is the focus of this study. The morphology indicates the existence of many uniform, dandelion-like TiO_2 nanostructures.

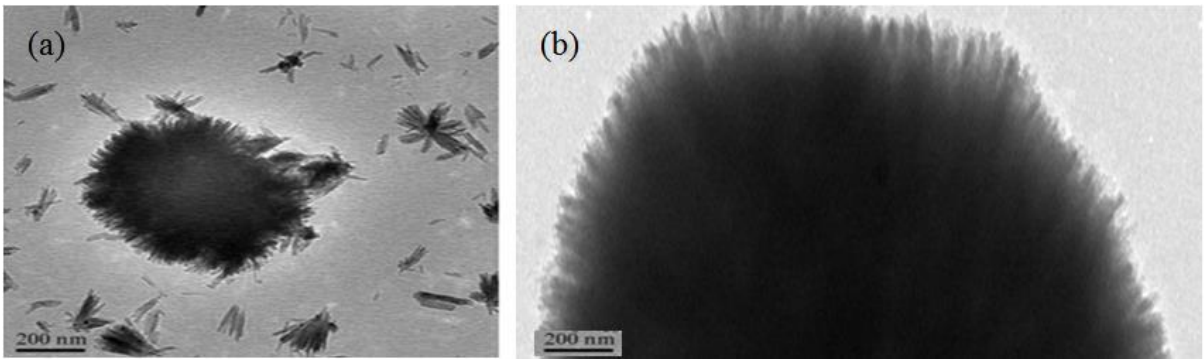

Figure 4.9: TEM images of the dandelion-like rutile TiO_2 synthesised for 24 h and hydrothermal treated at 100˚C: (a) typical well-crystallised dandelion-like TiO_2 nanosphere; (b) dandelion-like TiO_2 half nanosphere.

4.1.3.5 Energy-dispersive X-ray spectrometer (EDX)

EDX analyses (Figure 4.10(a)) showed that the rutile dandelion-like TiO_2 nanostructures were chemically composed of Ti, C and O elements. Since C grids are used for the study, observed C is due to the grid. Figure 4.10(b) shows that dandelion-like TiO_2 supported gold catalyst were chemically composed of Ti, C, O and Au elements, with C emanating from a carbon tape used to fix the sample-to-sample stud. The intended Au loading during the catalyst preparation was 1 wt%, however, 1.18 wt% was achieved as the data obtained from EDX.

From the elemental weight percentage analysis (inset tables) in Figure 4.10(a) and 4.10(b), it can be observed that there is a dominant quantity of Ti and the weight presence of O and Au in respective stoichiometric ratios.

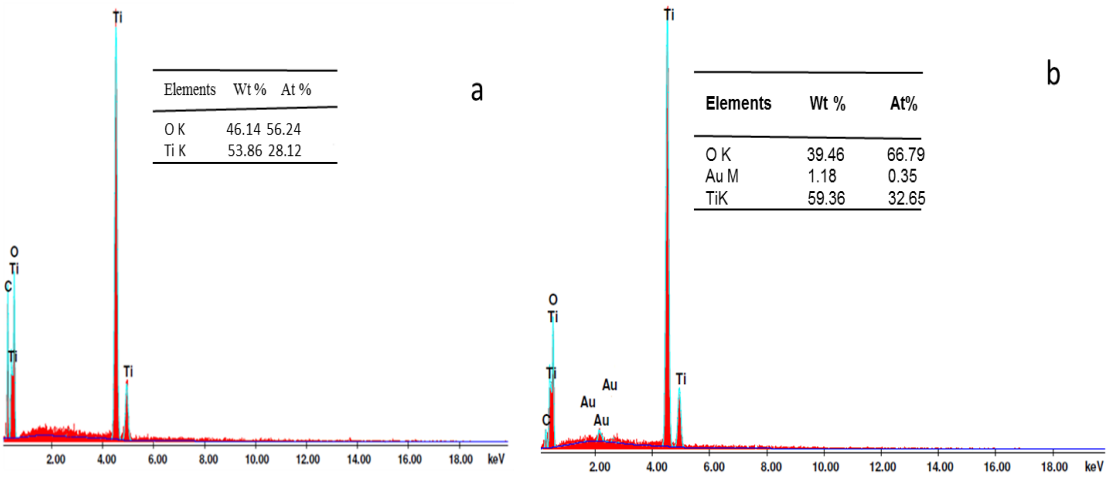

Figure 4.10: EDX spectrum of the pure rutile dandelion-like TiO_2 synthesised for 24 h and hydrothermally treated at 100˚C (a) and Au/TiO_2 (b). Inset is the composition tables.

4.1.4 Photocatalytic activity of 3D dandelion-like TiO_2 for reduction of Cr(VI) and Hg(II) in aqueous solution

4.1.4.1 Kinetic modelling and optimisation for Cr(VI) and Hg(II) photocatalytic reduction

A series of experiments was carried out to study the reduction behaviour of Cr(VI) and Hg(II) on dandelion-like TiO_2 nanostructures in different solution pH levels, initial concentrations and dandelion-like TiO_2 dosages and the results are shown in Figures 4.11 – 4.12 − it should be noted that the results shown are obtained after it was ascertained that an adsorption equilibrium had been reached and the lamp was turned on. For each experiment, the reduction rate constant for Cr(VI) and Hg(II) was calculated from the linear regression of a plot of the natural logarithm of the compound concentration as a function of irradiation time, that is, pseudo first-order kinetics equation using Eqs. 3.5 – 3.6.

a. Effect of the pH on the photocatalytic reduction of Cr(VI)

A series of experiments were conducted at different pH values ranging from 2 to 12, containing 20 mg/L Cr(VI) and 2 g/L of catalyst in order to investigate the influence of initial pH on the photocatalytic reactions of Cr(VI). The influence of initial pH on the Cr(VI) photoreduction was studied and the results are presented in Figure 4.11. It can be seen from the figure that efficient photoreduction is reached in the solution at pH of 2, and the photoreduction drastically decreases with the increasing pH up to 12. The reduction rate increase with decreasing pH of the Cr(VI) solution from 12 to 2. This can be attributed to the

neutralisation of the anionic sites and negative potential of the TiO_2 surface at lower pH. Furthermore, such a tendency can be explained based on the speciation of Cr(VI) as a function of pH alteration. Cr(VI) occurs in oxy anions as $HCrO_4^-$, $Cr_2O_7^{2-}$ and CrO_2^{4-} depending on the pH. In acidic medium (pH > 1), $HCrO_4^-$ predominates and converts to CrO_2^{4-} with increasing solution pH, owing to the acidity constant (pKa = 6.49 at 25ºC). At pH 2 to 4, Cr(VI) ion in the solution exists as $HCrO_4^-$ and $Cr_2O_7^{2-}$ (Nomanbhay et al., 2005), which act as strong oxidising agents, therefore, they are easily reduced.

At higher pH, that is about 6 to 12, the fraction of $HCrO_4^-$ and $Cr_2O_7^{2-}$ decreases gradually, but the fraction of CrO_4^{2-} species, which is a weaker oxidising agent, increases. Moreover, Cr(III) in the solution resulting from Cr(VI) photoreduction may precipitate as $Cr(OH)_3$ (Wang et al., 2004). This could scatter the entering light leading to the low photoreduction rate. The trend is consistent with that reported by Prairie et al. (1993). Since the best pH for the removal of Cr(VI) from aqueous solution by the dandelion-like TiO_2 was found to be 2, this indicates that the precipitation of ions to metal hydroxide was avoided throughout this study.

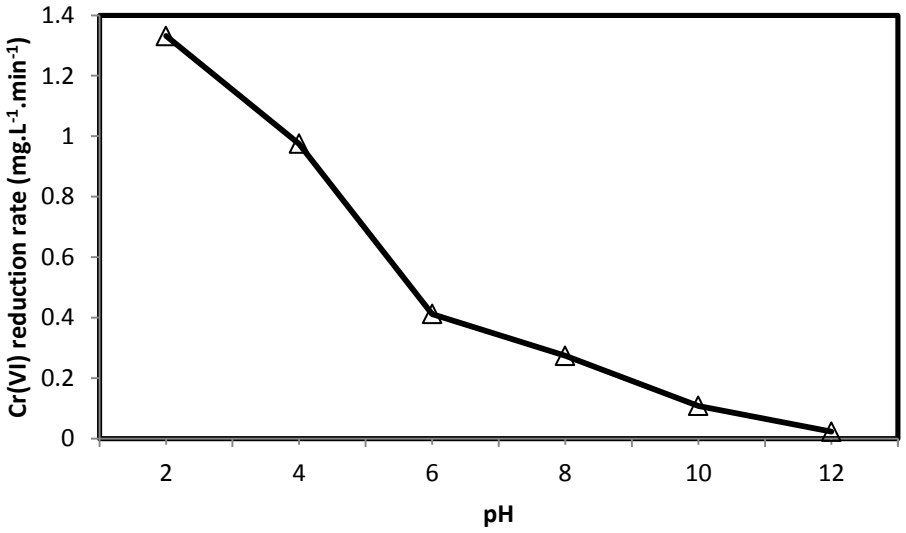

Figure 4.11: Influence of initial pH on the photocatalytic reduction rate of Cr(VI). Experimental conditions: [initial pH (2, 4, 6, 8, 10, and 12); catalyst dosage, 2 g/L and initial concentrations, 20 mg/L)].

b. Effect of initial Cr(VI) concentration on the photocatalytic reduction of Cr(VI)

From both mechanistic and application points of view, the study of dependence of the photoreduction rate on the substrate concentrations is important (Qamar et al., 2011). Hence, the effect of the initial concentration of Cr(VI) on the photoreduction efficiency was studied and the obtained results are illustrated in Figure 4.12. The photoreduction of Cr(VI) was studied between 10 to 50 mg/L at initial pH of 2 and catalyst dosage of 2 g/L. Figure 4.12 illustrates the effect of initial concentration on the removal efficiency of Cr(VI). As can be seen, the Cr(VI) reduction rate gradually decreased upon increasing the initial concentration of Cr(VI) in the solution from 10 to 50 mg/L. This can be attributed to the fact that with increasing initial concentration of Cr(VI), a large amount of UV radiation is absorbed by substrate before it reaches the surface of the dandelion-like TiO_2 nanostructures and then the reduction decreases (Ma et al., 2012). Moreover, at a fixed dosage of dandelion-like TiO_2, the total available electron–hole pairs will be limited to obtain a higher reduction efficiency of Cr(VI) at higher concentration (Testa et al., 2004). By observing the colour change of the dandelion-like TiO_2 nanostructure, the white-coloured nanostructure became yellow after adsorption of Cr(VI), and then gradually turned into pale green during the photocatalytic reduction of Cr(VI) to Cr(III). Therefore, for high initial Cr(VI) concentrations of Cr(VI) a yellow deposit on dandelion-like TiO_2 nanostructure was observed, which corresponds to the adsorption of anionic Cr(VI) species (Chen et al., 2005).

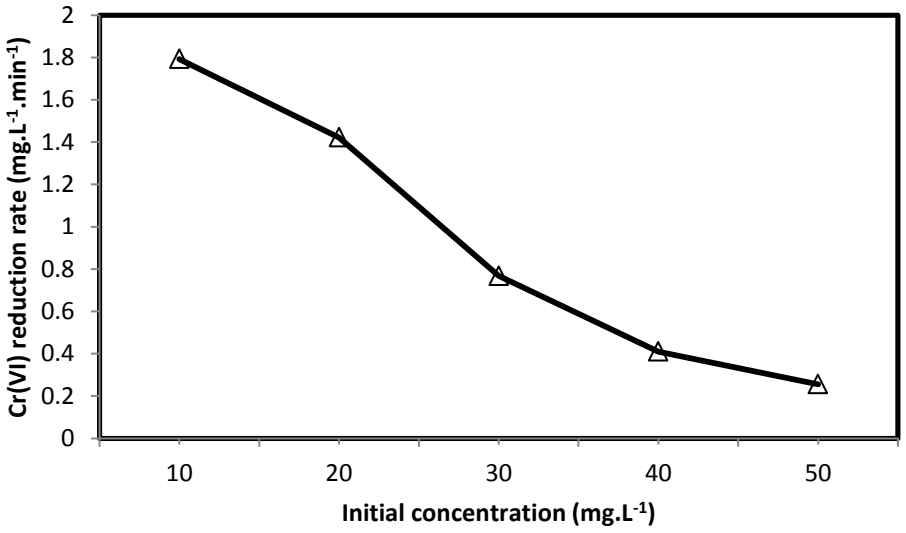

Figure 4.12: Influence of initial Cr(VI) concentration on the photocatalytic reduction rate of Cr(VI). Experimental conditions: [initial Cr(VI) concentration (10, 20, 30, 40, and 50 mg/L); catalyst dosage, 2 g/L and initial pH, 2)].

c. Effect of catalyst dosage on the photocatalytic reduction of Cr(VI)

Figure 4.13 shows the effect of catalyst concentration on the percentage of reduction of Cr(VI) in a solution. It was observed that with an increase in a catalyst dosage up to 2 g/L the reduction rate increases and thereafter decreases. This may be due to the fact that with an increase in catalyst dosage the number of photons absorbed by dandelion-like TiO_2 nanostructure and numbers of reacting molecules adsorbed on dandelion-like TiO_2 surface are increased. However, at high catalyst dosage (2 g/L) there was no further increase in the reduction rate, this might be due to the fact that no reacting molecules are available for adsorption and light scattering of dandelion-like TiO_2.

From this observation it can be presumed that with increase an in catalyst dosage there is an increase in the surface area of the dandelion-like TiO_2 catalyst available for adsorption and hence photoreduction. However, further increase in the catalyst dosage increases the solution opacity, leading to a decrease in the penetration of the light, thereby, affecting the reduction rate. Munoz and Domenech, (1990) & Chaudhary et al. (2012) reported similar results previously.

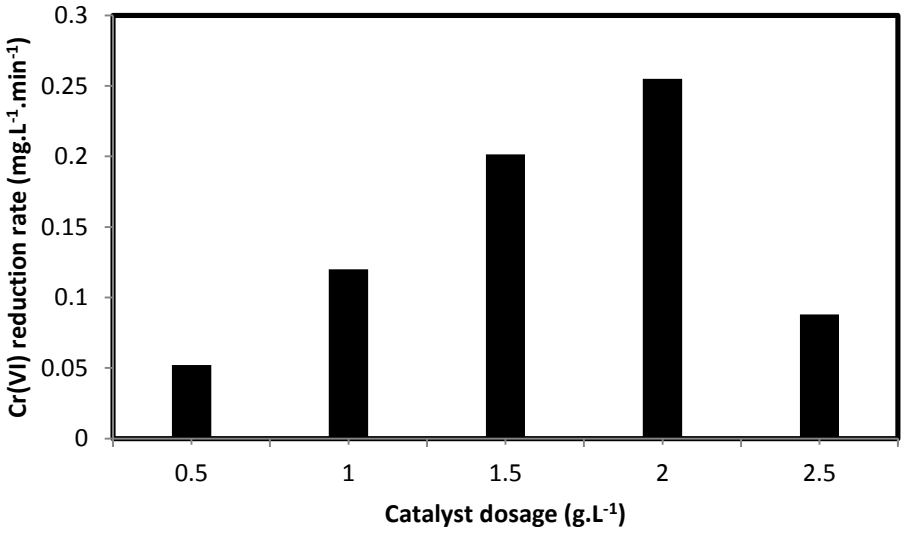

Figure 4.13: Influence of catalyst concentration on the photocatalytic reduction rate of Cr(VI). Experimental conditions: [catalyst dosage (0.5, 1, 1.5, 2 and 2.5 g/L) initial Cr(VI) concentration (20 mg/L) and initial pH, 2)].

d. Effect of the pH on the photocatalytic reduction of Hg(II)

The influence of initial pH on the Hg(II) photoreduction rate is studied and the results are presented in Figure 4.14. It can be seen from the Figure 4.14 that the photoreduction rate increases with an increase in the solution initial pH. This shows fact the photoreduction rate Hg(II) is more favourable at alkaline solution pH compare to acidic solution pH. Such a tendency can be explained on the basis of decrease in competition between protons (H^+ ions) and metal cations (Hg(II) ions) for the electrons and by decrease in the positive surface charge on the dandelion-like TiO_2 in a lower electrostatic repulsion between the surface of dandelion-like TiO_2 and Hg (II) ions. The low photoreduction of Hg(II) ions at acidic pH may be explained on the basis of the overall surface charge on the dandelion-like TiO_2 becoming positive and active sites being protonated, which will hinder the approach of positively charged Hg(II) ions.

In order to verify whether or not the decrease of the Hg(II) concentration could be due to the precipitation of the metal ions in the forms of metal hydroxides, a control experiment was carried out on the Hg(II) ions solution without photocatalyst. In Figure 4.14 (inset), when comparing the control (without a photocatalyst) and the sample (with photocatalyst) from pH 2 to 12, it is clear that the removal of Hg(II) ions from pH 2 to 8 was due to the photoreduction rather than by precipitation which accounted for 0%. This observation is supported by Karthika and Sekar (2012), who reported that when the pH is raised above 8 the Hg(II) ions precipitate to form hydroxyl species such as $Hg(OH)_2$ within the solution. Kannan and Malar (2005), also observed the precipitation of Hg(II) ions to form $Hg(OH)_2$, when the pH is raised above 9. Photoreduction at pH above 8 was not considered in this study in order to avoid any possible interference from metal precipitation in solution. Hence, the pH of 8 for the removal of Hg(II) from aqueous solution was used in all experiments in this work.

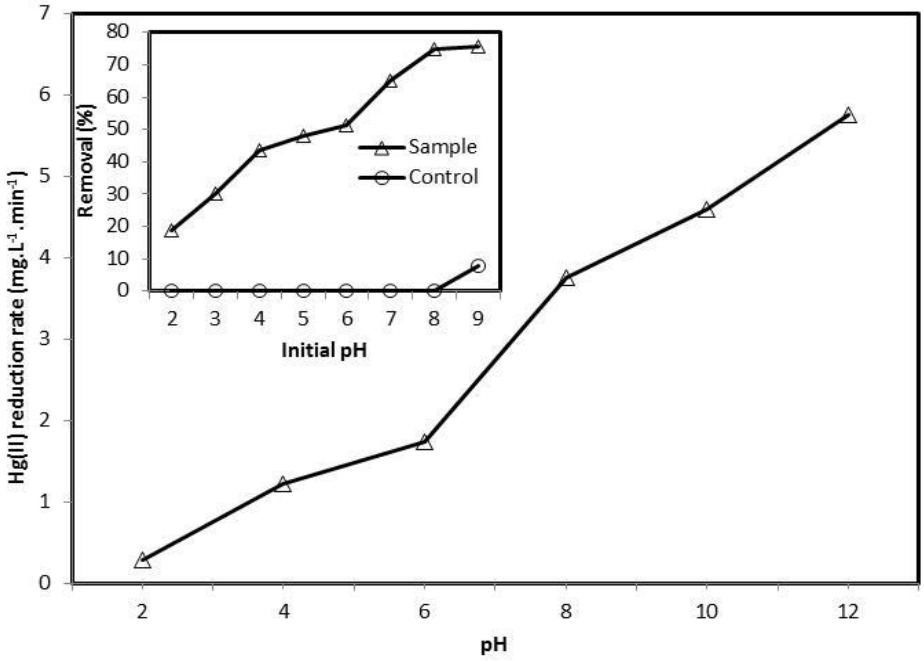

Figure 4.14: Influence of initial pH on the photocatalytic reduction rate of Hg(II). Inset shows the effect of pH on Hg(II) photoreduction and precipitation. Experimental conditions: [initial pH (2 - 12); initial Hg(II) concentration (100 mg/L) and catalyst dosage, 2 g/L].

e. Effect of initial Hg(II) concentration on the photocatalytic reduction of Hg(II)

To study the effect of initial Hg(II) concentration on the photoreduction efficiency of Hg(II), the experiments were conducted with initial Hg(II) concentrations varying from 20 to 120 mg/L. The results of the study of initial Hg(II) concentration on the photoreduction rate of the photoreduction process are summarised in Figure 4.15. According to the results, the photoreduction rate increased with an increase in the initial Hg(II) concentration up to 100 mg/L, and thereafter, the photoreduction rate decreased. With increasing initial Hg(II) concentration the number of the available photons at the dandelion-like TiO_2 catalyst surface reduces and the dandelion-like TiO_2 catalyst active sites deactivate, resulting in a decrease in the photoreduction rate. Deng et al. (2010) have reported similar results.

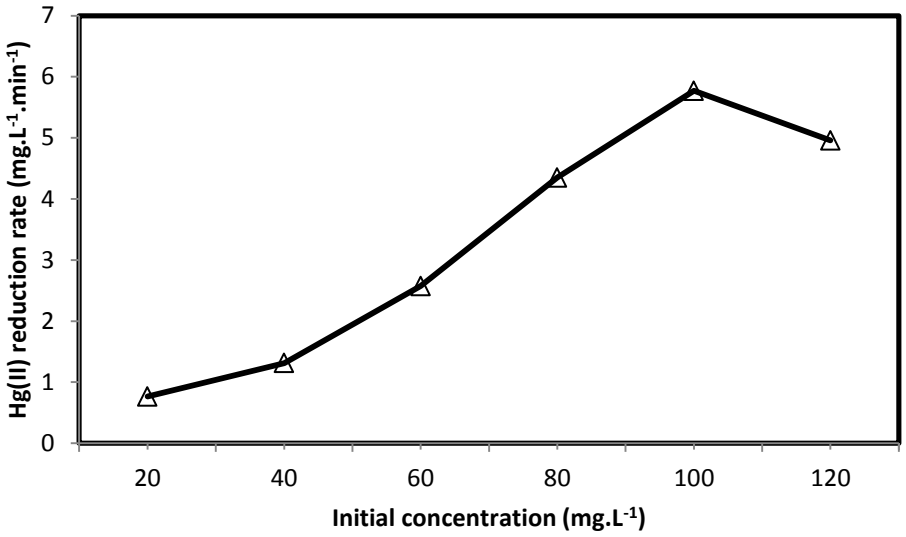

Figure 4.15: Influence of initial Hg(II) concentration on the photocatalytic reduction rate of Hg(II). Experimental conditions: [initial Hg(II) concentration (20, 40, 60, 80, 100 and 120 mg/L); initial pH, 8 and catalyst dosage, 2 g/L].

f. Effect of catalyst dosage on the photocatalytic reduction of Hg(II)

Figure 4.16 shows the effect of the catalyst dosage on the photoreduction rate of Hg(II) by varying the catalyst dosage from 0.5 to 2 g/L. By increasing the dandelion-like TiO_2 catalyst dosage up to 2 g/L the photoreduction rate increased, and thereafter, decreased. The enhancement in the reduction rate of Hg(II) increased with an increase in the catalyst dosage from 0.5 to 2 g/L can be attributed to the increase in the catalyst dosage which contributed to the increase in the active sites and number of photons adsorbed and thus increased Hg(II) reduction rate. Apparently, when the catalyst dosage was further increased beyond 2 g/L the photoreduction rate of Hg(II) decreased. This was probably due to the blockage of light caused by excessive catalyst dosage. These results are in agreement with previous studies done by Cristante et al. (2006), where they reported that the increase in the catalyst dosage beyond the optimum dosage has a negative effect on the photoreduction rate. Light blocking by excessive catalyst may account for the decreased photoreduction rate. The excessive catalyst prevented the irradiation of catalyst.

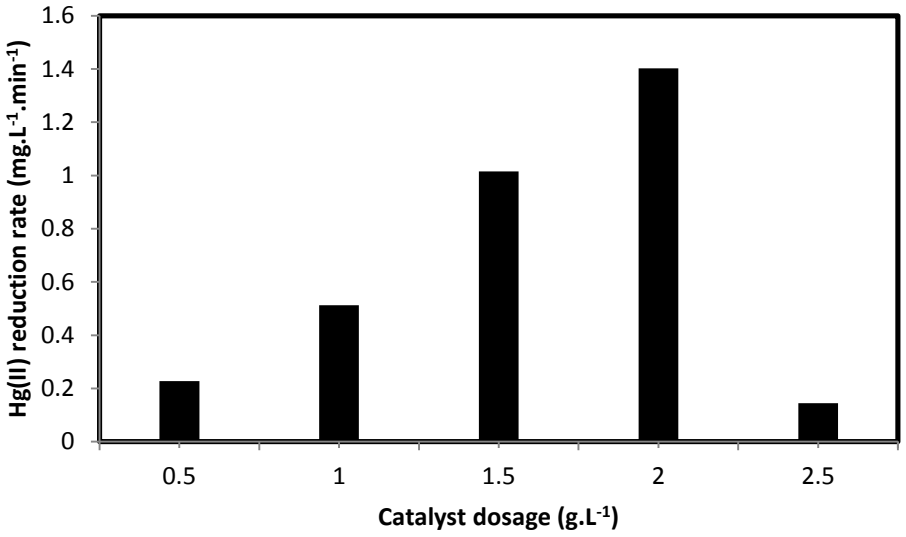

Figure 4.16: Influence of catalyst dosage on the photocatalytic reduction rate of Hg(II). Experimental conditions: [catalyst dosage (0.5, 1, 1.5, 2 and 2.5 g/L); initial pH, 8 and initial Hg(II) concentration (100 mg/L)].

4.1.4.2 Effect of calcination temperature on the photocatalytic activity of dandelion-like TiO_2

In Figure 4.17, the efficiencies of photocatalytic reactions of as-prepared dandelion-like TiO_2 powder was compared with dandelion-like TiO_2 calcined at different temperatures and the commercially available Degussa P25. The photolysis of selected model pollutants without photocatalyst was performed first to explore the role of UV light in photocatalytic oxidation processes (Figure 4.17 and 4.18). Approximately 1.25% of Cr(VI) was photolysed after 120 min irradiation, indicating that only UV light irradiation cannot effectively reduce Cr(VI). This confirms that the reduction of Cr(VI) comes from the photocatalytic effect of the TiO_2 powders.

The initial Cr(VI) concentration was 20 mg/L at pH 2 and 2 g/L of the 3D dandelion-like TiO_2 and Degussa P25 powders were used as photocatalysts. In the experiment, the photoreduction of Cr(VI) was evaluated over time as shown in Figure 4.17: The reduction efficiency of Cr(VI) was as follows a (81.25%) > b (75%) > c (58.75%) > d (23.75%) > e (20%) > f (17.5%) > g (1.25%), which is in accordance with the BET surface areas as shown in Table 4.1. In this study surface area, porosity and crystal structure should be key factors affecting the photocatalytic activity of the catalysts. The as-prepared 3D dandelion-like TiO_2 achieved excellent photocatalytic activity, slightly higher than Degussa P25 at the same experimental conditions. This can be attributed to the larger surface area of the

synthesised 3D dandelion-like TiO_2 structure, as it is well known that large surface area could provide more active sites and absorb more reactive species. A large surface area contains more active sites and photocatalytic reaction centres for the adsorption of reactant molecules, which favours photocatalytic activity. It has been reported by Zhao et al. (2005), that keeping dimensionality, size, and crystal structure well controlled may bring some novel and unexpected properties, and that a well-controlled dandelion-like TiO_2 nanostructure structure should be an important factor for superior activity of the dandelion-like TiO_2 (Bai et al., 2008). Therefore, it is more important to keep a high surface area and good crystallinity, in order to achieve a high photocatalytic activity. Poor crystallinity defects in samples always leads to the recombination of electrons and holes at defect position.

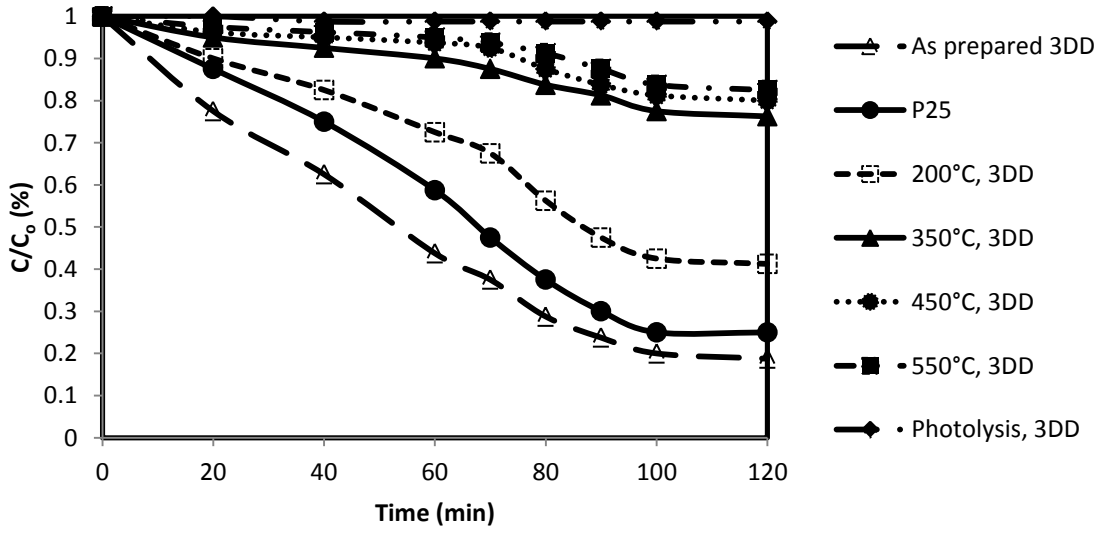

Figure 4.17: Photoreduction curves of Cr(VI) using 3D dandelion-like TiO_2 and the P25 powder. The initial composition of the solution is: Cr (VI), 20 mg/L; catalyst dosage, 2 g/L and pH, 2.

A photolysis experiment of irradiating the solution containing Hg(II) at 100 mg/L without dandelion-like TiO_2 shows no decrease in Hg(II) concentration. However, when dandelion-like TiO_2 particles were added into the solution, the white dandelion-like TiO_2 turned black with time, Hg(0) being produced. Therefore, the photo-reduction of Hg(II) occurs only in the presence of the semiconductor powders.

Figure 4.18 shows that calcination temperature has a significant effect on the Hg(II) reduction efficiencies. The photocatalytic activity of 3D dandelion-like TiO_2 samples decreases with

increasing calcination temperature. The photocatalytic efficiency decreases gradually in the order a (74%) > b (66%) > c (38.75%) > d (21.25%) > e (16.25%) > f (12.5%) > g (1.25%), in agreement with the decrease of the surface areas of the samples (Table 4.1), which results in the decrease of the active site on the surface of particles. As a result, excellent photocatalytic activity has been achieved in the case of as-prepared 3D dandelion-like TiO_2 sample, which is slightly superior to that of P25 under identical experimental conditions. These results suggest that a balance between high crystalline quality and the higher surface area can achieve high photocatalytic activity of 3D dandelion-like TiO_2 nanoparticles.

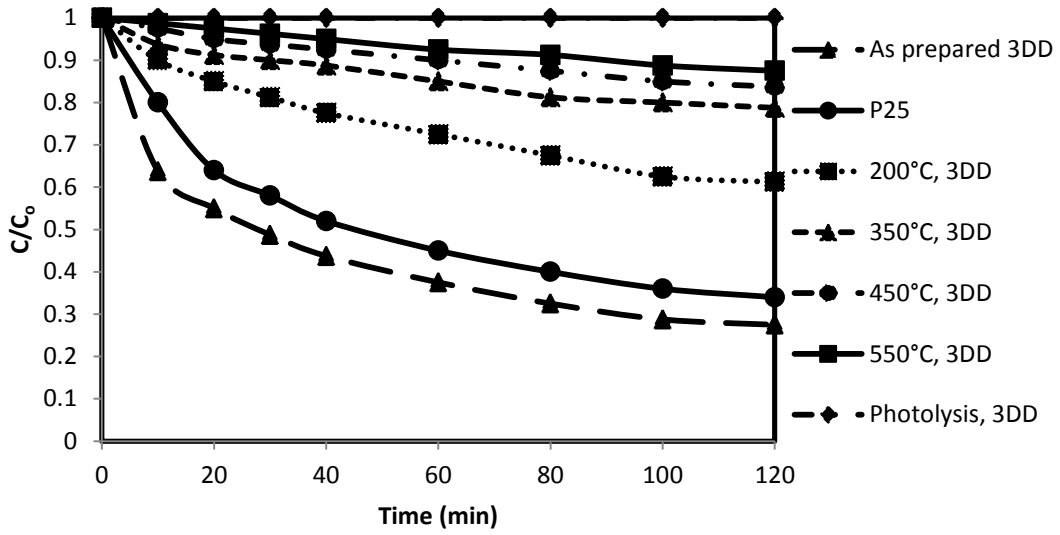

Figure 4.18: Hg(II) reduction of: 3D dandelion-like TiO_2 and the P25 powder. The initial composition of the solution is: Hg (II), 100 mg/L; catalyst dosage, 2 g/L and pH, 8.

4.1.4.3 Influence of Au nanoparticles on photocatalytic activity of dandelion-like TiO_2

As shown in Figure 4.19A and 4.20B, Au nanoparticles loaded on rutile-TiO_2 enhanced photocatalytic activity under UV light irradiation by 17 and 20% for Cr(VI) and Hg(II) reduction, respectively. The improved UV activity of these photocatalysts is attributed to the better charge separation by electron transfer from the conduction band (CB) of TiO_2 to Au nanoparticles (Subramanian et al., 2004 &Silva et al., 2011), whereas the observed activity can be attributed to photo excitation of Au nanoparticles and charge separation.

As shown in Figure 4.19A and 4.19B the control experiments indicated that the photocatalytic reaction hardly proceeded in the absence of any catalyst. The photocatalytic activity of the Au/TiO_2 catalyst was higher than that of TiO_2 photocatalyst. After 120 min, up to 98% of Cr(VI) and 92% of Hg(II) were reduced in the presence of Au/TiO_2 catalyst. The higher photocatalytic activity was attributed to the mesoporous and larger surface area of the open dandelion-like TiO_2 photocatalyst. The Au cluster deposited on dandelion-like TiO_2 surface functions as the electron trap centre, and the perimeters between Au and TiO_2 act as the active site for toxic metal removal. Moreover, the Au nanoparticles dispersed on the surface of dandelion-like TiO_2 enhanced photocatalytic activity due to its ability to act as electron transfer sites on the TiO_2 nanostructure. Therefore, the deposition of gold nanoparticles had a beneficial role primarily in increasing the removal of selected (Cr(VI) and Hg(II)) toxic heavy metals.

It is also of great significance to note that the Au deposited on rutile dandelion-like TiO_2 are promising materials for solar photocatalysts. The photoreduction of both Cr(VI) and Hg(II) were 58.75 and 38.75%, respectively under irradiation by sunlight. Since rutile TiO_2 does absorb in the 400 – 410 nm range, some charge transfer from TiO_2 to Au could take place. As expected, the rutile phase of TiO_2 is visible light active due to its band gap of 3.0 eV. Therefore, results can be explained by the Au nanoparticles on the rutile TiO_2, which is reported to be effective to narrow band gap of the photocatalyst. This resulting in solar photocatalytic activity of the Au deposited on the rutile dandelion-like TiO_2.

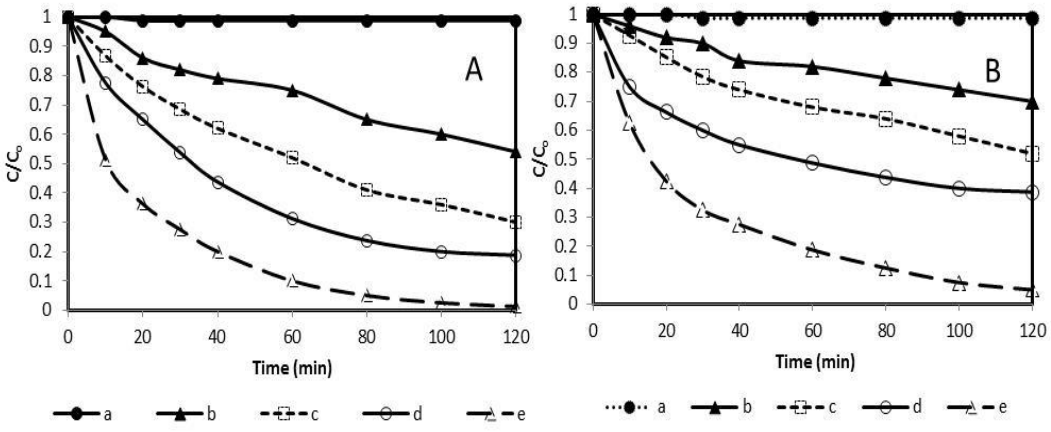

Figure 4.19: Reduction of (A) Cr(VI) and (B) Hg(II); (a) photolysis, (b) 3D dandelion-like TiO_2 sunlight, (c) Au/TiO_2 under sunlight (d) 3D dandelion-like TiO_2 under UV (e) Au/TiO_2 under UV. The initial composition of the solution were: Cr (VI), 20 mg/L; pH 2 and Hg(II), 100 mg/L; catalyst dosage, 2 g/L; pH, 8.

4.1.4.4 Influence of wavelength and different photocatalysts phases

The effect of different light sources on the photoreduction efficiency is shown in Figure 4.20. The experimental results indicated that the wavelength and intensity of the light used for photo activation has a significant impact on the Cr(VI) reduction efficiency. The shorter wavelengths and light intensity lead to higher reduction. As it can be seen in Figure 4.20, the order of reduction efficiency using dandelion-like TiO_2 was shown to be UVC > Sunlight > UVLED. UVC lamp as a light source resulted in the highest reduction that may be due to the shorter wavelength. However, when the experiment was carried out with sunlight and UVLED light sources, Cr(VI) photoreduction efficiency was found to be low compared to the experimental run using UVC lamp. This indicates that photoreduction of Cr(VI) with sunlight and UVLED light is possible, but not efficient.

On the other hand Cr(VI) photoreduction using Degusa P25 was found to follow the same order (UVC > sunlight > UVLED) in this study. However, Cr(VI) photoreduction efficiency decreased by 6,11 and 14% under UVC, UVLED and sunlight, respectively. The high activity of the dandelion-like TiO_2 as compared to P25 TiO_2 under UVLED and sunlight can be explained by the rutile phase of the dandelion-like TiO_2 which is visible light active, whereas the anatase phase is visible light inactive due to its slightly large band gap. Superior activity of the dandelion-like TiO_2 than P25 under UVC can be attributed to the high surface area and flower-like nanostructure of the dandelion-like TiO_2 obtained in this study. It has been reported by Wang et al. (2011), that flower-like structures may play an important role in enhancing the UV photocatalytic activity of TiO_2 due to effective light scattering inside the gaps between nano-flakes, resulting in the photogenerated electrons and holes to participate effectively in the photocatalytic degradation of contaminants. Therefore, UVC lamps are the best source for Cr(VI) photoreduction under experimental conditions of this study. Hence, the UVC lamp was used in the subsequent study. Similar results were observed for Hg(II) and the data is shown in Fig 3A 1 in the appendix.

However, it should be noted that the light sources of UVLED and sunlight can save a lot of energy in comparison to the traditional UVC lamp. Using UVLED and sunlight as light sources can enhance not only the safety with less UV intensity but also the energy usage efficiency.

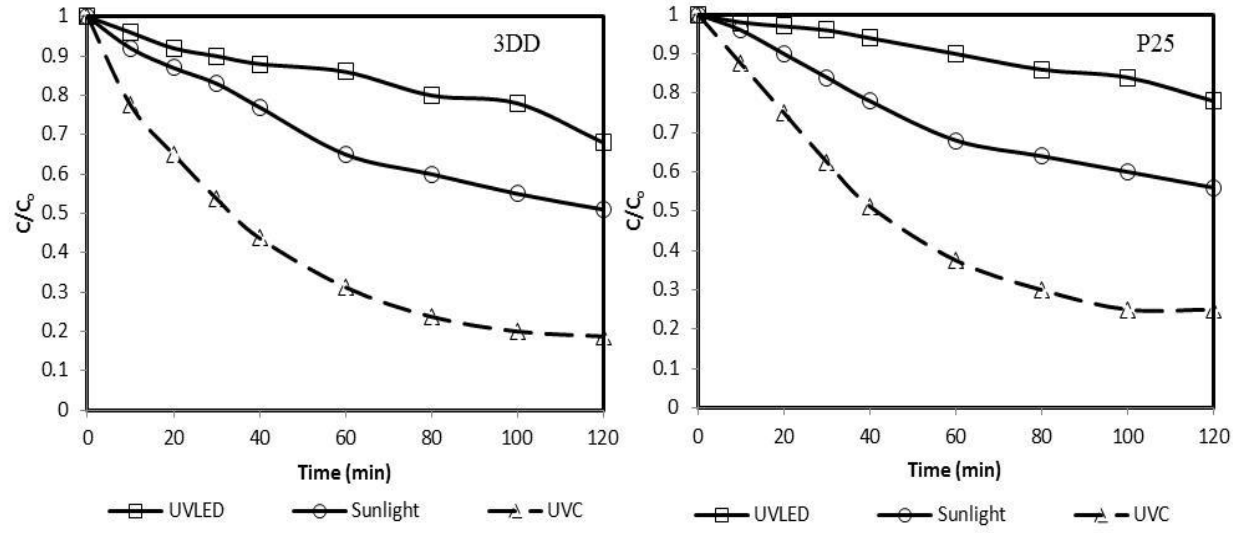

Figure 4.20: Photoreduction of Cr(VI) using 3D Dandelion-like TiO_2 (3DD) and P25-TiO_2 (P25) under UVLED, Sunlight and UVC. The initial composition of the solution was: Cr (VI) initial concentration, 20 mg/L; catalyst dosage, 2 g/L; pH, 2.

4.1.5 Adsorption and photoreduction of Cr(VI) and Hg(II) with dandelion-like TiO_2

It is important to carry out a dark reaction (adsorption reaction) of Cr(VI) and Hg(II) TiO_2 before carrying out the photocatalysis reaction. This is due to the fact that if photocatalysis of Cr(VI) and Hg(II) was performed without the dark reaction, it would be difficult to measure the amount of Cr(VI) and Hg(II) reduction that occurred due to photocatalysis alone. Because both adsorption and reduction processes would take place concurrently and the final Cr(VI) and Hg(II) reduction would be due to the result of both removal by adsorption and photoreduction by photocatalysis. Therefore, dark reaction followed by photocatalysis would enable an accurate breakdown of the percentage removal of Cr(VI) and Hg(II) due to photocatalysis. Moreover, even if adsorption on dandelion like-TiO_2 can completely reduce both Cr(VI) and Hg(II) to their nontoxic forms, it is still important to integrate it with photoreduction. This is due to the well-known fact that adsorption alone can only transfer pollutants from the solution to the adsorbent surface, whereas photoreduction removes the pollutants.

Figure 4.21 adsorption and photoreduction with activity of the dandelion-like TiO_2. Prior to irradiation, the suspensions were magnetically stirred in the dark for 60 min to achieve the adsorption/desorption equilibrium between TiO_2 and selected pollutants. The adsorption experimental results showed that approximately 12 and 11% of Cr(VI) and Hg(II),

respectively was adsorbed on TiO_2 surface after 40 min. Adsorption process almost completed within 40 min and no significant change was observed at the end of 60 min. However, under irradiation with the UV lamp, the Cr(VI) was photoreduced to Cr(III) this was obseved by the colour change of white dandelion-like TiO_2, which lost its original white colour to pale green. The pale green deposit on the dandelion-like TiO_2 is claimed to be Cr(III) (Chen et al., 2005). On the other hand, the white dandelion-like TiO_2 turned black with time, the black deposit on the surface of the catalyst was reported to be Hg(0) in other studies (Wang et al., 2004). Therefore, photoreduction process was shown to have a dramatic accelerating influence on the Cr(VI) and Hg(II) reduction, which was approximately 81 and 61% for Cr(VI) and Hg(II) reduction, respectively. This can be attributed to the fact that the adsorption of both Cr(VI) and Hg(II) occurs up to a maximum level where equilibrium is attained and thereafter no more adsorption can occur. While on the otherhand, there is no photoreduction equilibrium to be attained as both Cr(VI) and Hg(II) are photoreduced rapidly as they are adsorbed on the dandelion like-TiO_2 surface. The overall removal of Cr(VI) and Hg(II) was approximately 91 and 71%, respectively. These results indicate that the photoreduction should start after the completion of the adsorption process for the treatment of wastewater containing Cr(VI) and Hg(II), to eliminate the effect of adsorption on the reactions.

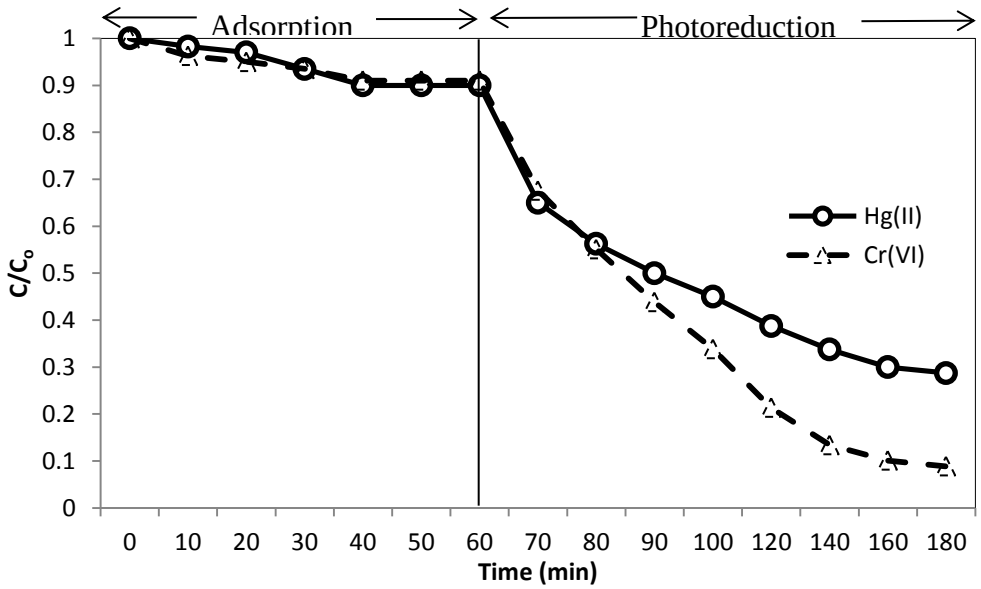

Figure 4.21: Cr(VI) and Hg(II) reduction by adsorption and photoreduction processes. The initial composition of the solution were: Cr (VI), 20 mg/L; pH, 2 and Hg(II), 100 mg/L; catalyst dosage, 2 g/L; pH, 8.

4.1.6 The adsorption isotherms studies

The adsorption isotherms for the Cr(VI) and Hg(II) removal were studied from the time versus reduction efficiency curves in Figure 4.21. The adsorption equilibrium data are represented conveniently by adsorption isotherms, which correspond to the relationship between the mass of the solute adsorbed per unit mass of adsorbent q_e and the solute concentration for the solution at equilibrium C_e. Adsorption isotherm is one of the most important data to understand the mechanism of the adsorption systems and describing the equilibrium situation. In this study, the experimental data obtained in Figure 4.21 were fitted to the Langmuir and Freundlich adsorption isotherms.

4.1.6.1 Langmuir model

Langmuir isotherm, given by equation (3.8) was used to analyse the Cr(VI) and Hg(II) adsorption data. The experimental data obtained were fitted to the Langmuir adsorption isotherms applied to equilibrium adsorption assuming mono-layer coverage of the adsorption onto a surface with a finite number of identical sites and no interactions between adsorbed molecules. It also assumes that no transmigration of adsorbed molecules on the adsorption surface. The plots of C_e/q_e against C_e give a straight line (Figure 4.22) showing the applicability of Langmuir isotherm. Values of q_m were 9.85 and 22.52 mg/g and k_L values were 0.566 and 0.254 L/mg for both Cr(VI) and Hg(II), respectively. It was found that the Langmuir isotherm fitted the sorption data well for both Cr(VI) and Hg(II) adsorption by dandelion-like TiO_2 as the correlation coefficients (R^2) were 0.9332 and 0.9796, respectively. However, R^2 for Hg(II) obtained with Freundlich isotherm (Figure 4.23) was 0.6646 which is lower than 0.9796. Therefore, the experimental data better fits Langmuir model and the Langmuir equation could be used to describe the Hg(II) adsorption on dandelion-like TiO_2 surfaces. Hg(II) adsorption is a monolayer adsorption process, indicating the chemisorption property between Hg(II) ion and the active sites on dandelion-like TiO_2.

The essential dimensionless constant called the equilibrium parameter or a separation factor, R_L, which perfectly determines the favourability and shape of the isotherm of the adsorption process by applying Eq. (3.9). The R_L value indicates the shape of the isotherm as follows: R_L>1, unfavorable adsorption; R_L=1, linear adsorption; 0<R_L<1, favorable adsorption; R_L= 0, irreversible adsorption (Ngah et al., 2002). The values were found to be 0.0812 and 0.0379 for the adsorption of both Cr(VI) and Hg(II), respectively, onto dandelion-like TiO_2. As

the R_L values obtained lies between 0 and 1, the adsorption process for both Cr(VI) and Hg(II) ions by dandelion-like TiO_2 were considered to be favourable.

4.1.6.2 Freundlich model

The Freundlich model (Freundlich, 1906) is an empirical equation and is based on multi-molecular layer adsorption on an energy heterogeneous adsorbent surface, suggesting that binding sites are not equivalent. The experimental data on adsorption of Cr(VI) and Hg(II) were fitted to Freundlich adsorption isotherm, which is known to be the earliest relationship describing the adsorption equilibrium and is expressed by Eq.(3.10).

The linear plots of $\text{Log}\, q_e$ versus $\text{Log}\, C_e$ (Figure 4.23) give a straight line showing the applicability of Freundlich isotherm. If the value of n is between 1 and 10, which corresponds to $1/n$ values < 1, it shows a favourable adsorption. In this adsorption study the constants were found to be k_F = 15.51 and 12.19 and n = 3.16 and 2.01 for both Cr(VI) and Hg(II), respectively, which indicate that the adsorption of both Cr(VI) and Hg(II) was favourable. The correlation coefficient (R^2) value for Freundlich model for Hg(II) was 0.6646, which is lower than 0.9, indicating that the Freundlich model does not fit the experimental data well. Therefore, the experimental data of Hg(II) adsorption can be well described by Langmuir model. On the other hand correlation coefficient (R^2) value for Freundlich model (R^2 = 0.9896) was greater than the coefficient for Langmuir model (R^2 = 0.9896) and thus the correlation coefficient of Freundlich isotherm was closer to one as compared to the Langmuir isotherm. Therefore, the value of correlation coefficient showed that the Cr(VI) adsorption data better fitted the Freundlich equation, which proved that the adsorption of Cr(VI) on dandelion-like TiO_2 is a multi-molecular layer physisorption process.

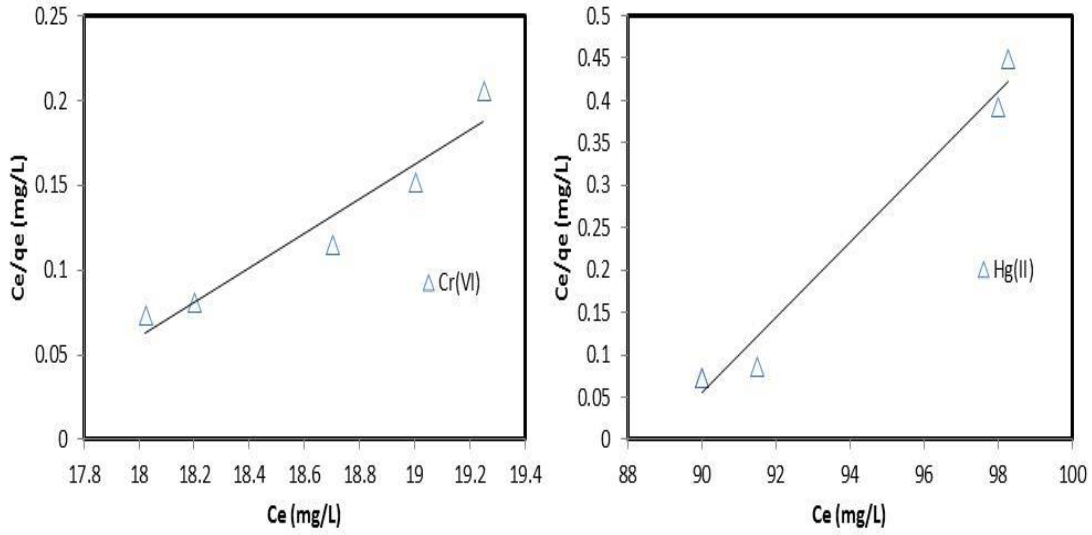

Figure 4.22: Langmuir plot for adsorption of Cr(VI) and Hg(II) on dandelion-like TiO_2.

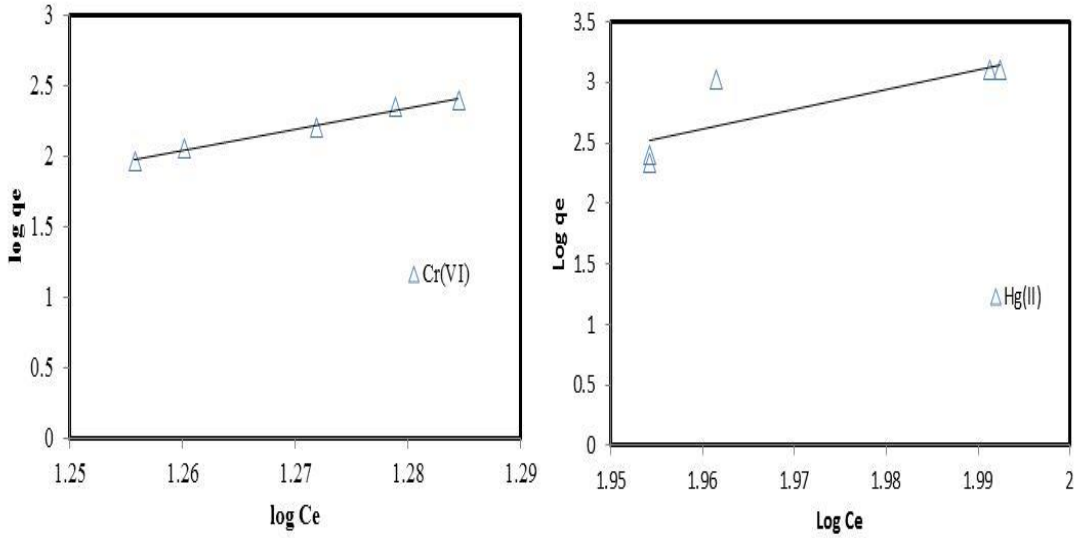

Figure 4.23: Freundlich plot for adsorption of Cr(VI) and Hg(II) on dandelion-like TiO_2.

4.1.7 Summary

Dandelion-like TiO_2 nanostructures were successfully synthesised by hydrothermal method with reaction at 100˚C, using $TiCl_4$ and H_2O as starting material. The dandelion-like TiO_2 nanostructures were characterised using a range of techniques such as XRD, SEM, TEM, EDX and BET. XRD analysis shows the presence of pure rutile phase (JCPDS No. 21-1276), while SEM images revealed the presence of spherical morphology of the particles. EDX data

confirmed the composition of Ti to O ratio to be 1:2. From TEM analysis, the average particle size of dandelion-like TiO_2 nanoparticles was found to be 17 nm. BET surface area of the dandelions-like TiO_2 was 81 $m^2.g^{-1}$ with pores of about 3.2 nm. The experimental results showed that the hydrothermal reaction time and reaction temperature could critically affect the formation of the dandelion-like TiO_2 nanostructure. The results reported in this work also suggest that the dandelion-like TiO_2 can be easily scaled-up and reproduced. The increase in calcinations temperature results in the decrease of the BET surface area. The formation mechanism of the dandelion-like TiO_2 nanostructure was proposed as follows; (i) nucleation and nanoparticles formation; (ii) formation of spheres through self-assembly growth; (iii) further growth and (iv) agglomeration of the dandelions to form sheet-like rutile TiO_2.

Dandelion-like TiO_2 appear as promising material for the reduction of both Cr(VI) and Hg(II) from aqueous solutions using UV/TiO_2 photocatalysis process. The photoreduction strongly depends on the parameters such as initial pH, initial concentration, contact time, UV wavelength and photocatalyst dosage. The photoreduction of Cr(VI) and Hg(II) using dandelion-like TiO_2 obeyed the pseudo-first-order rate equation. Equilibrium adsorption data for Cr(VI) and Hg(II) better fitted the Freundlich and Langmuir isotherm models, respectively. Deposition of gold nanoparticles on TiO_2 enhanced the photocatalytic activity by 17 and 31% for Cr(VI) and Hg(II), respectively. The obtained dandelion-like TiO_2 structure with rutile phase structure exhibited excellent photocatalytic activity, which is higher than P25 titania powder under different light sources. The order of the reduction rate using different light sources was shown to be UVC > Sunlight > UVLED. The performance of dandelion-like TiO_2 was excellent for Cr(VI) and Hg(II) reduction, however, the use of suspended TiO_2 is rather impractical. This is because TiO_2 particles are difficult to separate from the treated wastewater stream. This study attempted to immobilise further the dandelion-like TiO_2 on Ca-alginate on the next section, thus making the environmental application of UV/TiO_2 photocatalysis technology easier for implementation.

4.2 Photocatalytic treatment of heavy metals and citric acid using Alg/TiO_2 beads.

In order to avoid separation problems, which has been mentioned already for slurry applications, dandelion-like TiO_2 nanoparticles were used as immobilised photocatalyst. The rutile dandelion-like TiO_2 was immobilised on calcium alginate (Alg/TiO_2). In order to investigate the possibility and feasibility of using heterogeneous photocatalysis for co-treatment of selected toxic heavy metals and citric acid, this research was carried out in six

parts. The first part investigated the surface morphology and elemental composition of the Alg/TiO_2 beads. The second part investigated the effects of various experimental parameters such as initial pH of solution to be degraded, catalyst dosage, initial concentration of Cr(VI), Hg(II) and citric acid, contact time on the photocatalytic degradation of Cr(VI), Hg(II) and citric acid. The third part investigated the synergic effects of the two conjugated reactions (photooxidation and photoreduction) on the reduction of Cr(VI) and Hg(II) and photooxidation of citric acid. The effects of hydraulic rention time and UV light intensity was investigated. The fourth part investigated the reusability of the Alg/TiO_2. Finally the studies on the real wastewater containing citric acid and toxic heavy metals contaminated acid mine drainage were carried out on the fifth part.

4.2.1 Characterisation of Alg/TiO_2

4.2.1.1 Scanning electron microscopy (SEM)

The surface morphologies of both calcium alginate (Alg/C) and immobilised dandelion-like TiO_2 (Alg/TiO_2) were examined using SEM. As shown in Figure 4.24(a), large cracks appeared on the rough surface of the Alg/C beads, this can be attributed to the Alg/C beads possibly not being rigid enough to withstand the vacuum environment during SEM analysis. Figure 4.24(b) shows that the TiO_2 nanostructures are flower-like in shape. SEM characterisation in Figure 4.24(c) reveals that the TiO_2 nanoparticles are dispersed well on the Alg/C surface. This is confirmed by tiny particles, which were evenly dispersed on the surface of the Alg/C and they were the encapsulated TiO_2 particles. The TiO_2 particles are evident as small brighter spots, while the calcium alginate substrate is dark and larger. Figure 4.24(d) confirms the spherical shape of the Alg/TiO_2 beads. Also, it can be clearly observed that the surface of the Alg/TiO_2 beads was rough but uniform. Liu et al. (2013) obtained similar results.

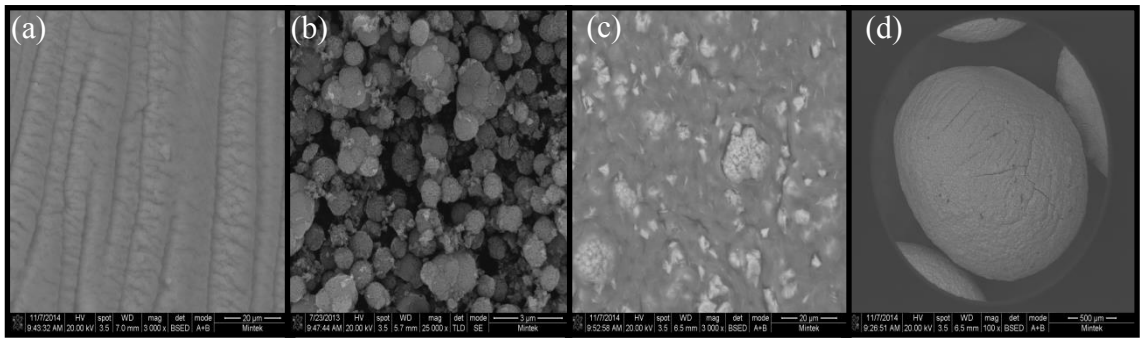

Figure 4.24: SEM analysis for (a) calcium alginate (b) dandelion-like TiO_2 (c) dandelion-like TiO_2 /calcium alginate (Alg/TiO_2) and (d) spherical individual Alg/TiO_2.

4.2.1.2 Energy-dispersive X-ray (EDX)

Figure 4.25 shows that the Alg/TiO_2 beads were chemically composed of Ti, Ca, Cl and O elements. The large Ti peak was observed in the spectrum confirms the presence of Ti nanoparticles in biopolymer Alg/C. It is observable that some Cl ions are present on the surface of the sample; this might be due to the $CaCl_2$ solution that was used during the preparation of the alginate beads. The O peak can be attributed to the presence of the carboxyl groups in alginate and the TiO_2, which was used in the preparation of Alg/TiO_2 beads. The C element was from the carbon grid.

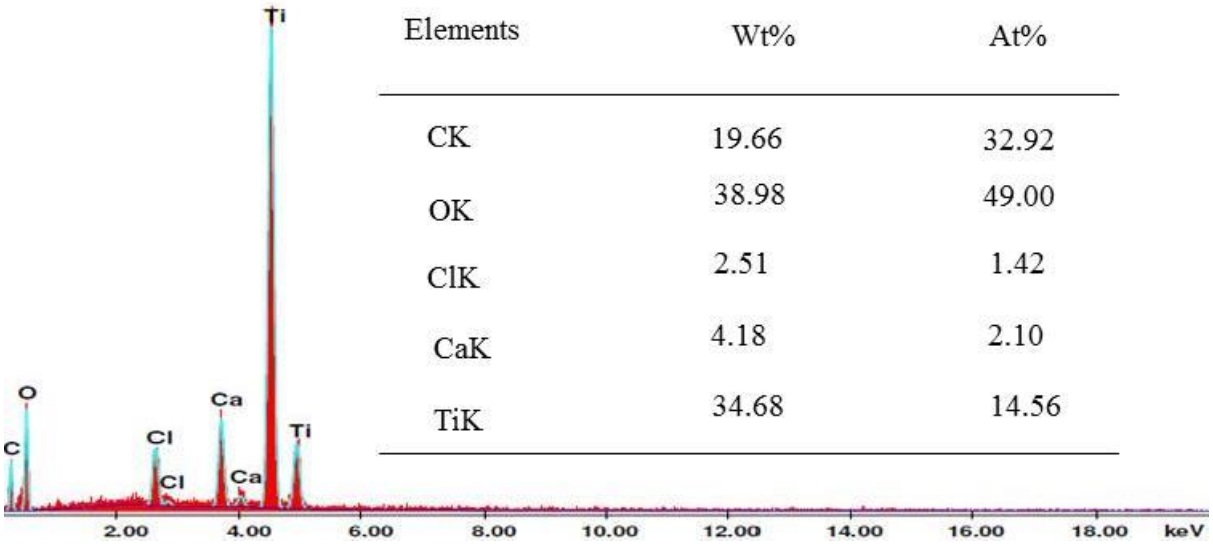

Elements	Wt%	At%
CK	19.66	32.92
OK	38.98	49.00
ClK	2.51	1.42
CaK	4.18	2.10
TiK	34.68	14.56

Figure 4.25: EDX spectrum of prepared Ti nanoparticles entrapped Ca-alginate beads (Alg/TiO_2).

4.2.1.3 X-ray diffraction (XRD)

The XRD measurement in Figure 4.26 shows the XRD pattern corresponding to: a. dandelions-like TiO_2; b. Alg/TiO_2 and c. Ca-alginate. The Bragg diffraction peaks of rutile TiO_2 and Alg/TiO_2 at $2\theta = 32^\circ$, 24.2°, 48.2° and 64° are the main peaks observed in the diffraction analysis. The observed 2θ values are consistent with the standard JCPDS values (JCPDS No. 21-1276), which corresponds to rutile phase of TiO_2 (Jin et al., 2012). The intensity of diffraction peaks for Alg/TiO_2 composites are lower than that for TiO_2. The presence of Ca-alginate reduces the mass volume percentage of TiO_2 and sequentially weakens diffraction peaks of TiO_2 (Sirtori et al., 2012). The XRD pattern of Ca-alginate did

not reveal any crystalline phase, only the presence of an amorphous solid. This confirms that the Ca-alginate is amorphous in nature (Sirtori et al., 2012).

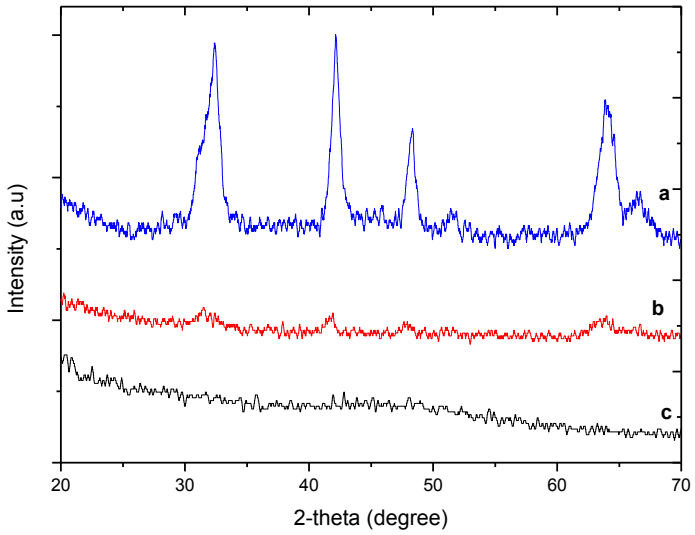

Figure 4.26: XRD patterns of dandelion-like TiO_2 (a), Alg/TiO_2 (b) and calcium alginate (c).

4.2.2 Optimum conditions and kinetic modelling

All the investigations were carried out as batch experiments for the two metal ions (Cr(VI) and Hg(II)), as well as organic compound (citric acid). This section also evaluated the kinetics rate expression which can be used to model the photocatalytic reduction of Cr(VI) and Hg(II) as function of time using Alg/TiO_2. Based on experimental data obtained, the kinetics rate expression of the reactions was assumed to be the pseudo-first-order with respect to the initial concentration, Eq. 4.4 and Eq. 4.5 in Section 4.1.4.1 were used.

4.2.2.1 Control experiments

Control experiments were carried out without the Alg/TiO_2, with Alg/TiO_2 in the dark and blank beads without TiO_2 under UV. The control experiments were designed to exhibit possible effects of photolysis, adsorption and photocatalytic activity of the beads alone in the system. The results of the selected model pollutants, namely Cr(VI), Hg(II) and citric acid control experiments are shown in Figure 4.27 – 4.2.7.

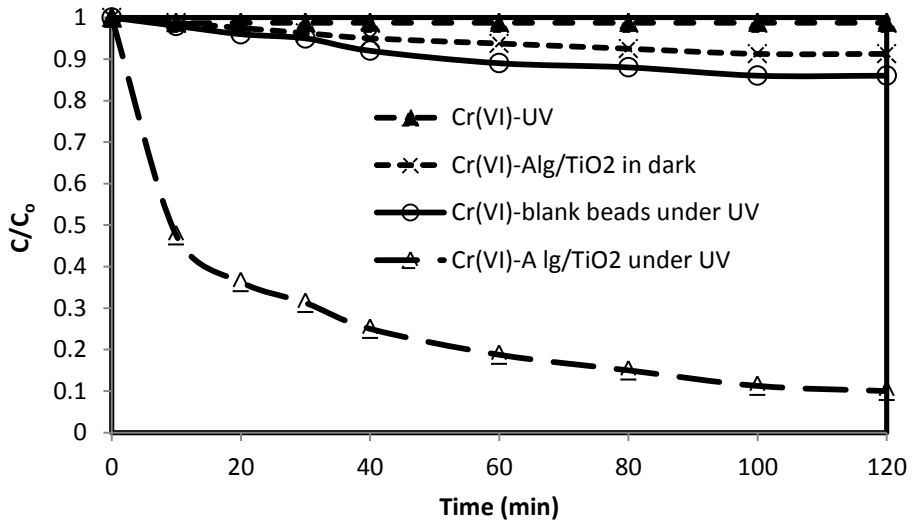

Figure 4.27: Comparison of photoreduction performance with UV (without Alg/TiO_2), Alg/TiO_2 in dark, blank beads and Alg/TiO_2 under UV. (Experimental conditions: initial pH, 2; initial Cr(VI) concentration, 20 mg/L; catalyst dosage, 2 g/L).

Figure 4.27 shows the effects of photolysis, adsorption and the blank beads on the Cr(VI) reduction. To investigate the extent of Cr(VI) reduction by UV irradiation only (photolysis), a solution containing 20 mg/L of Cr(VI) was irradiated by UV lamp for 120 min at pH 2. As shown in Figure 4.27 no observable reduction of Cr(VI) was observed without Alg/TiO_2 catalyst. This indicates that Cr(VI) cannot be reduced by UV irradiation alone. These results agree with those reported by Wang et al. (2008), who demonstrated that no reduction of Cr(VI) was observed during photolysis. The reduction efficiency of Cr(VI) was approximately 9.4 for the control experiment conducted using blank beads under UV irradiation. The results may be attributed to photoreduction of Cr(VI) through the photoinduced electron transfer between excited Cr(VI) ion and the blank beads (Mytych et al., 2003).

The effect of adsorption of Cr(VI) on Alg/TiO_2 was investigated in the presence of Alg/TiO_2 in the dark. A solution containing 20 mg/L of Cr(VI) and 2 g/L of Alg/TiO_2 was stirred in the dark for 120 min at pH 2. It was found that the reduction efficiency of Cr(VI) during the adsorption was approximately 6%. This confirms that adsorption of Cr(VI) by Alg/TiO_2 is negligible. However, when the system was exposed to UV light, rapid increase in the reduction of Cr(VI) was observed. The results support the fact that UV light energy plays an important role in the reduction of Cr(VI) in the presence of Alg/TiO_2.

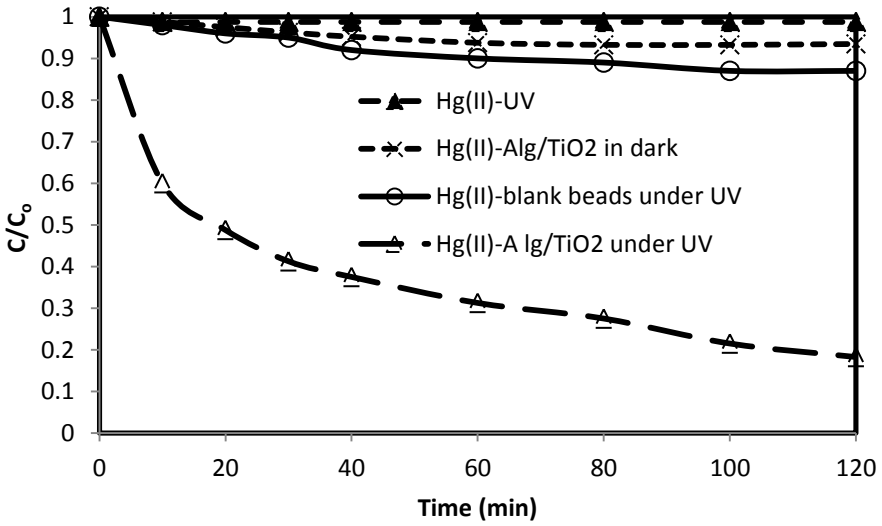

Figure 4.28: Comparison of the photoreduction performance with UV (without Alg/TiO_2), Alg/TiO_2 in dark, blank beads and Alg/TiO_2 under UV. (Experimental conditions: initial pH, 8; initial Hg(II) concentration, 100 mg/L; catalyst dosage, 2 g/L).

Photolytic experiments were performed without addition of Alg/TiO_2 in order to determine whether any photochemical reactions could occur in the absence of catalyst. As shown in Figure 4.28 there is no photolytic reduction of Hg(II) observed in the absence of Alg/TiO_2 under UV light after 120 min of irradiation at pH 8. As shown in Figure 4.28 approximately 9.2% of Hg(II) was reduced using blank beads under UV irradiation. These results can be attributed to the photoreduction via the photo induced electron transfer between the excited Hg(II) ion and the blank beads (Jerome, 1994). The adsorption of Hg(II) onto the Alg/TiO_2 surface was evaluated by analysing the Hg(II) reduced in the solution after stirring 2 g of Alg/TiO_2 and 100 mg/L of Hg(II) solution for 120 min in the dark at pH 8. The results indicated negligible dark adsorption of Hg(II) onto the Alg/TiO_2 surface. The results indicate that the UV light energy is important in Hg(II) reduction.

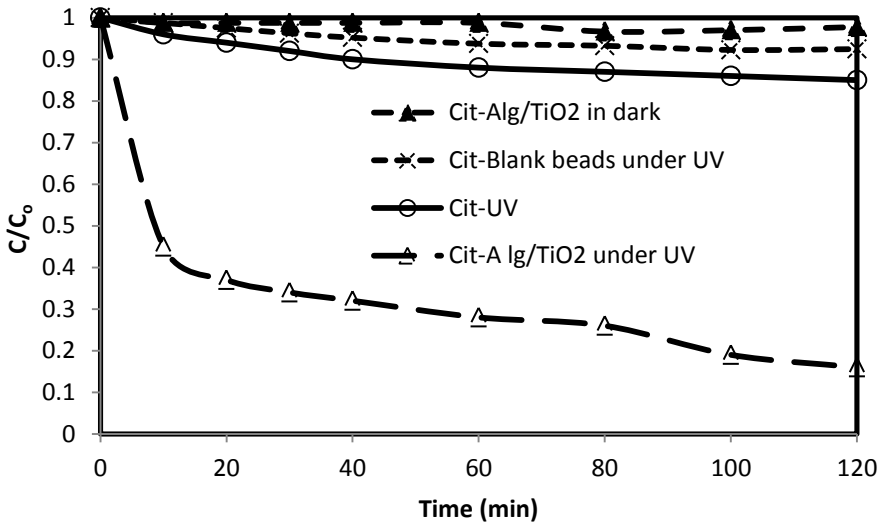

Figure 4.29: Comparison of photodegradation of citric acid with UV (without Alg/TiO_2), Alg/TiO_2 in dark, blank beads and Alg/TiO_2 under UV. (Experimental conditions: initial pH, 2; initial citric acid concentration, 60 mg/L; catalyst dosage, 1.5 g/L).

The results of citric acid control experiments are shown in Figure 4.29. Experiments with UV irradiation alone (without Alg/TiO_2) were carried out to investigate the extent of citric acid degradation by UV irradiation alone. Briefly, UV light illuminated a solution containing 60 mg/L citric acid for 120 min at pH 2. As can be seen in Figure 4.29, photochemical reaction of citric acid was approximately 20% after 120 min UV irradiation. This indicates that citric acid can partially be degraded by UV irradiation in the without Alg/TiO_2. Lee et al. (2003) obtained similar results. As illustrated in Figure 4.29 about 15% of citric acid was reduced using blank beads under UV irradiation. These results can be attributed to an electron transfer molecule between excited citric acid and the blank beads (Augugliaroa et al., 2012). As shown in Figure 4.29, it was found that the degradation of citric acid was negligible when the citric acid solution was not irradiated with UV light. Briefly, 1.5 g of Alg/TiO_2 and 60 mg/L of citric acid solution was stirred in the dark for 120 min at pH 2. Approximately 5% of citric acid was degraded after 120 min of adsorption in the dark. In contrast, when the system was exposed to UV light, rapid increase in the degradation of citric acid was observed. This means that photolysis, photodegradation using the beads alone and adsorption using Alg/TiO_2 cannot effectively degrade citric acid.

4.2.2.2 Photoreduction and kinetic modelling of Cr(VI)

a. Effect of initial pH

The reduction of Cr(VI) at different initial pH over time under different pH values is shown in Figure 4.30. The Cr(VI) reduction gradually declined with an increase in pH. Higher reduction efficiency was obtained when experiments were performed in acidic solutions than that in alkaline solutions. At pH = 2, the reduction efficiency was 88.75%, but, at pH = 12, the reduction efficiency was only 8.75%. These findings are similar to those obtained from the suspended form of dandelion-like TiO_2 in Section 4.1.4.1.The reduction of Cr(VI) in acidic and alkaline conditions probably occurs via the following reactions (Tuprakay and Liengcharernsit, 2005 & Wang et al., 2010):

$$Cr_2O_7^{2-} + 14H^+ + 6e^- \rightarrow 2Cr^{3+} + 7H_2O \quad (4.11)$$

$$Cr_2O_7^{2-} + 14H_2O + 3e^- \leftrightarrow 2Cr(OH)_3 + 5OH^- \quad (4.12)$$

The photocatalytic reduction of Cr(VI) to Cr(III) consumes protons in acidic solution and produces hydroxyls in alkaline solution (Shao et al., 2009). As the pH value increased, the photoreduction rate of dichromate ions gradually decreased since the increase in pH reduced the adsorption of dichromate ions onto the surface of the photocatalyst. Also, at alkaline pH, $Cr(OH)_3$ covered the surface active position of TiO_2 so that the Cr(III) deposits on TiO_2 depressed the photocatalytic activity. These results are in agreement with those reported by Aarthi and Madras, (2008) & Shao et al. (2009), who discussed the influence of different pH values of photocatalyst on the reduction of Cr(VI) by UV/TiO_2 photoreduction processes.

The linear trend observed in Figure 4.30B shows that the photoreduction of Cr(VI) at the condition of the reaction follows a pseudo-first-order kinetics. As pH values increased, the photoreduction rate of dichromate ions gradually decreased because the increase of pH value reduced the adsorption of dichromate ions onto the surface of the TiO_2. At high pH values, $Cr(OH)_3$ covered the surface active sites of TiO_2 so that the Cr(III) deposits on TiO_2 depressed the photocatalytic activity (Chen et al., 2005). Similar observation was reported for photoreduction of Cr(VI) by Ma et al. (2012).

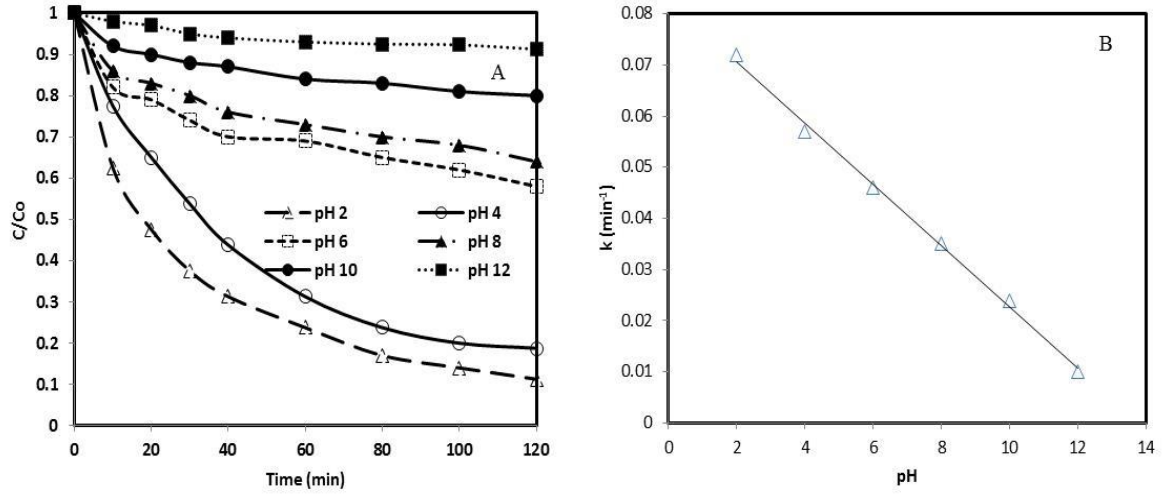

Figure 4.30: Effect of initial pH on the reduction of Cr(VI) and the effect of initial pH value on the rate constant in solution (20 mg/L, 250 mL) with 2 g/L of Alg/TiO_2.

b. Effect of photocatalyst dosage

Photoreduction patterns of Cr(VI) at different catalyst dosage of Alg/TiO_2 are shown in Figure 4.31. It was observed that the photoreduction efficiency increased when the catalyst dosage was increased from 1 to 2 g/L. However, further increase in catalyst dosage to 2.5 g/L decreased the photoreduction efficiency. These findings were same to those obtained by the pure dandelion-like TiO_2 and the reason attributed to this phenomenon was similar to those stated in Section 4.1.4.1. Decreased photoreduction efficiency at higher catalyst dosage has been observed in photocatalytic reactions by Shaban et al. (2013). This behavior may be attributed to the shielding at higher concentrations where the TiO_2 photocatalyst reduces the penetration of light to the solution. Wang et al. (2004) & Ma et al. (2012) have also observed that photoreduction of Cr(VI) increased with increasing amount of photocatalyst, reaching the highest value at catalyst dosage of 2 g/L and then decreased.

Figure 4.31B shows the apparent rate constant as a function of Alg/TiO_2 dosage using the pseudo-first-order kinetics. As it can be seen, the photoreduction of Cr(VI) was successfully fitted using pseudo-first-order kinetic, as confirmed by the obtained straight line. The photoreduction reaction rate increased as the Alg/TiO_2 dosage increased, indicating that the increase of Alg/TiO_2 dosage aided the photocatalytic reaction.

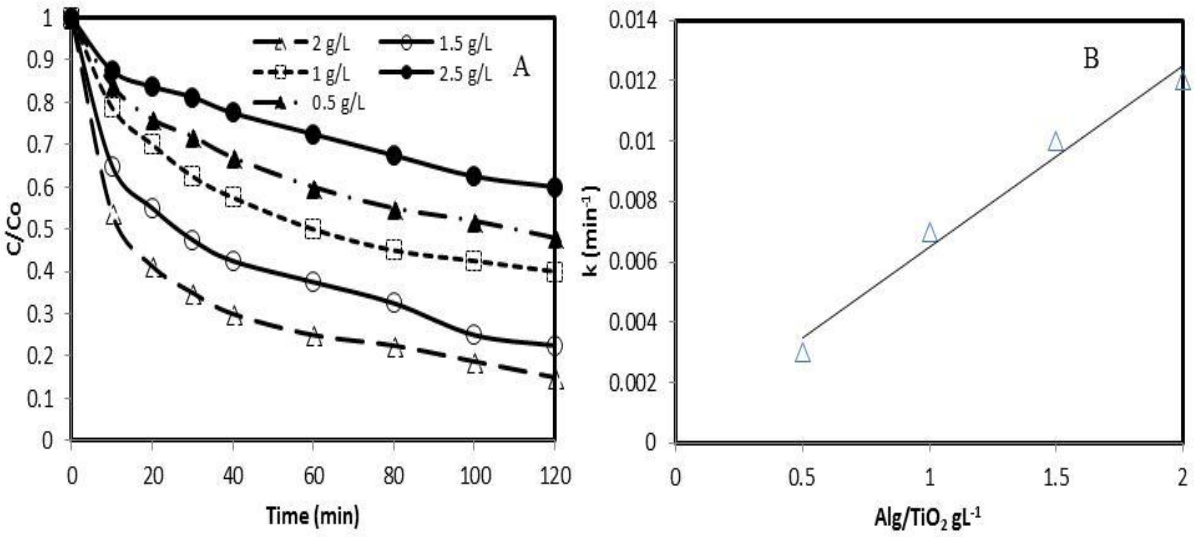

Figure 4.31: Effect of photocatalyst dosage on the reduction of Cr(VI) and the effect of photocatalyst dosage on the rate constant in solution (20 mg/L, 250 mL) with pH 2.

c. Effect of initial concentration and contact time

The effect of initial Cr(VI) concentration and contact time on Cr(VI) photoreduction efficiency was investigated over a dosage range of 10 to 50 mg/L. As illustrated in Figure 4.32A, Cr(VI) reduction efficiency gradually decreases with increasing initial concentration of Cr(VI) from 10 to 50 mg/L. After 120 min, the percentage of Cr(VI) was at 88.7% at concentration of 10 mg/L and 42.5% at concentration of 50 mg/L under same operating conditions. The observed results were identical to those obtained by the pure dandelion-like TiO_2 in Section 4.1.4.1 and this phenomenon can be attributed to the increasing initial Cr(VI) concentration, while the light intensity, catalyst amount and irradiation time are constant, resulting in fewer active sites on the catalyst available for photoreduction of Cr(VI) to Cr(III) (Tuprakay et al., 2005; Chen et al., 2011 & Mekatel et al., 2012). At higher concentration the path length of photons entering the solution decreased, and a fewer photons reached the catalyst surface. This decrease in the penetration of light might be attributed to the higher colour intensity. Furthermore, an increase in Cr(VI) concentration can lead to the saturation of the limited number of accessible active sites on the photocatalyst surface, resulting in a reduction in the Cr(VI) photoreduction efficiency.

The results in Figure 4.32B show a well linear relationship of apparent rate constant as function of initial concentration. According to the results, the reaction rate was decreased

with increasing the initial Cr(VI) concentration. This is attributed to the reduced number of reached photons at the TiO_2 surface.

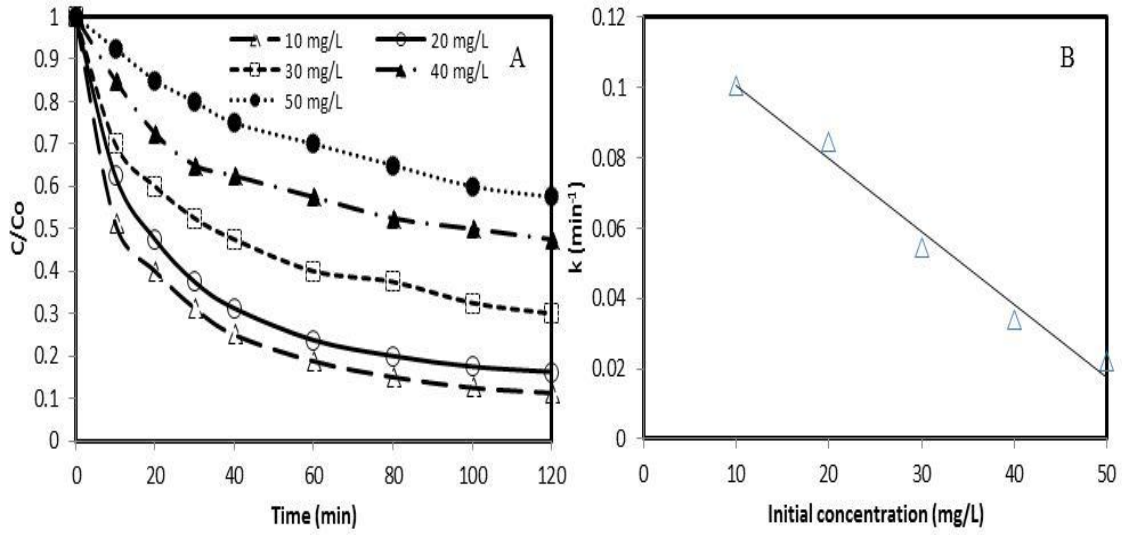

Figure 4.32: Effect of initial Cr(VI) concentration on the reduction of Cr(VI) and the effect of initial concentration on the rate constant in solution (250 mL) with optimum catalyst dosage of 2 g/L and pH 2.

4.2.2.3 Photoreduction and kinetic modelling of Hg(II)

a. Effect of initial pH

In this work, pH of Hg(II) solution was adjusted to a range of values from 2 to 9, all other parameters were kept constant, and the results are shown in Figure 4.33A. At low pH, the reduction of Hg(II) was found to be lower than that at high pH. These results were identical to those obtained by the pure dandelion-like TiO_2 and the reasons for this phenomenon were similar to those stated in Section 4.1.4.1d. Photoreduction of Hg(II) onto Alg/TiO_2 increased from 18.7 to 78% when pH of the solution was increased from 2 to 8. This can be attributed to the surface sites of Alg/TiO_2, which are protonated at low pH and deprotonated at high pH. The low reduction efficiency of Hg(II) observed at low pH might be due to the competition between Hg(II) and H^+ cations for electrons at this pH. Kannan and Malark. (2005) have reported similar observations. Moreover, the like-charges of the Alg/TiO_2 and Hg(II) ions will repel each other due to the surface charges of the Alg/TiO_2 and that of Hg(II) ions which are both positive in the solution. However, as the pH increases, there is a greater possibility for the positive Hg(II) ions to be attracted to increasingly negatively charged Alg/TiO_2

catalyst. Moreover, there is also a possible decrease in competition between H^+ and Hg(II) cations for the electrons. At pH values greater than 8, higher reduction of Hg(II) can be attributed to the possible precipitation of Hg(II) to $Hg(OH)^+$ or $Hg(OH)_2$ which can lead to a higher reduction of Hg(II) within the solution (Zhang and & Bishop, 2002). Therefore, throughout the experiments in this study, the initial pH was kept at 8 to avoid precipitation of Hg(II) ions.

The linear trend of Hg(II) rate constant as function of pH shown in Figure 4.33B indicates that the reaction obeys a pseudo first-order kinetics. As it can be seen in Figure 4.33B increasing the pH values led to the enhancement of the rate constant *k*. Wang et al. (1993) & Khalil et al. (2002) have reported similar results.

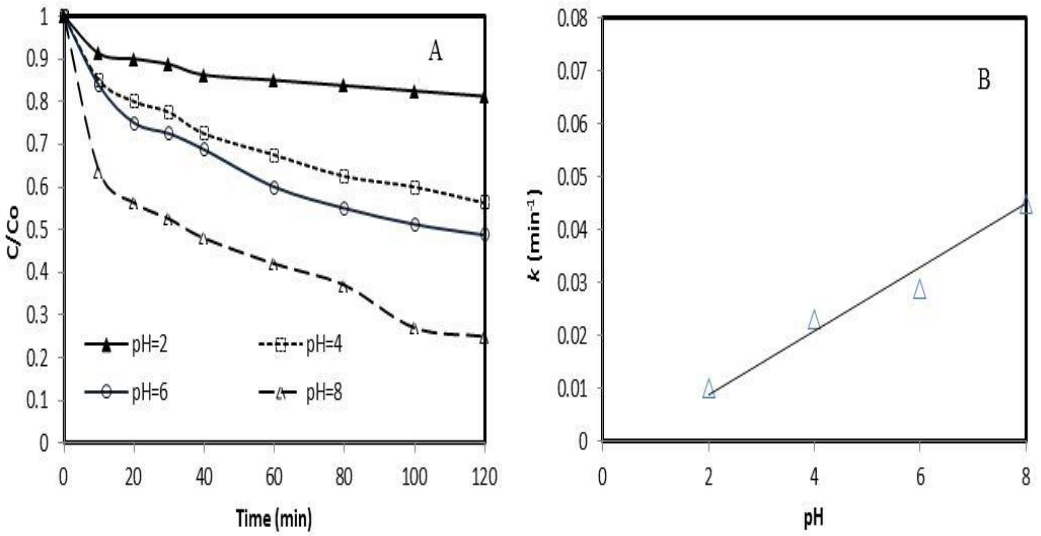

Figure 4.33: Effect of initial pH on the reduction of Hg(II) and the effect of initial pH value on the rate constant in solution. (Experimental conditions: initial Hg(II) concentration of 100 mg/L and 2 g/L of Alg/TiO_2 catalyst).

b. Effect of photocatalyst dosage

In order to investigate the effect of catalyst mass on Hg(II) phodoreduction efficiency, 250 mL of solution (100 mg/L) was used with each of 0.5, 1.5, 2 and 2.5 g/L of Alg/TiO_2 for 120 min. The results from Figure 4.34A indicate the photoreduction efficiency of Hg(II) increased with the increase in catalyst dose from 1 to 2 g/L. Further increment in catalyst concentration to 2.5 g/L leads to decrease in photoreduction efficiency. The results obtained were identical to those obtained by the as-prepared dandelion-like TiO_2 and the motivations accounting for

this phenomenon was similar to those stated in Section 4.1.4.1. The observed increment in the photoreduction efficiency at a catalyst concentration of 2 g/L is due to the increase of the total number of active sites on the photocatalyst surface, resulting in an increase in the number of e- which can take part in the photoreduction of Hg(II). At a higher catalyst dosage beyond the optimum (2 g/L), there is a decrease in the number of surface active sites due to the aggregation of Alg/TiO_2 particles. Thus resulting in a reduction in surface area available for light absorption and hence a drop in photoreduction effiency. The kinetic relationship of Hg(II) rate constant versus catalyst dosage is given in Figure 4.34B. The Hg(II) rate constant depends on the amount of catalyst and the experimental data fits well pseudo-first order kinetic model.

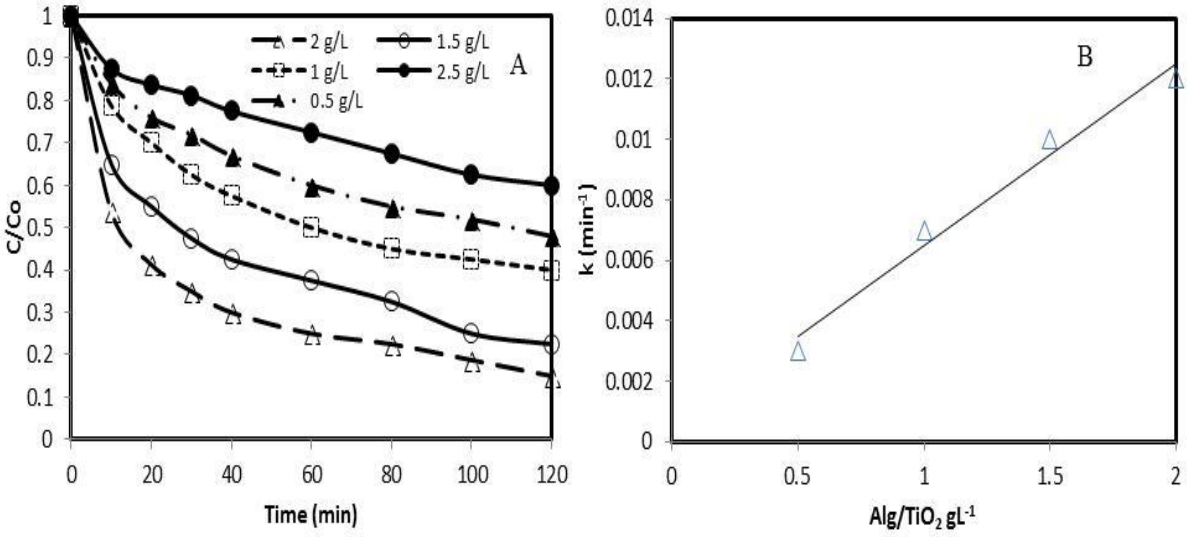

Figure 4.34: Effect of photocatalyst dosage on the reduction of Hg(II) and the effect of photocatalyst dosage on the rate constant in solution (100 mg/L, 250 mL) with pH 8.

c. Effect of initial concentration and contact time

The influence of initial Hg(II) concentration and contact time on the photoreduction efficiency of Hg(II) was examined by irradiating the 2 g/L of TiO_2 at pH 8 with initial Hg(II) concentrations ranging from 20 to 100 mg/L. The photoreduction efficiency of Hg(II) at different initial concentrations is summarised in Figure 4.35A. After 120 min irradiation, 45 and 81.5% of Hg(II) initially present in solution was reduced at initial Hg(II) concentrations of 20 and 100 mg/L, respectively. According to the results, photoreduction efficiency increased with increasing initial concentration of Hg(II) and the increase being more

pronounced during the first 60 min of irradiation time. These results were identical to those obtained by the pure dandelion-like TiO_2 in Section 4.1.4.1 and this can be attributed to the increase in initial concentration of Hg(II) ions which cause a decrease in the number of photons reaching the catalyst surface (Deng et al., 2010). As the concentration of Hg(II) increases above 80 mg/L low photoreduction efficiency was observed. This can be attributed to the deactivation of the active sites of the catalyst, resulting in a reduction of the photoreduction efficiency. The slope and the intercept of the linear plot of Hg(II) rate constant *k* as function initial Hg(II) concentration is shown in Figure 4.35B. As indicated in Figure 4.35B increasing initial Hg(II) concentration enhanced the reaction rate constant *k*.

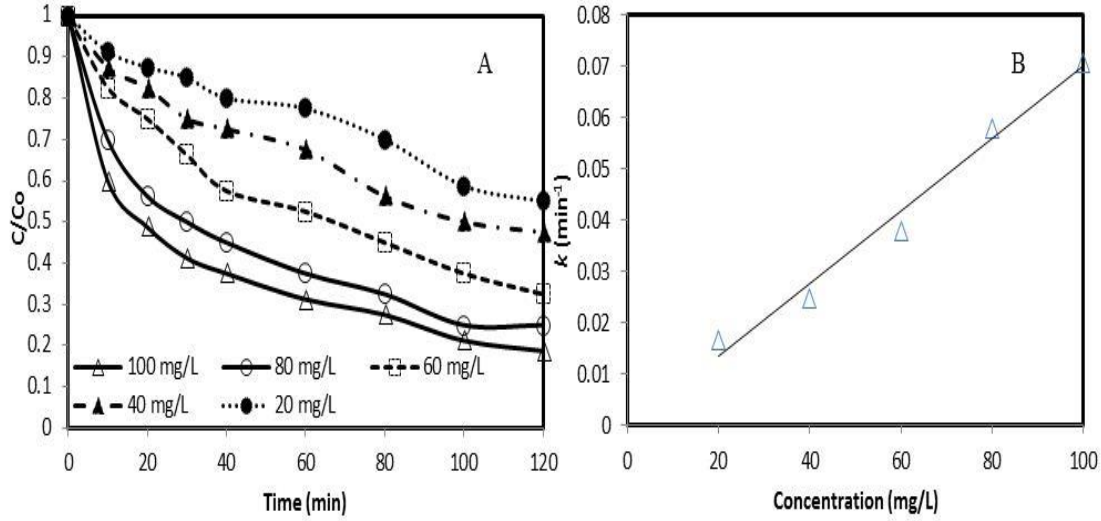

Figure 4.35: Effect of initial Hg(II) concentration on the reduction of Hg(II) and the effect of initial concentration on the rate constant in solution (250 mL) with optimum catalyst dosage of 2 g/L and pH 8.

4.2.2.4 Photodegradation and kinetic modelling of citric acid

a. Effect of initial pH

Figure 4.36A shows the experimental results of the role of pH on the photocatalytic degradation of citric acid. It was observed that the degradation efficiency was approximately 90% (at pH=2) in the acidic pH and decreased to 20% (at pH=12) as the pH was increased. Similar results were reported by Meichtry et al. (2010) and Quici et al. (2007), where the degradation of citric acid was more significant in acidic conditions. Pelizzetti et al. (1993) reported that the acid-base behaviour of catalyst surface influences the photocatalytic degradation. The pK_{a1}, pK_{a2} and pK_{a3} values of citric acids are 3.13, 4.76 and 6.40 (Pelizzetti

et al., 1993), respectively. Since TiO_2 is charged positively at the solution pH (less than the pzc) and citric acid has a dominantly negative charge at acidic pH, the adsorption of citric onto the TiO_2 is electrostatically favourable. Therefore, citric acid degradation was more favourable at acidic pH. The kinetic analysis data of citric acid constant rate *k* as function of initial pH is illustrated in Figure 4.36B. The obtained results show that the pseudo-first order fits well with the experimental data. The citric acid constant rate *k* was found to increase when decreasing the initial pH values.

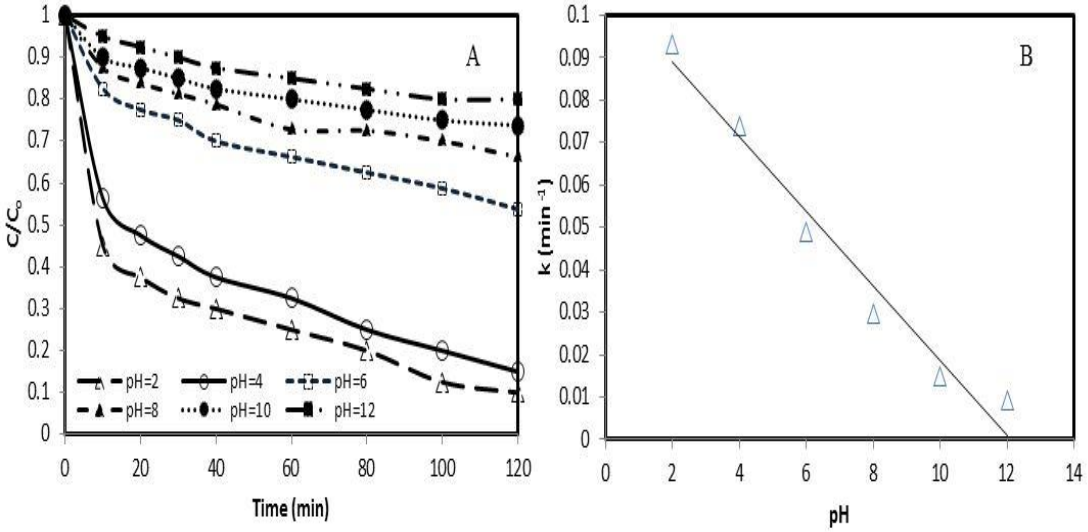

Figure 4.36: Effect of initial pH on the oxidation of citric acid and the effect of initial pH value on the rate constant in solution (20 mg/L, 250 mL) with 1.5 g/L of Alg/TiO_2.

b. Effect of photocatalyst dosage

The amount of catalyst was varied from 1 to 2 g/L in 250 mL of constant citric acid solution of 60 mg/L concentration. Figure 4.37A shows the results obtained when studying the effect of catalyst dosage on the degradation rate of citric acid. By increasing the dosage of catalyst up to 1.5 g/L the degradation rate was increased and thereafter decreased. The degradation efficiency was enhanced by increasing the catalyst dosage from 0.5 to 1.5 g/L. This was due to the increase in the catalyst surface area, which increases absorption of photons and also increases the surface adsorption extent of pollutants. The decrease beyond the optimum catalyst dosage of 1.5 g/L was because of the decrease in the light penetration and deactivation of activated molecules due to collision with the ground state molecules (Nezamzadeh-Ejhieh et al., 2010). The relationship of the citric acid rate constant as function of catalyst dosage is shown in Figure 4.37B, demonstrating a linear relationship between

citric acid rate constant *k* and catalyst dosage. The linear trend observed shows that the experimental data obeys pseudo-first order reaction. The rate constant *k* increases with increasing the catalyst amounts; this can be attributed to the increase in the number of active surfaces on the catalyst.

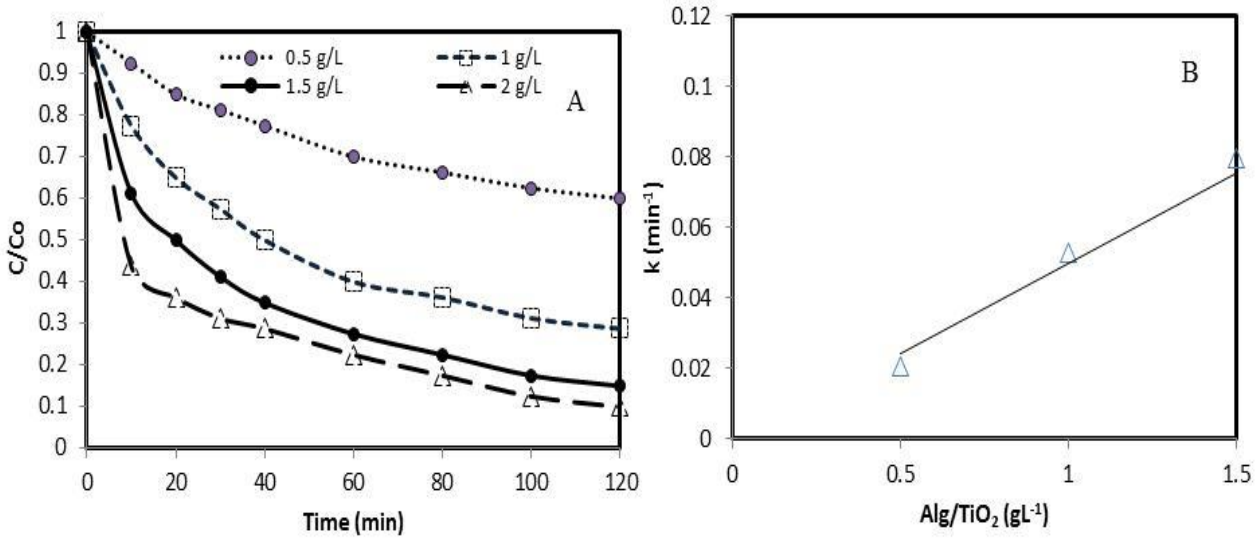

Figure 4.37: Effect of photocatalyst dosage on the reduction of citric acid and the effect of photocatalyst dosage on the rate constant in solution (20 mg/L, 250 mL) with pH 2.

c. Effect of initial concentration and contact time

The effect of the initial concentrations of citric acid and contact time on the citric acid degradation rate was investigated as shown in Figure 4.38A, with 1.5 g/L Alg/TiO_2 and at pH 2. The photocatalytic degradation efficiency of citric acid increases with the decrease in the initial citric acid concentration. As it can be seen in Figure 4.38A, the best degradation efficiency of 90% was obtained at initial concentration of 20 mg/L. The degradation efficiency increases from 52.5 to 90% after 120 min illumination when citric acid initial concentration decreases from 120 mg/L to 20 mg/L. It was reported in the literature, that the photocatalytic reaction occurs between the adsorbed substrate (citric acid) and $OH^{\bullet}$ generated on Alg/TiO_2 surface. The concentration of adsorbed citric acid increases with an increase in initial citric acid concentration. However, as the light intensity, Alg/TiO_2 dosage amount and irradiation time are constant, the concentration of $OH^{\bullet}$ remains practically unchanged. Thus reduces the photocatalytic degradation at higher initial citric acid concentration due to a lower $OH^{\bullet}$/citric acid ratio, although adsorbed citric acid concentration increases.

The relationship of the citric acid rate constant *k* as function of the initial citric acid concentration is illustrated in Figure 4.38. There is a linear relationship between the rate constant *k* and initial citric acid concentration, indicating that the experimental data fits well the pseudo-first order reaction. This is because as the number of citric acid molecules increase, the amount of light (quantum of photons) penetrating the citric acid solution to reach the catalyst surface is reduced owing to the hindrance in the path of light.

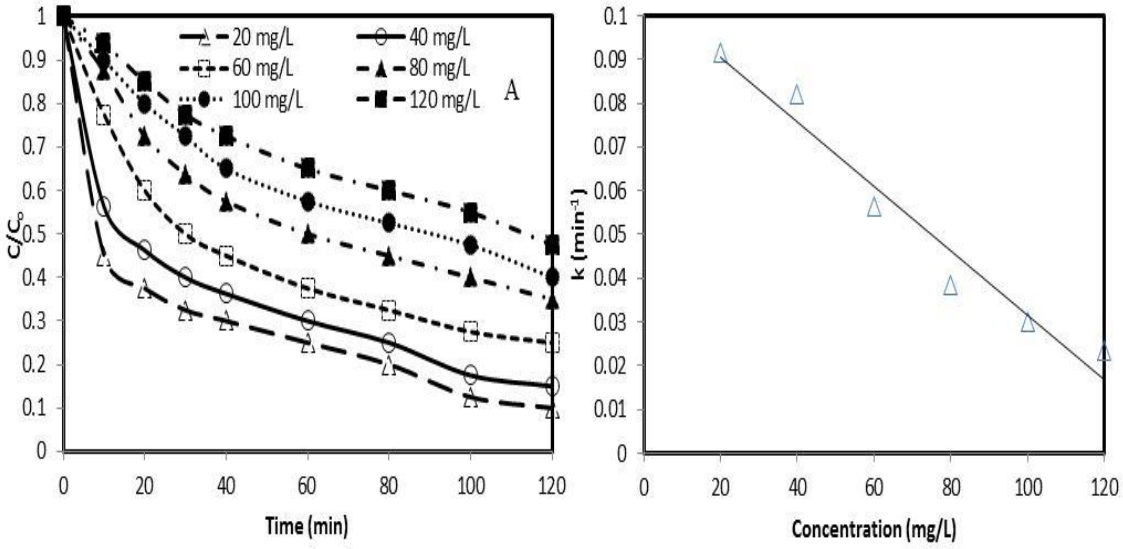

Figure 4.38: Effect of initial citric acid concentration on the reduction of citric acid and the effect of initial citric acid concentration on the rate constant in solution (250 mL) with optimum catalyst dosage of 1.5 g/L and pH 2.

4.2.2.5 Synergic effects of photooxidation and photoreduction reactions

a. Influence of citric acid

The influence of citric acid on photoreduction of Cr(VI) is shown in Figure 4.39A. In the presence of 20 and 40 mg/L of citric acid, 62.5 and 90% was removed after 120 min irradiation, respectively. While, after 60 min irradiation, 100 and 97.5% was removed in the presence of 60 and 80 mg/L, respectively. The photoreduction efficiency increases with the increase in the initial citric acid concentration from 20 to 60 mg/L. Further increase in the initial citric acid concentration to 80 mg/L leads to a decrease in the photoreduction efficiency. The observed fast photoreduction of Cr(VI) at 60 mg/L can be attributed to the minimum electron-hole recombination due to sufficient concentration of the hole scavenger. At this initial citric acid concentration the oxidation of citric acid consumes photogenerated

holes rapidly and efficiently from Alg/TiO_2 particles, which suppresses electron-hole recombination and accelerates photoreduction Cr(VI) on Alg/TiO_2. Previous studies reveal that the presence of organic compounds as a hole scavenger can accelerate the photoreduction of Cr(VI) (Yang et al., 2010, Dozzi et al., 2012 and Chaudhary et al., 2012). When increasing the initial citric acid concentration beyond 80 mg/L, the tendency towards saturation of limited number of accessible active sites on the Alg/TiO_2 increases, resulting in a decrease in photoreduction rate.

As has been discussed, Cr(VI) was reduced through photocatalytic reduction by the photogenerated electrons from TiO_2 photocatalyst and redox between the excited citric acid. The over-reaction in this photocatalysis is the reduction of Cr(VI) to Cr(III) and the oxidation of citric acid to CO_2 which is generally depicted as follows:

$$4Cr_2O_7^{2-} + C_6H_5O_7^{3-} + 41H^+ + 6e^- \xrightarrow{hv,\, Alg/TiO_2} 8Cr^{3+} + 6CO_2 + 23H_2O \qquad (4.14)$$

Figure 4.39B shows the kinetic analysis of Cr(VI) reduction in the absence and presence of citric acid. Plotting Ln (C_0/C) as function of illumination time (t) yields a straight line, this confirms that the experimental data obtained can be described by the pseudo-first-order kinetic. After the addition of citric acid as a hole scavenger, the pseudo-first-order Cr(VI) photoreduction rate was higher than before the addition. A similar observation has been reported by Yang et al., 2010.

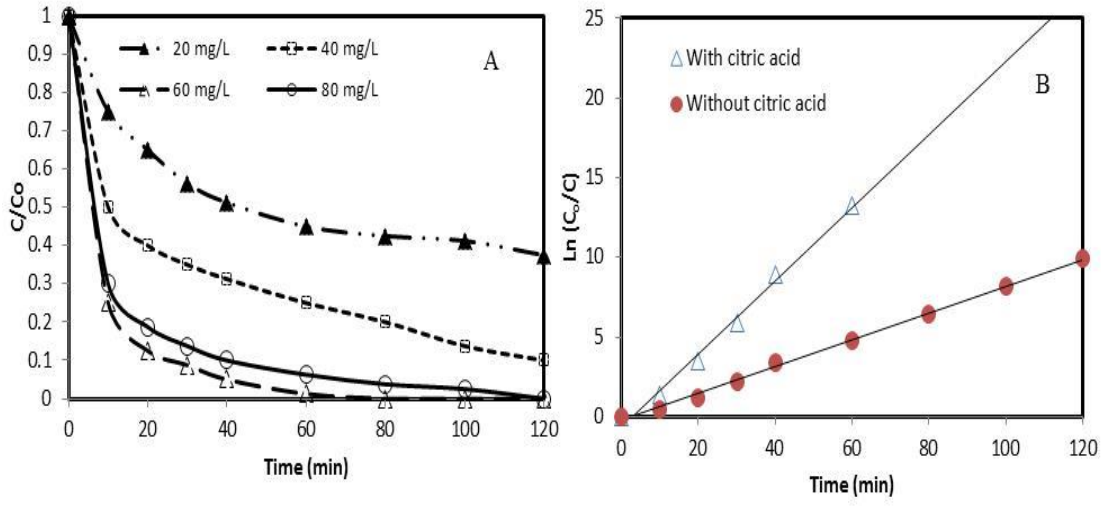

Figure 4.39: Influence of citric acid concentration on the Cr(VI) photoreduction in solution and the linear plot fitting of pseudo-first-order kinetics model. (Experimental conditions; pH 2, 20 mg/L initial Cr(VI) concentration and 2 g/L catalyst dosage).

The influence of citric acid on the photoreduction of Hg(II) is illustrated by Figure 4.40A. As can be clearly seen from Figure 4.40, the irradiation time required for complete removal of Hg(II) was extended as the initial citric acid concentration decreased. From Figure 4.40A the Hg(II) reduction at initial citric acid concentration of 20 and 40 mg/L was about 60 and 76.25% at 120 min irradiation time. While, after 100 min irradiation time, 98 and 100% was removed in the presence of 60 and 80 mg/L, respectively. These results indicated that the Hg(II) photoreduction efficiency was enhanced by citric acid concentration. This can be attributed to initial citric acid concentration, which sufficiently enhances charge separation of photo-induced hole/electron pairs by simultaneous redox reactions (Deng et al., 2010). Citric acid acts as sacrificial electron donor, accelerating the reduction of Hg(II) to Hg(0). Bussi et al. (2002) also reported that the citric acid could promote the reduction of Hg(II) in aqueous solution. The reaction occurring in the presence of TiO_2 via the reduction of Hg(II) to Hg(0) and the oxidation of citric acid to CO_2 is as follows (Bussi et al., 2002):

$$Hg^{2+} + C_6H_5O_7^{3-} + H+ + 16e_{catalyst}^{-} \xrightarrow{hv, Alg/TiO_2} Hg^0 + 6CO_2 + 12H_2O \qquad (4.15)$$

The plot of Ln (*Co/C*) against the irradiation time (*t*) in the presence and absence of citric acid is shown in Figure 4.40B, demonstrating a linear relationship both in the single system and binary system. The experimental data, both in the single system and binary system, obeys a pseuso-first order kinetic model. It can be pointed out that the addition of citric acid led to the enhancement of the reaction rate constant. This fact could be ascribed to the oxidation of citric acid, which consumes photo-excited holes efficiently and thereby supressing the electron-hole recombination.

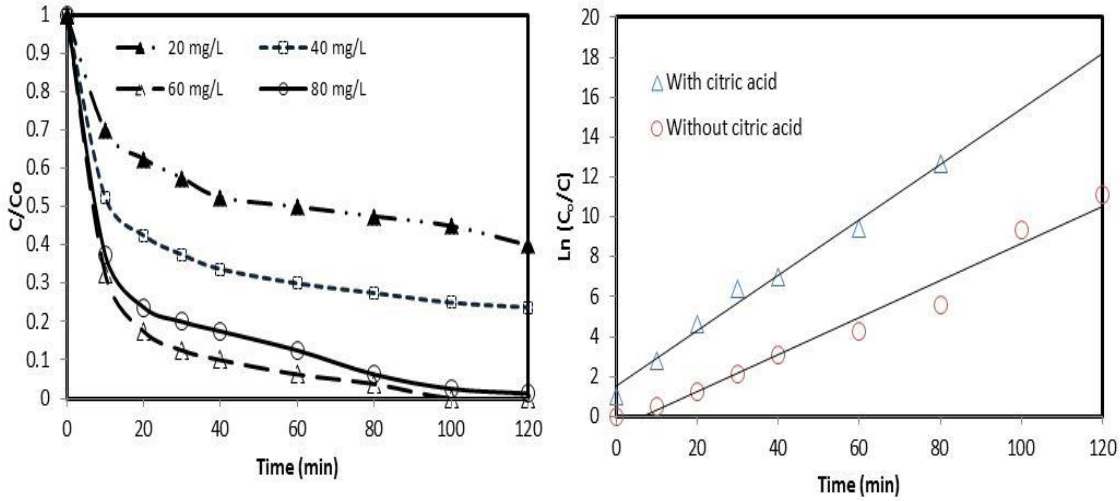

Figure 4.40: Influence of citric acid concentration on the Hg(II) photoreduction and in solution (Experimental conditions; pH 8, 100 mg/L initial Hg(II) concentration and 2 g/L catalyst dosage).

b. Evaluation of reduction efficiency in the photocatalytic systems used

In order to identify the most suitable and economical system for complete photoreduction of Cr(VI) to Cr(III) and Hg(II) to Hg(0), as well as complete mineralisation of citric acid the following experiments were done in this study. The experiments were conducted in single, binary and ternary systems, namely Cr(VI)-UV, Cr(VI)-Cit-UV, Cr(VI)-Alg/TiO_2-UV, Cr(VI)-Cit-Alg/TiO_2-UV, Cr(VI)-Cit-Hg(II)-Alg/TiO_2-UV for photoreduction of Cr(VI) and Hg(II)-UV, Hg(II)-Cit-UV, Hg(II)-Cit-Alg/TiO_2-UV, Hg(II)-Cit-Cr(VI)-Alg/TiO_2-UV for photoreduction Hg(II).

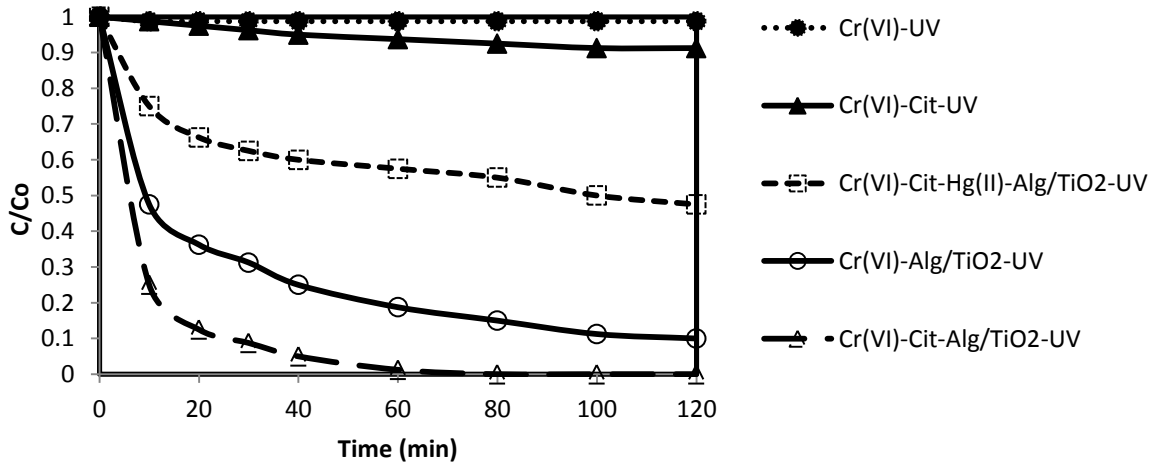

Figure 4.41: Reduction of Cr(VI) in single, binary and ternary systems (Metal ions were complexed 1Cr(VI):5Hg(II) ratio with 60 mg/L of citric acid; pH, 2; Alg/TiO_2, 2 g/L).

Figure 4.41 illustrates the reduction of Cr(VI) under different conditions as function of irradiation time. The photoreduction efficiency of Cr(VI) was in sequence as Cr(VI)-Cit-Alg/TiO_2-UV > Cr(VI)-Alg/TiO_2-UV > Cr(VI)-Cit-Hg(II)-Alg/TiO_2-UV > Cr(VI)-Cit-UV > Cr(VI)-UV. Direct photolytic interactions in the single and binary systems of Cr(VI) and citric acid resulted in low reduction of Cr(VI), implying no severe interaction between Cr(VI) and citric acid under photolysis. Photoreduction of Cr(VI) is almost completely reduced after an irradiation time of only 60 min on the Cr(VI)-Cit-Alg/TiO_2-UV system. In the case of Cr(VI)-Cit-Hg(II)-Alg/TiO_2-UV, approximately 52.5% of Cr(VI) was reduced as shown in Figure 4.50. The addition of Hg(II) retarded the photocatlytic reduction of Cr(VI), this may be attributed to both Hg(II) and Cr(VI) competing for electrons.

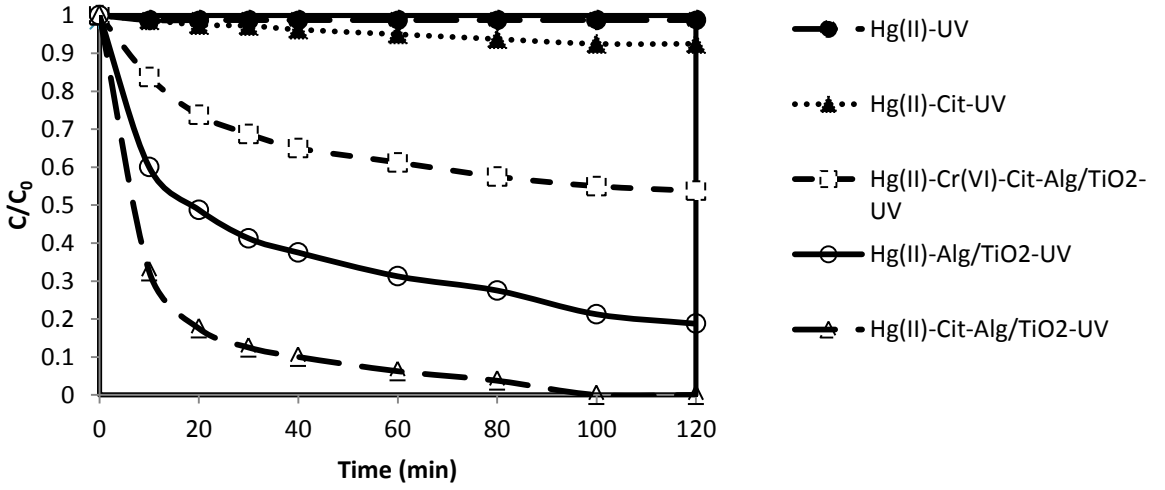

Figure 4.42: Reduction of Hg(II) in single, binary and ternary systems (Metal ions were complexed 5Hg(II): 1Cr(VI) ratio with 60 mg/L of citric acid, pH = 8, Alg/TiO_2 = 2 g/L).

Figure 4.42 shows the reduction of Hg(II) under different conditions. The reduction of Hg(II) was as follows Hg(II)-Cit-Alg/TiO_2/UV > Hg(II)-Alg/TiO_2-UV > Hg(II)-Cr(VI)-Cit-Alg/TiO_2-UV > Hg(II)-Cit-UV > Hg(II)-UV as shown in Figure 4.42. The reduction percentages Hg(II) in single and binary systems in the presence of Alg/TiO_2 was approximately 78.5 and 100%, respectively, after 100 min of irradiation. The reduction of Hg(II) in the ternary system after 120 min irradiation was 46.25%. The inhibitory effect of Cr(VI) on Hg(II) reduction may also be attributed to the competition for electrons between Cr(VI) and Hg(II). Consequently, the reduction of the system with both Cr(VI) and Hg(II)

should be lower than that occurring in the presence of Hg(II) alone. It can be observed that direct photolysis in the single and binary systems reduced Hg(II) to 1.25 and 7.5%, respectively after 120 min irradiation.

c. Effect of ferric ion on the photocatalytic reduction of Cr(VI) and Hg(II) by citric acid

The reduction of both metal ions sharply increased with the addition of Fe(III) as shown in Figure 4.43 and 4.44. The enhancement of reduction of Cr(VI) and Hg(II) by the addition of Fe(III) may be explained as follows. In the acid solution, Fe(III) should be present as Fe^{3+} which is easily reduced to Fe^{2+} by catching the electrons provided by photocatalyst. Based on the reduction of Fe^{3+}, there should be a competition between Cr(VI) or Hg(II) and Fe^{3+} in the photoreduction. Consequently, the reduction of Cr(VI) or Hg(II) should be lower than that occurring in the absence of Fe^{3+}. This is in contrast with the results obtained in this study. The results obtained can possibly be explained by Fe^{2+} resulted from the Fe^{3+} oxidation is oxidised back rapidly by OH radicals present in the solution with releasing an electron, which is used for Cr(VI) or Hg(II) reduction (Wang et al 2004). The capturing OH radical and donating electron are the two conditions which are good for enhancement of Cr(VI) or Hg(II) reduction.

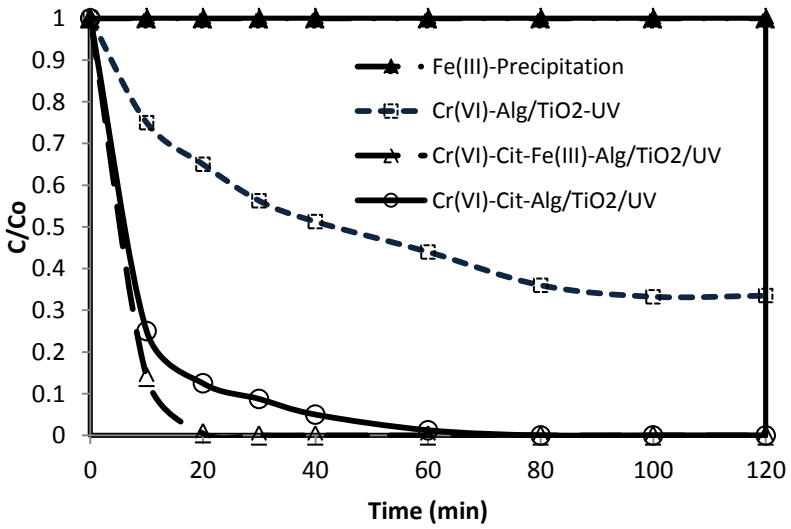

Figure 4.43: Influence of Fe(III) on the Cr(VI) photoreduction in solution (Experimental conditions; pH, 2; 20 mg/L, initial Cr(VI) concentration; 20 mg/L, Fe(III) and 2 g/L, catalyst dosage).

Given the focus on photoreduction, Fe(III) precipitation experiments were carried out as shown in Figure 4.43. As can be seen in Figure 4.43, Fe(III) was not removed in the solution due to precipitation to form $Fe(OH)_3$. These results are in agreement with the findings of Meltzer et al. (2007), who observed Fe(III) precipitating to $Fe(OH)_3$ at pH of 3.5 to 7. Petrucci et al. (2002), reported on a species distribution diagram of hydrolytic metal species in a solution as a function of pH, where it appears that for Fe(III) ions metals precipitation is only expected to occur above pH

Figure 4.43 shows the Cr(VI)-citric acid complex photocatalytic reduction-oxidation profiles at pH 2 with 2 g/L of Alg/TiO_2 in the absence and in the presence of Fe(III). It can be seen in Figure 4.43 that the addition of Fe(III) improves Cr(VI) photoreduction. In the absence and presence of Fe(III) approximately 91.25 and 100%, respectively, of Cr(VI) was reduced after 30 min irradiation. This can be attributed to the Fe(III), which can maintain the acidic pH during the process. Similar results were reported for the reduction of Cr(VI) by the UV/TiO_2 process for solution at acidic pH by Munoz and Domenech (1990), Wang et al. (2004) & Xu et al. (2013). They assumed the enhancement of reduction of Cr(VI) under acidic conditions was due to the acid pH which can be maintained by ferrous iron generated by a photocatalytic reduction of Fe(III). They further proposed the promoting effect of Fe(III) on the reduction of Cr(VI) to be explained by the following reaction.

$$Fe(III) + e^- \xrightarrow{h\nu,\ Alg/TiO_2} Fe(II) \qquad (4.16)$$

$$3Fe(II) + Cr(VI) \rightarrow 3Fe(III) + Cr(III) \qquad (4.17)$$

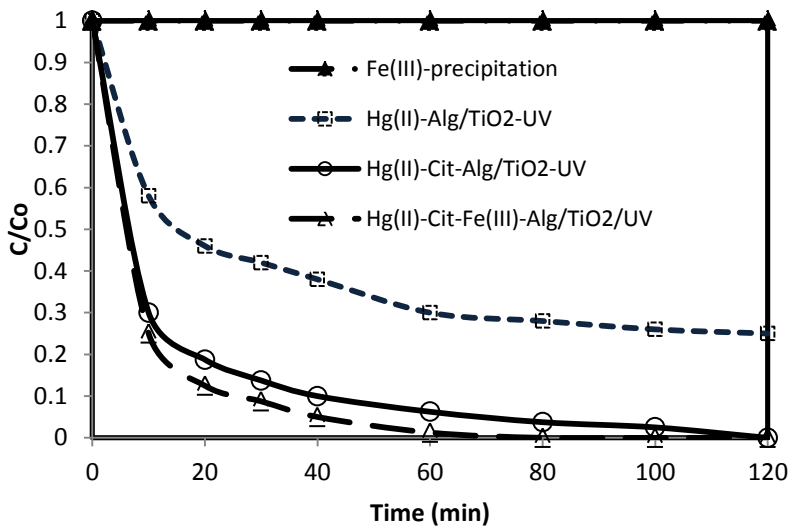

Figure 4.44: Effects of Fe(III) on the Hg(II) photocatalytic degradation in solution (Experimental conditions; pH, 8; 100 mg/L, initial Hg(II) concentration; 100 mg/L, Fe(III) and 2 g/L, catalyst dosage).

In the present study, an Fe(III) precipitation experiment was carried out to check if precipitation was likely to occur in the solution at pH of 8. As can been shown in Figure 4.44, Fe(III) was found to not precipitate to $Fe(OH)_3$ at pH of 8. Similar observation has been reported by Meltzer et al. (2007), who observed the precipitation of Fe(III) ions to $Fe(OH)_3$ over the pH range of 3.5 to 7.

To investigate the effect of Fe(III) ions on reduction of Hg(II), the initial concentration of Hg(II) and citric acid were kept at 100 and 60 mg/L, respectively in the solution at initial pH of 8. The presence of Fe (III) accelerated the photoreduction of Hg(II), which increased from approximately 93 to 100% after 60 min irradiation as shown in Figure 4.44. The fast reaction between Hg(II) and citric acid in the presence of Fe(III) can be attributed to photoreaction products generated during photoreduction process. These products like Fe(II), $HO_2/O_2^{\bullet-}$ or $CO_2^{\bullet-}$, catalyse the reduction of Hg(II) (Sun et al., 2009). Previous studies reported by Chen and Ray (2001), also observed that Hg(II) can be reduced to much lower concentration in the presence of Fe(III). They further suggested that Fe(III) can be absorbed by TiO_2 and, subsequently, easily photoreduced to Fe(II) by accepting photo-reduced electrons on the surface of the TiO_2 catalyst. In the presence of Fe(III), Hg(II) is also reported by Chen and Ray (2001) to be photoreduced by the following redox reactions:

$$Fe(III) + e^{-} \xrightarrow{hv,\ Alg/TiO_2} Fe(II) \quad (4.18)$$

$$Hg(II) + 2Fe(II) \rightarrow Hg + 2Fe(III) \quad (4.19)$$

4.2.3 Photodegradation mechanism for co-treatment of Cr(VI) and Hg(II) and citric acid

From the results already presented and discussed the scheme shown in Figure 4.45 might be suggested for the mechanism of the simultaneous photocatalytic reduction of Cr(VI) or Hg(II), and degradation of citric acid in the presence of Alg/TiO_2 photocatalyst under irradiation of UV light. The photocatalytic reduction of Cr(VI) and Hg(II) by Alg/TiO_2 in both the presence and absence of organic compounds has been extensively investigated for its application to the reduction of metal ions and the oxidation of organic compounds. The mechanism has been reported by Wang et al. (2009) to involve the charge transfer complex formed between TiO_2 and small molecular weight organic acids. The mechanism of photocatalysis on TiO_2 particles involves generated electron/hole pairs that must be trapped in order to avoid recombination. In the absence of organic compounds hydroxyl ions (OH^-) are the likely traps for holes, leading to the formation of hydroxyl radicals, which are strong oxidant agents. The traps for electrons are adsorbed oxygen species, leading to the formation of superoxide species (O_2^-) which are unstable, reactive and may evolve in several ways (Barakat et al., 2011).

$$TiO_2 + hv \rightarrow TiO_2\ (e^- + h^+) \quad (4.20)$$

$$TiO_2–OH_s^- + h^+ \rightarrow TiO_2–OHs^{\bullet} \quad (4.21)$$

$$O_{2(ads)} + e^- \rightarrow O_2^- \quad (4.22)$$

However, in the presence of organic acid, strong oxidising agents (hydroxyl ions ($OH^{\bullet}$)) would be produced by either oxidising of the pollutant directly or water. This synergism is based on the photogenerated electrons and holes on the surface of n-TiO_2 semiconductor. Irradiation of TiO_2 by UV light with energy ($h\upsilon$) greater than or equal to the bandgap energy ($h\upsilon \geq E_{BG}$) of TiO_2 promotes electron in the valence band (VB) to the conduction band (CB), and a positive hole is formed in the valence band (Eq. 4.23). The positive holes mediate the oxidation of citric acid by the formation of hydroxyl radicals, and the electrons mediate

reduction of Cr(VI) or Hg(II) by the formation of superoxide radicals. At the external TiO_2 surface, the positive hole and the excited electron either recombine or become involved in redox reactions with adsorbed groups.

Charge carrier generation:

$$TiO_2 + hv \rightarrow TiO_2\ (e^- + h^+) \quad (4.23)$$

Photoreduction of Cr(VI):

$$Cr_2O_7^{2-} + 14H^+ + 6e^- \rightarrow 2Cr^{3+} + 7H_2O \quad (4.24)$$

Photoreduction of Cr(VI):

$$Hg^{2+}{}_{(ads)} + 2e- \rightarrow Hg^0{}_{(ads)} \quad (4.25)$$

Generation of oxygen via water oxidation:

$$2H_2O + 4h^+{}_{vb} \rightarrow O_2 + 4H^+ \quad (4.26)$$

Photooxidation of citric acid (direct hole attach)

$$h^+{}_{vb} + Cit \rightarrow CO_2 + H_2O \quad (4.27)$$

Generation of hydroxyl radicals in the aqueous medium (hole pathway):

$$H_2O + h^+{}_{vb} \rightarrow {}^{\bullet}OH + H^+ \quad (4.28)$$

Photooxidation of citric acid (hydroxyl radical attach):

$$^{\bullet}OH + Cit \rightarrow CO_2 + H_2O \quad (4.29)$$

The conduction band electrons (e^-_{cb}) can reduce Cr(VI) to Cr(III) (Eq. 4.24) (Rodenas et al., 2000 & Testa et al., 2001), while Hg(II) can be reduced to Hg(0) (Eq. 4.25) (Chen and Ray, 2001) and the valence band hole (h^+v_b) can oxidise water to generate O_2 (Eq. 4.26). Therefore, the net photocatalytic reaction is the three-electron-reduction of Cr(VI) to Cr(III) with oxidation of water to oxygen, which is a kinetically slow four-electron process (Testa et al., 2001 & Schrank et al., 2002). While the Hg(II) is completely reduced to zero (Chen and Ray, 2001). The photocatalytic reductions of Cr(VI) and Hg(II) alone are quite slow. This results in the photogenerated electrons and holes recombination on surface of the semiconductor within a very short time, causing a reduction in the photocatalytic efficiency. Therefore, adding electron donors (sacrificial reagents or hole scavengers) to react irreversibly with the photogenerated VB holes (h^+_{vb}) is reported to suppress the electron-hole recombination (Bolton et al., 1996 & Li et al., 2001). If citric acid as an organic pollutant present in wastewater, the positive hole (h^+_{vb}) would oxidise either pollutant directly (Eq. 4.27) or water to produce hydroxyl radicals (•OH) which are strong oxidising agents (Eq.

4.28). Therefore, in the presence of citric acid, as a sacrificial electron donor, the photogenerated holes are rapidly scavenged from the TiO_2 particles, suppressing electron-hole recombination on immobilised TiO_2 and accelerating the reduction of Cr(VI) and Hg(II) by photogenerated electron (Schrank et al., 2002 & Deng et al., 2010).

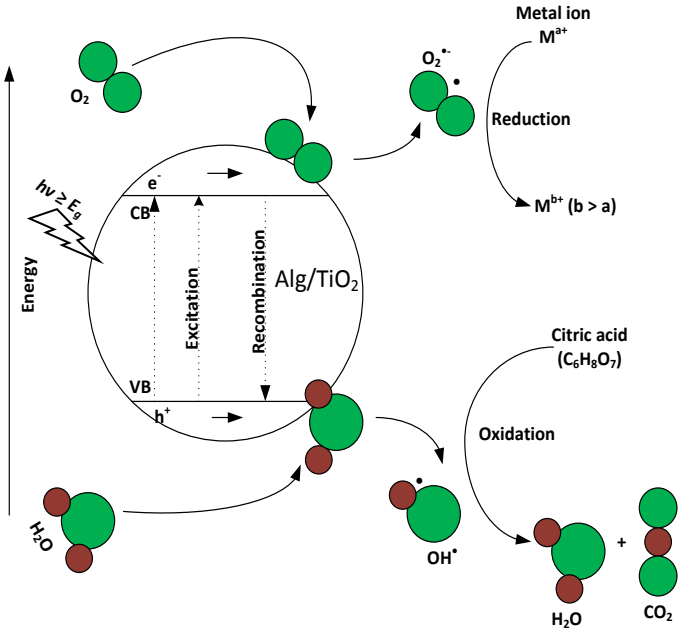

Figure 4.45: Mechanism of Alg/TiO_2-semiconductor photocatalysis process. Schematic of simultaneous photocatalytic reduction of Cr(VI) or Hg(II) and oxidation of citric acid.

4.2.4 Reusability of photocatalyst

One of today's main industrial wastewater treatment strategies is focused on the development of green technologies and management practices for environmental benefit. The catalyst lifetime is an essential parameter of the photocatalytic process, because its use for a longer period leads to a significant cost reduction of the treatment. The catalyst was recycled four times to investigate the number of times it can be reused after a photocatalytic treatment. After the optimised conditions (initial Cr(VI) concentration, 20 mg/L; initial Hg(II) concentration, 100 mg/L; Alg/TiO_2 dosage, 2 g/L; Cr(VI) initial pH, 2; Hg(II) initial pH, (8) for the photoreduction of the effluent were determined, the catalyst was recovered by separating the Alg/TiO_2 from the solution and then added into 100 mL $CaCl_2$ solution (4%) and stirred for 120 min at 25ºC and rinsed with high purity water. After regeneration, the catalyst was air-dried at room temperature and used to study its reusability.

As shown in Figure 4.46 Alg/TiO_2 demonstrated good stability after recovery and catalyst reuse is effective for both photoreduction of Cr(VI) and Hg(II). The first cycle reduced 100% of the both Cr(VI) and Hg(II) after 120 min of irradiation. Subsequently, the second cycle reduced 96 and 85% of the Cr(VI) and Hg(II), respectively. While the third cycle reduced 92 and 75% of the Cr(VI) and Hg(II), respectively. After these cycles, the efficiency markedly decreased, as illustrated in the fourth cycle, where the reduction efficiency decreased to 72 and 63% for Cr(VI) and Hg(II), respectively. However, the reduction efficiency of both Cr(VI and Hg(II) was still significant after four times of Alg/TiO_2 reuse. Agglomeration and sedimentation of the Cr(VI) and Hg(II) on the surface of the Alg/TiO_2 particles after each cycle of photoreduction is a possible cause of the observed decrease on the reduction efficiency, because each time the photocatalyst is reused new parts of the catalyst surface become unavailable for Cr(VI) and Hg(II) adsorption. In addition, this prevents excitation of photons during photocatalytic reduction process, reducing the efficiency of the catalytic reaction. Furthermore, the decrease in the removal efficiency may be due to the non-negligible adsorbed molecules on the Alg/TiO_2 surface and thus hinder the formation of electron-hole pairs which is crucial in photoreduction of Cr(VI) and Hg(II). Liu et al. (2013) utilised a pure recycled TiO_2-impregnated glutaraldehyde crosslinked alginate beads in the reduction of toxic heavy metals and observed that the reduction ratio remained at 100% after three times of reuse. Therefore, it can be concluded that the reusability of Alg/TiO_2 in Cr(VI) and Hg(II) photoreduction goes towards green chemistry key principles.

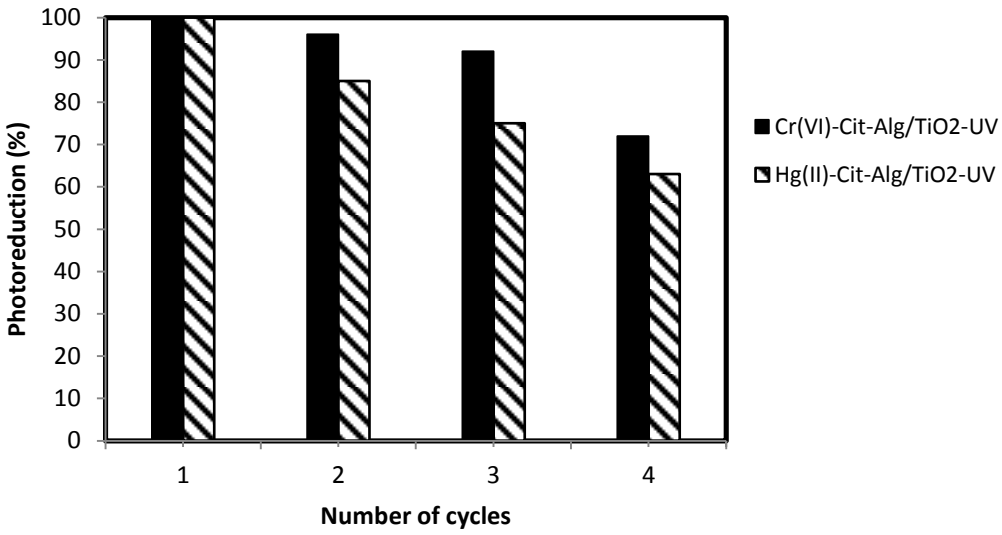

Figure 4.46: Reusability of Alg/TiO_2 photocatalyst.

4.2.5 Evaluation of photocatalytic reactor system

In this section, the optimised experimental parameters and the best photocatalytic systems discussed in the previous sections are used to evaluate the effectiveness of the photocatalytic reactor designed in this study. The effects of UV irradiation wavelength and light intensity and reaction time on the reduction rate of Cr(VI) and Hg(II) in binary systems are introduced and the results are discussed. Moreover, the ability to treat complex systems is of paramount practical importance since it is the actual case in the environment. For this reason an assessment of the performance of the photocatalytic reactor in terms of Cr(VI) and Hg(II) reduction and the treatment of a AMD real wastewater sample contaminated by both inorganic and organic species are presented in this study.

4.2.5.1 Effects of light intensity

In order to study the effect of light intensity on the reduction, experiments were conducted by varying UVC lamp power i.e 16 W, 24 W and 32 W. This emitted radiation wavelengths between 100 to 280 nm. The optimised values of initial concentration of Cr(VI), Hg(II) and citric acid, Alg/TiO_2 dosage and initial pH were used. The recycle flow rate was kept constant as 400 mL/min. It has been observed in Figure 4.47 and 4.48 that the rate of photocatalytic reaction increases with increasing the light intensity. This can be attributed to the fact that more electron-hole pairs will be generated due to an increased number of photons striking the semiconductor surface with an increase in the intensity of light. Therefore, more electrons will be available for reduction, resulting into the increase in rate of reaction.

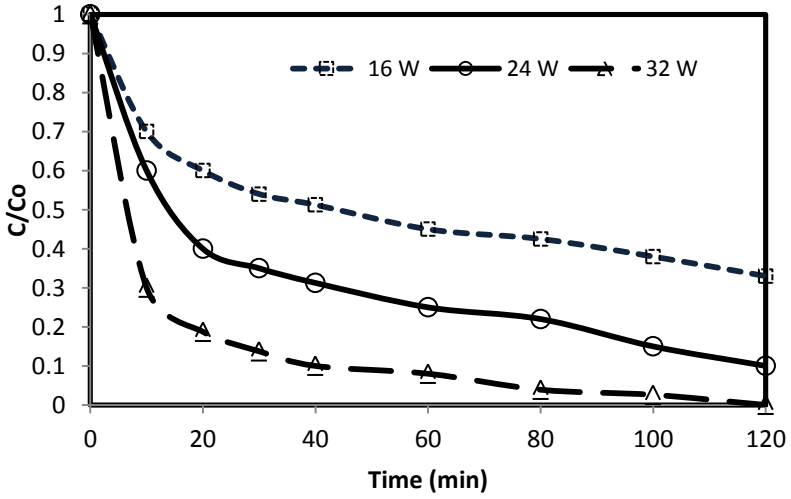

Figure 4.47: Effect of light intensity on rate of Cr(VI) reduction. Experimental conditions: initial Cr(VI) concentration, 20 mg/L; initial citric acid concentration, 20 mg/L; Alg/TiO_2 dosage, 2 g/L; initial pH, 2.

The percentage of Cr(VI) reductions under the UVC lamp power of 16 W, 24 W and 32 W are shown in Figure 4.47. At UVC power of 32 W, 60 min after irradiation the reduction of Cr(VI) was found to be 94.75%, then reduction efficiency increased with time and reached about 100% at 120 min. With UVC power of 24 W, 60 min after irradiation the reduction of Cr(VI) was found to be 84%, then reduction efficiency slowly increased with time and reached about 91% at 120 min. At UVC power of 16 W, 60 min after irradiation the reduction efficiency reached 62%, then reduction efficiency slightly increased with time, and reached about 75% at 120 min. The highest Cr(VI) reduction efficiency was found at the highest UVC lamp power used in this study (32 W). This result can be attributed to the radiation absorption of the photocatalyst and sufficient energy to overcome the photocatalyst band gap. Similar results were reported by Qamar et al. (2006) & Sharma et al. (2008), who observed an increase in the removal efficiency with an increase in light intensity during photocatalytic degradation.

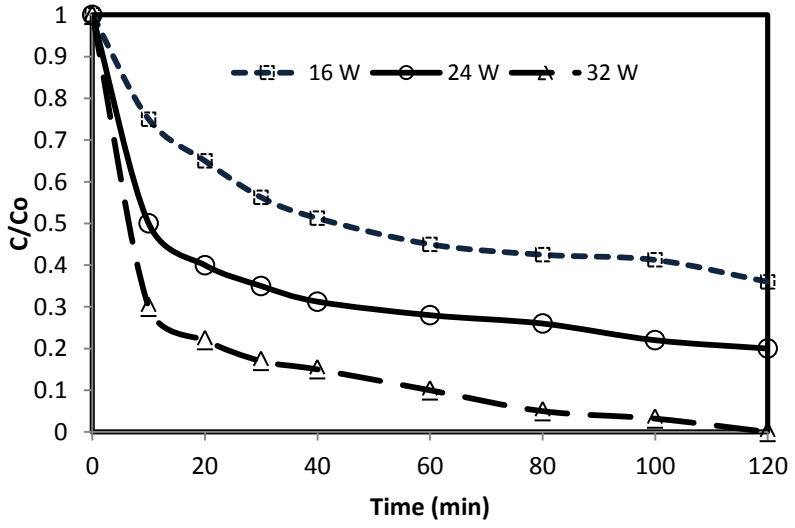

Figure 4.48: Effect of light intensity on rate of Hg(II) reduction. Experimental conditions: initial Hg(II) concentration, 100 mg/L; initial citric acid concentration, 100 mg/L; Alg/TiO_2 dosage, 2 g/L; initial pH, 8.

As shown in Figure 4.48, using different intensity of light source i.e. 16 W, 24 W and 32 W UVC lamps, increased the reduction of Hg(II) significantly. The increase in reduction was about 16.25% from 16 W to 24 W and 16.75% from 24 W to 32 W. At UVC power of 32 W, 60 min after irradiation the reduction of Hg(II) was approximately 90.75%, then reduction

efficiency increased with time and reached almost 98% at 120 min. At UVC power of 24 W, 60 min after irradiation the reduction of Hg(II) was approximately 72.68%, then reduction efficiency increased with time and reached about 81.25% at 120 min. At UVC power of 16 W, 60 min after irradiation the reduction efficiency was approximately 51%, then reduction efficiency increased with time, and reached about 65% at 120 min. The highest Hg(II) reduction efficiency was also found at the highest intensity of light source used in this study (32 W). The obtained results can be attributed to the fact that more electron-hole pairs will be generated due to an increased number of photons striking the semiconductor surface with an increase in the intensity of light. Therefore, more electrons will be available for Hg(II) reduction, resulting in an increase in rate of reaction. Similar results were obtained in the studies reported by Magrini et al. (1990), who observed an increase in radiation intensity with an increase in the removal rate for the organic contaminants. Therefore, it can be concluded that increasing light intensity will increase the reduction of Hg(II).

4.2.5.2 Application to real wastewater sample

Influent acid mine drainage (AMD) wastewater was collected from Witwatersrand gold fields Western basin (WB) and Mogale alloys ferrochrome mine discharge (FMD). The initial characteristics of influent wastewater were determined (Table 4.2). There was very little detectable change in water chemistry pH along the surface drainage waters pH, where AMD was collected. The pH readings of AMD measured on the field on the 14 November 2013 were: pH between 2.55 and 2.74 and pH between 2.26 and 2.28 for WB and FMD, respectively. The pH readings of AMD measured at Mintek laboratory on the 15 November 2013 were: pH between 2.57 and 2.75 and pH between 2.28 and 2.30 for WB and FMD, respectively. The AMD treated in this study typical showed strongly acidic pH and contained significant level of sulphates. The acidic characteristic of the AMD results from the percolation of water through sulphide minerals, commonly pyrite, which oxidises and dissociates when in contact with air and water. Therefore, Fe^{2+} is released and rapidly oxidises to Fe^{3+}, which precipitates as hydroxides. A cyclic series reaction takes place starting with the oxidation of Fe^{2+} to Fe^{3+}, Fe^{3+} which is easily reduced to Fe^{2+} by pyrite, releasing Fe^{2+}, which increases the acidity of the solution (Johnson et al., 2006).

Table 4.2: Physiochemical characterisation of the AMD used in toxic heavy metal removal studies.

Parameter (units)	Witwatersrand gold fields Western basin (WB)	Mogale alloys ferrochrome mine discharge (FMD)
pH	2.75	2.30
SO_4^{2-} (mg/L)	6126	5563
Fe (mg/L)	160.3	271.8
Al^{3+} (mg/L)	75	81
Ca^{2+} (mg/L)	83	182
Mg^{2+} (mg/L)	58	196
Mn^{2+} (mg/L)	3.121	22.253
Sn^{2+} (mg/L)	< 0.05	< 0.05
Cu^{2+} (mg/L)	< 0.05	< 0.05
Ag^{+} (mg/L)	< 0.05	< 0.05
Cr^{6+} (mg/L)	< 0.05	+ 20
Hg^{2+} (mg/L)	+ 100	< 0.05

* +, concentration was below detection, and then spiked into AMD wastewater.

The effect of reaction time on the photoreduction of Cr(VI) and Hg(II) from real AMD samples was studied between 10 to 180 min; results are shown in Figure 4.49. The Cr(VI)-AMD-Alg/TiO_2-UV system shows an increase from 26 to 61% reduction of Cr(VI) from 10 to 160 min, respectively. However, prolonging the reaction time to 180 min resulted in no increase in Cr(VI) photoreduction. The addition of citric acid to Cr(VI)-AMD-Alg/TiO_2-UV system resulted in an increase in Cr(VI) reduction and shorter reaction time. The Cr(VI) reduction was 40.5 and 88% between 10 to 140 min irradiation time, respectively. A further increase of reaction time to 180 min resulted in no increase in the reduction rate of Cr(VI). The reduction processes of Hg(II)-AMD-Alg/TiO_2-UV and Hg(II)-Cit-AMD-Alg/TiO_2-UV increase the reduction percentage of Hg(II) to 10 and 24% after 10 min irradiation, respectively. By prolonging the reaction time from 10 min to 160 min the reduction of Hg(II) was increased from 47 to 70%, respectively. However, the Hg(II) reduction remained unchanged with reaction time increased to over 160 min, which means maximum reduction limit of photocalysis for Hg(II).

These results indicate that the use of a recycled photocatalytic reactor designed for the purpose of this work is economical considering the shorter reaction time of 160 min achieved. This is because the economics of the photocatalysis treatment process depends on the power consumption of the radiation source, which is a function of the radiation time. Therefore, high energy will be required if the photocatalysis treatment process is to be operated for long periods. The long contact time of 160 min as compared to 120 min obtained using synthetic wastewater in the absence of other ions in this study, might be due to the some other ions present in real AMD wastewater (Table 4.2) which cannot be removed by photocatalysis due to their low positive standard reduction potential. It has been reported by Prairie et al. (1994), that the ability to remove toxic heavy metals depends on the standard reduction potential and a more positive standard potential than 0.4 V is required. In this case, electrons generated by the conduction band of Alg/TiO_2 will be hardly transferred to these ions with low positive standard reduction potential. Therefore as explained above the photoreduction of such ions might not be possible. However, these ions can be adsorbed on the Alg/TiO_2 surface and blocking the active sites of the Alg/TiO_2 catalyst (Abdullah et al., 1990). Thus, having a retarding effect on reduction of Cr(VI) and Hg(II). The reductants (citric acid or water) were required for the reduction of Cr(VI) and Hg(II). Hence the AMD contaminated with toxic heavy metals samples was spiked with citric acid. Furthermore, the optimisation studies in this study suggested that the rates of oxidation (citric acid) and reduction (Cr(VI) or Hg(II)) were intrinsically interrelated.

As seen from Figure 4.49, Cr(VI) was reduced more as compared to Hg(II). This trend might be explained by considering the thermodynamics of the photocatalytic reaction as explained earlier. The redox potential level to reduce the oxidation states of Cr(VI) and Hg(II) from hexavalent to trivalent and divalent to zero-valent, are +1.33 and +0.855 respectively. The positions of Cr(VI) and Hg(II) redox potentials lie below the flat band of TiO_2 as their standards potentials are more positive than 0.4 V. In this case, electrons generated by the conduction band of Alg/$Ti0_2$ can be transferred to both Cr(VI) and Hg(II) ions. However, photoreduction of Cr(VI) is expected to be high compared to Hg(II) due to their differences in standard potentials.

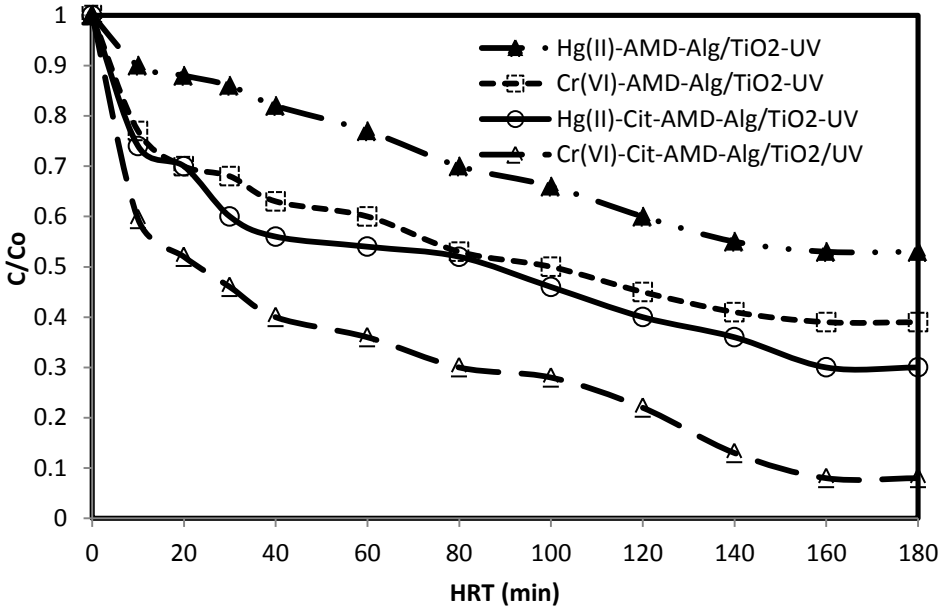

Figure 4.49: Reduction of Cr(VI) and Hg(II) contaminated AMD in the presence and absence of citric acid. [Experimental conditions for Cr(VI) reduction: initial Cr(VI) concentration, 20 mg/L; initial citric acid concentration, 60 mg/L; Alg/TiO_2 dosage, 2 g/L; initial pH, 2.30 and experimental conditions for Hg(II) reduction: initial Hg(II) concentration, 100 mg/L; initial citric acid concentration, 80 mg/L; Alg/TiO_2 dosage, 2 g/L; initial pH, 2.75].

4.2.6 Summary

The co-treatment of selected toxic heavy metals such as Cr(VI) and Hg(II), and citric acid in aqueous solution was successfully achieved using immobilised dandelion-like TiO_2 on calcium alginate under UV irradiation. The control experiments were investigated in this study and were designed to investigate possible effects of photolysis, adsorption and photocatalytic activity of the beads alone in the photocatalytic system. Results from control experiments indicated that the removal of Cr(VI), Hg(II) and citric acid by photolysis can be negligible. It was, therefore, reasonable to assume that photocatalysis was the dominant process for the removal of Cr(VI), Hg(II) and citric acid.

The effects of experimental parameters such as initial pH, Alg/TiO_2 dosage, initial concentration of Cr(VI), Hg(II) and citric acid and contact time were studied for the removal of Cr(VI), Hg(II) and citric acid by photocatalysis. It was found that the photocatalysis was highly dependent on these parameters. For Cr(VI) reduction, the highest reduction was obtained under initial pH, Alg/TiO_2, initial concentration and contact time in this study, which

were pH of 2, 2 g/L, 20 mg/L and 120 min, respectively. While for Hg(II) the highest reduction was obtained under the optimal experimental conditions in this study, with a Hg(II) solution that had a pH of 8, 2 g/L of Alg/TiO_2, an initial Hg(II) concentration of 100 mg/L and 120 min. The highest degradation of citric acid was obtained at pH of 2, 1.5 g/L of Alg/TiO_2, an initial citric acid concentration of 20 mg/L and 120 min. The kinetic model of the photoctalytic degradation of Cr(VI), Hg(II) and citric acid fits well with pseudo-first-order kinetics.

The effect of citric acid on the Cr(VI) and Hg(II) reduction was investigated in this study. Heterogeneous photocatalysis process was found to be able to simultaneously remove the citric acid and Cr(VI) or Hg(II). Citric acid acted as a hole scavenger. In the binary system, the reduction of Cr(VI) and Hg(II) was faster than in the single and ternary systems. It can be concluded that the presence of citric acid significantly improves the photoreduction of Cr(VI) and Hg(II) ions into less-toxic Cr (III) ion and Hg(0), respectively, as a function of concentration. The best approximate initial concentration of citric acid was 60 and 80 mg/L for the complete reduction of Cr(VI) and Hg(II), respectively. Addition of ferric ions to Cr(VI)-citric acid complex and Hg(II)-citric acid complex enhanced the reduction of Cr(VI) and Hg(II), and the complete removal of both Cr(VI) and Hg(II) were accomplished within 30 and 60 min of irradiation time, respectively. The reusability of Alg/TiO_2 was investigated in this study and reduction efficiency of both Cr(VI and Hg(II) was found to be still significant after four times of Alg/TiO_2 reuse. It could consequently be concluded that Alg/TiO_2 could be a very effective photocatalyst material for the removal of studied toxic heavy metals (Cr(VI) and Hg(II)) along with citric acid.

The final sets of experiments were carried out in the recycle photocatalytic reactor designed in this study using synthetic and real wastewater. The effectiveness of reduction of Cr(VI) and Hg(II) in AMD and effects of experimental parameters such as light intensity and reaction time were investigated. The photocatalytic reduction was found to increase with an increase of light intensity. It was found that the reaction time of 140 min led to an 88% reduction of Cr(VI). On the other hand the reaction time of 160 min led to a 70% reduction of Hg(II).

CHAPTER 5: CONCLUSIONS AND RECOMMENDATIONS

The efficiency of UV/TiO_2 photocatalysis process in the treatment of Cr(VI), Hg(II) and citric acid effluent was investigated. The study focused on the co-treatment of citric acid and toxic heavy metals in wastewater using as-prepared dandelion-like TiO_2 as photocatalyst. In the study, dandelion-like TiO_2 powder was synthesised. Composite catalysts of dandelion-like TiO_2 with Au (Au/TiO_2) and calcium alginate (Alg/TiO_2) were prepared and used as photocatalysts. The UV/TiO_2 photocatalytic studies were carried out in single and binary photocatalytic systems. With this study, recommendations were suggested for future studies.

5.1 Conclusions

5.1.1 Synthesise of dandelion-like TiO_2 powder and application

The dandelion-like TiO_2 was successfully synthesised using hydrothermal method. The experimental results showed that the hydrothermal reaction time and reaction temperature can critically affect the formation of the dandelion-like TiO_2. On the other hand, the increase in quantity of TiO_2 (scale-up) was found to not affect the chemical characteristics and composition of dandelion-like TiO_2. The obtained dandelion-like TiO_2 exhibited excellent photocatalytic activity, which is higher than P25 titania powder.

5.1.2 Characterisation of dandelion-like TiO_2 powder

The dandelion-like TiO_2 structures were characterised using a range of techniques such as XRD, SEM, TEM, EDX and BET. XRD analysis shows the presence of pure rutile phase, while SEM images revealed the presence of spherical morphology of the particles. EDX data confirmed the composition of Ti to O ratio to be 1:2. From TEM analysis, the average particle size of dandelion-like TiO_2 was found to be 17 nm. BET surface area of the dandelions-like TiO_2 was 81 $m^2.g^{-1}$ with pores of about 3.2 nm.

5.1.3 Modification of dandelion-like TiO_2 powder

Au nanoparticles were deposited onto dandelion-like TiO_2 by deposition-precipitation method. This enhanced the photocatalytic activity of dandelion-like TiO_2 by 17 and 31% for Cr(VI) and Hg(II) reduction, respectively. A composite catalyst of dandelion-like TiO_2 immobilised on Ca-alginate was prepared using one-step encapsulation method. The XRD analysis showed that the Bragg diffraction peaks of rutile dandelion-like TiO_2 decrease due to the amorphous solid Ca-

alginate. Also, the SEM analysis of the Alg/TiO_2 composite catalyst showed that the dandelion-like TiO_2 nanoparticles were well dispersed on the calcium alginate surface. The spherical Alg/TiO_2 gel beads aided the solid-liquid separation for UV/TiO_2 photocatalysis process, but also reduced photocatalytic efficiency due to light scattering and the possibility of Alg/TiO_2 reuse.

5.1.4 Photocatalytic treatment of citric acid and toxic heavy metals

Photocatalytic experiments were carried out and it was found that the UV/TiO_2 photocatalytic efficiency depends on the type of pollutants, initial pH of the solution, photocatalyst dosage, contact time and substrate initial concentration. The photocatalytic efficiency decreased with increasing the initial concentration and initial pH of Cr(VI) and citric acid solution. While for Hg(II) the photocatalytic efficiency decreased with decreasing the initial concentration and initial pH. Kinetic experiments showed that the UV/TiO_2 photocatalytic process fits well with pseudo-first-order kinetics under the experimental conditions in this study.

5.1.5 Photocatalytic co-treatment of citric acid and toxic heavy metals

UV/TiO_2 photocatalytic process was found to be able to simultaneously reduce the Cr(VI) and Hg(II) with citric acid. In a binary system, the reduction of Cr(VI) and Hg(II) was faster than in single and ternary systems. It was concluded that the presence of citric acid significantly improved the photoreduction of Cr(VI) and Hg(II) ions into less-toxic Cr (III) ion and Hg(0), respectively, as a function of concentration. Also, the addition of ferric ions to Cr(VI)-citric acid complex and Hg(II)-citric acid complex are shown to enhance the reduction of Cr(VI) and Hg(II), where a complete reduction was accomplished within 30 min and 60 min of irradiation time, respectively.

5.1.6 Reusability of Alg/TiO_2

Reusability of Alg/TiO_2 composite was investigated in this study. The photocatalytic activity of both Cr(VI) and Hg(II) was still significant after four times of Alg/TiO_2 composite reuse. Therefore, it was established that, the reusability of Alg/TiO_2 composite in Cr(VI) and Hg(II) photoreduction is possible. Consequently, it can also be concluded that Alg/TiO_2 could be an economical photocatalyst for the removal of toxic heavy metals such as Cr(VI) and Hg(II) along with citric acid.

5.1.7 Influence of UV irradiation wavelength and light intensity

The effect of UV wavelength was investigated using different light sources in a batch reactor. The experimental results indicated that the order of Cr(VI) and Hg(II) reduction efficiency using

different light sources was shown to be UVC > Sunlight > UVLED. It was also found that the dandelion-like TiO_2 could be an efficient photocatalyst under both UV and solar lights. The influence of light intensity was only investigated for the recycle photocatalytic reactor as the reactor was designed with different UV light intensities. It was generally observed that photocatalytic reduction of Cr(VI) and Hg(II) along with citric acid increased with an increase of light intensity.

5.2 Recommendations

In order to have a further investigation to improve the outcomes of this research area, the following recommendations for future studies are proposed:

5.2.1 Characterisation of dandelion-like TiO_2 powder

The above study was constrained by the limited laboratory resources such as diffuse reflectance spectroscopy (DRS). A natural progression would involve characterising the Au/TiO_2 composite by DRS spectroscopy (to confirm the presence of surface plasmon) and measuring the band gap.

5.2.2 Photocatalytic co-treatment of citric acid and toxic heavy metals

The results in this study can be applied in wastewater management scenarios, particularly in the removal of Cr(VI) and Hg(II) along with citric acid in wastewater using UV/TiO_2 photocatalytic treatment process. However, it will be essential to perform a comprehensive study further exploring the application of the Alg/TiO_2 composite for the removal of other toxic heavy metals and ions present in AMD. This will ensure that the effect of anions, competing cations and organics present in actual wastewater systems along with AMD, can be investigated in detail to explore the use of Alg/TiO_2 composite in real wastewater. Finally, to study the toxicity of the intermediates formed and various methods for the disposal of the final solution produced from the experiments of this study. Therefore, an appropriate disposal method would ensure the effluent disposed off to the environment is free from toxic substances.

REFERENCES

AARTHI, T. & MADRAS, G. 2008. Photocatalytic reduction of metals in presence of combustion synthesized nano-TiO_2. *Catalysis Communications,* 9(5):630-634.

ABDULLAH, M., LOW, G. & MATHEWS, R.W. 1990. Effects of common inorganic ions on rates of photocatalytic oxidation of organic carbon over illuminated titanium dioxide. *Journal of Physical Chemistry,* 94:6820.

AKLIL, A., MOUFLIHB, M. & SEBTI, S. 2004. Removal of heavy metal ions from water by using calcined phosphate as a new adsorbent. *J. Hazard. Mater,* 112:183–190.

ALGARIN, P.C. 2008. Effects of Zn doping and high energy ball milling on the photocatalytic properties of TiO_2. Master's thesis. Florida, USA: University of South Florida.

ANANDAN, S. & YOON, M. 2003. Photocatalytic Activity of the Nano-sized TiO_2-supported Y-Zeolites. *Journal of Photochem. and Photobiol,* 9:5-18.

ANI, J. K., SAVITHRI, S. & SURENDE, G. D. 2005. Characteristics of titania nanoparticles synthesized through low temperature aerosol process. *Aerosol and air quality research,* 5:1-13.

ANPO, M., SHIMA, T., KODAMA, S. & KUBOKAWA, Y. 1987. Photocatalytic hydrogenation of propyne with water on small-particle titania: size quantization effects and reaction intermediates. *Journal of Physical Chemistry,* 91:4305-4310.

APHA. 1995. Standard methods for the examination of water and wastewater. Washington, DC: American Public Health Association.

ASSADI, A., DEHGHANI, M.H., NASSERI, N.R.S., & MAHVI, A.H. 2012. Photocatalytic reduction of hexavalent chromium in aqueous solutions with zinc oxide nanoparticles and hydrogen peroxide. *Environment Protection Engineering,* 38:5277-20401.

AUGUGLIAROA, V., BELLARDITA, M., LODDOA, V., PALMISANOA, G., PALMISANOA, L. & YURDAKALB S. 2012. Overview on oxidation mechanisms of organic compounds by TiO_2 in heterogeneous photocatalysis. *Journal of Photochemistry and Photobiology*,13:224–245.

BAHNEMANN, D. 2004. Photocatalytic water treatment: solar energy applications. *Sol. Energy*, 77:445-459.

BAI, X., XIE, B., PAN, N., WANG, X. & WANG, H. 2008. Novel three-dimensional dandelion-like TiO_2 structure with high photocatalytic activity, *Journal of Solid State Chemistry*, 181:450-456.

BAO, X., YAN, S.S., CHEN, F. & ZHANG, J. 2005. Preparation of TiO_2 photocatalyst by hydrothermal method from aqueous peroxotitanium acid gel. *Materials Letters*, 59:412-415.

BARAKAT, M.A. 2011. New trends in removing heavy metals from industrial wastewater. *Arabian Journal of Chemistry*, 4:361–37.

BHATKHANDE, D.S., PANGARKAR, V.G. & BEENACKERS, A.A. 2001. Photocatalytic Degradation for Environmental Applications- a Review. *J. Chem. Technol. Biotechnol*, 77: 102–116.

BOLTON, J. R. 1996. Solar photoproduction of hydrogen: A Review. *Solar Energy*, 57:37-50.

BUSSI, J., OHANIAN, M., VAZQUEZ, M. & DALCHIELE, D.A. 2002. Photocatalytic Removal of Hg from Solid Wastes of Chlor-Alkali Plant. *J. Environ. Eng*, 128:733.

CATANO, F.A., HINCAPRE, E.A., MARIN, J.M., RESLREPO, G.M. & VALENCIA, S.H. 2012. A comparative study between TiO_2 and ZnO photocatalyst – photocatalytic degradation of cibacron yellow. FN –2R dye, *Lat. Am. app. res*, 42:33-38.

CHAUDHARY, R. & THAKUR, R.S. 2012. Photocatalytic treatment of industrial wastewater containing chromium as a model pollutant-effect on process parameters and kinetically studies. *J. renewable sustainable energy,* 4:53-121.

CHEN, D. & RAY, A.K. 1999. Photocatalytic kinetics of phenol and its derivatives over UV irradiation TiO_2. *Appl.Catal.B: Environ,* 23:143-157.

CHEN, H., SHAO, Yl., XU, Z., WAN, H., WAN, Y., ZHENG, S. & ZHU, D. 2011. Effective catalytic reduction of Cr(VI) over TiO_2 nanotube supported Pd catalysts. *Applied Catalysis B: Environmental,*105:255-262.

CHEN, S.F. & CAO, G.Y. 2005. Study on the photocatalytic reduction of dichromate and photocatalytic oxidation of dichlorvos. *Chemosphere,* 60:1308-1315.

CHEN, X.B. & MAO, S.S. 2007. Titanium dioxide nanomaterials: synthesis, properties, modifications and applications. *Chemical Reviews,* 107:2891–2959.

CHEN, C.C., LU, C.S., CHUNG, Y.C. & JAN, J.L. 2007. UV light induced photodegradation of malachite green on TiO2 nanoparticles. *J. Hazard. Mater,* 141:520-528.

CHEN, D. & RAY, A.K. 2001. Removal of toxic metal ions from wastewater by semiconductor photocatalysis. *Chem. Eng. Sci,* 5:1561–1570.

CHONG, M.N., JIN, B., CHOW, C.W.K. & SAINT, C. 2010. Recent developments in photocatalytic water treatment technology: A review. *Water Res,* 44:2997–3027.

COLO´N, G., HIDALGO, C. & NAVI´O, J.A. 2001. Photocatalytic deactivation of commercial TiO_2 samples during simultaneous photoreduction of Cr(VI) and photooxidation of salicylic acid. *J. Photochem. Photobiol. A,* 138:79–85.

CRISTANTE, V. M., ARAUJO, A. B., JORGE S, M. A., FLORENTINO, A.O., VALENTE, J. P. S. & PADILHA, P. M. 2006. Enhanced photocatalytic reduction of Hg(II) in aqueous medium by 2-aminothiazole-modified TiO_2 particles. *J. Braz. Chem. Soc,* 17 (3): 453-457.

DEGEN, A. & KOSEC, M. 2002. Effect of pH and impurities on the surface charge of zinc oxide in aqueous solution. *J Eur Ceram Soc*, 20:667-673.

DENG, L., DENG, N., MOU, L. & ZHU, F. 2010. Photo-induced transformation of Hg(II) species in the presence of Nitzschia hantzchiana, ferric ion, and humic acid. *Journal of Environmental Science*, 22:76-83.

DONG, X., TAO, J., Li, Y.Y. & ZHU, H. 2009. Enhanced photoelectrochemical properties of F-containing TiO_2 sphere thin film induced by its novel hierarchical structure. *Applied Surface Science*, 255(16):7183-7187.

DOU, B.L., DUPONT, V., PAN, W.G & CHEN, B.B. 2001. Removal of aqueous toxic Hg(II) by synthesized TiO_2 nanoparticles and TiO_2/montmorillonite. *Chemical Engineering Journal*, 2:166-631.

DOZZI, M.V., SACCOMANNI, A. & SELLI, E. 2012. Cr(VI) photocatalytic reduction: Effects of simultaneous organics oxidation and of gold nanoparticles photodeposition on TiO_2. *Journal of Hazardous Materials*, 211-212:188-195.

ECCLES, H. 1999. Treatment of metal-contaminated wastes: why select a biological process Trends. *Biotechnol*, 17:462-465.

FREUNDLICH, H. Adsorption in solution. 1906. *Phys. Chem. Soc*, 40:1361-1368.

FU, F. & WANG, Q. 2010. Removal of heavy metal ions from wastewaters: A review. *Journal of Environmental Management*, 92:407-418.

FUJISHIMA, A. & HONDA, K. 1972. Electrochemical photolysis of water at a semiconductor electrode. *Nature*, 238: 37-38.

FUJISHIMA, A., RAO, T.N. & TRYK, D.A. 2000l. Titanium dioxide photocatalysis. *J. Photochem. Photobiol. C: Photochem. Rev*, 1:1-21.

FUJISHIMA, Al., ZHANG, X. T. & TRYK, D. A. 2008. TiO_2 photocatalysis and related surface phenomena. *Surface Science Reports,* 63:515–582.

GABERELL, M., CHIN, Y., HU, S.J. & SULZBERGER, B. 2003. Role of dissolved organic matter composition on the photoreduction of Cr(VI) to Cr(III) in the presence of iron. *Environ. Sci. Technol,* 4:403–4409.

GHERBI, Rl., NASRALLAH, N., AMRANE, A., MAACHI, R &TRARI, M. 2011. Photocatalytic reduction of Cr(VI) on the new hetero-system $CuAl_2O_4/TiO_2$. *J Hazard Mater,* 186:1124–1130.

GKIKA, El., TROUPIS, A., HISKIA, A. & PAPACONSTANTINOU, E. 2005. Photocatalytic reduction and recovery of mercury by polyoxometalates, *Environ. Sci. Technol,* 39:4242–4248.

GLATZMAIER, G.C. 1991. Innovative solar technologies for treatment of concentrated organic wastes. *Sol. Energy Mater.*, 24:672.

GLATZMAIER, G.C. NIX, R.G. & MEHOS, M.S. 1990. Solar destruction of hazardous chemicals. *J. Environ. Sci. Health A*, 25:571-581.

GUETTAI, N. & AMAR, H.A. 2005. Photocatalytic oxidation of methyl orange in presence of titanium dioxide in aqueous suspension. Part II: Kinetics study. *Desalination,* 185:427–437.

HABIBI, M.H. & VOSOOGHIAN, H. 2005. Photocatalytic degradation of some organic sulfides as environmental pollutants using titanium dioxide suspension. *J. Photochem. Photobiol*, 174:45-52.

HARIKUMAR, P.S. & LITTY, J. 2012. Kinetic and thermodynamics studies of as (III) adsorption onto iron nanoparticles entrapped ca-alginate beads. *International Journal of Plant, Animal and Environmental Sciences,* 2:159-156.

HARIKUMAR, P.S., LITTY, J. & DHANYA, A. 2013. Photocatalytic degradation of textile dyes by hydrogel supported titanium dioxide nanoparticles. *Journal of Environmental Engineering & Ecological Science*,2:2050-1323.

HARIKUMAR, P.S, LITTY, J. & MANJUSHA, C.M. 2011. Bio synthesis of silver nanoparticles and its application in microbial treatment of drinking water. Nano *Science and Nano Technology*, 5:23-27.

HERRMANN, J.M. 1999l. Heterogeneous photocatalysis: fundamentals and applications to the removal of various types of aqueous pollutants. *Catal. Today*, 53:115-129.

HOFFMAN, M.R., MARTIN, S.T., CHOI, W. & BAHNEMANN D.W. 1995. Environmental applications of semiconductor photocatalysis. *Chemical Reviews,* 95:69-96.

HOSONO, E., FUJIHARA, S., KAKIUCHI, K. & IMAI, H. 2004. Growth of submicrometer scale rectangular parallelepiped rutile TiO_2 films in aqueous $TiCl_3$ solutions under hydrothermal conditions. *J. Am. Chem. Soc,* 126:7790–7791.

HSU, C.C. & Wu, N.L. 2005. Synthesis and photocatalytic activity of ZnO/ZnO_2 composite, *J. Photochem. Photobiol. A Chem*, 172(3):269-274.

HU, X.L., YU, J.C. & GONG, J.M. 2007. Fast Production of self-assembled a-Fe_2O_3 hierarchical nanoarchitectures. *J. Phys. Chem. C*, 111: 11180-11185.

IBHADON, A.O. & PAUL, F. 2013. Heterogeneous photocatalysis: recent advances and applications: An review. *Catalysts,* 3:2073-4344.

IDRIS, A., HASSAN, N., ISMAIL, N.S.M., MISRAN, E., YUSOF, N.M., NGOMSIK, Al. & BEE, A. 2010. Photocatalytic magnetic separable beads for chromium(VI) reduction. *Water Res*, 44:1683–1688.

JEROME, O.N. 1994. Mechanistic steps in the photoreduction of mercury in natural waters. *The science of the Total Environment*, 154(1):1-8.

JIA, Z., LI, Y. & LIU, J. 2006. Morphological control and photodegradation behaviour of rutile TiO_2 prepared by a low-temperature process. *Materials Letters,* 60:1753–1757.

JIANG, J., GU, F., SHAO, W. & LI, C. Z. 2012. Facile synthesis of mesoporous tin oxide spheres and their applications in dye-sensitized solar cells. *Industrial and Engineering Chemistry Research,* 51:2838–2845.

JIN, Yl., YAN-LIN, L., YUAN, W., XIAO-PING, L., SHE-JUN, H. & WEI-SHAN, L. 2012. Synthesis of dandelion-like TiO_2 microspheres as anode materials for lithium ion batteries with enhanced rate capacity and cyclic performances. *International journal of minerals, metallurgy and materials,* 19:1058.

JOHNSON, K.L. & YOUNGER P.L. 2006. The co-treatment of sewage and mine waters in aerobic wetlands. *Engineering geology,* 85: 53-61.

KALIDHASAN , S., GANESH, M., SRICHARAN, S. & RAJESH, N. 2009. Extractive separation, determination of chromium in tannery effluents and electroplating waste water using tribenzylamine as the extractant. *J. Hazard. Mater,* 165:886–892.

KAMAT, P.V. 2010. Graphene-based nanoarchitectures. Anchoring semiconductor and metal nanoparticles on a two-dimensional carbon support. *J. Phys. Chem. Lett,* 1:520–527.

KANNAN, N & MALAR, J.S. 2005. Removal of mercury(II) ions by adsorption onto dates nut and commercial activated carbons: A comparative study. *Indian journal of chemical engineering,* 12:522-527.

KARTHIKA, C & SEKAR, M. 2012. Removal of Hg (II) ions from aqueous solution by Acid Acrylic Resin A Study through Adsorption isotherms Analysis. *I Res. J. Environment Sci,* 1:34-41.

KHALIL, L.B., ROPHAEL, M.W. & MOURAD, W.E. 2002. The removal of the toxic Hg(II) from water by photocatalysis. *Applied Catalysis B: Environmental,* 36:125-130.

KHIN, M.M., NAIR, A.S., BABU, V.J., MURUGAN, R & RAMAKRISHNA, S. 2012. A review on nanomaterials for environmental remediation. *Energy and Environmental Science,* 5:8075–8109.

KIELBASSA, S., HABICH, A., SCHNAIDT, J., BANSMANN, J., WEIGL, F., BOYEN, H.G., ZIEMANN, P. & JURGEN, R. 2006. On the morphology and stability of Au nanoparticles on TiO_2(110) prepared from micelle stabilized precursors. Langmuir, 22: 7873–7880.

KORMANN, C., BAHNEMANN, D.W., HOFFMANN, M.R. 1991. Photolysis of chloroform and other organic molecules in aqueous TiO_2 suspensions. *Environ. Sci. Technol.* 25, 494-500.

KOSMULSKI M. 2006. pH-dependent surface charging and points of zero charge. III. Update. *J Colloid Interface Sci.* 298(2):730-41.

KRISHNA, D., KRISHNA, K.S. & SREE R.P. 2013. Response surface modelling and optimization of chromium (VI) removal from aqueous solution using borasus flabellifer coir powder. *International journal of applied science and engineering,* 2: 213-226.

KUBACKA, A., FERNANDEZ-GARCIA, M. & COLON, G. 2012. Advanced nanoarchitectures for solar photocatalytic applications. *Chemical Society Reviews,* 112: 1555–1614.

KURNIAWAN, T.A., CHAN, G.Y.S., LO, W.H. & BABEL S. 2006. Physicochemical treatment techniques for wastewater laden with heavy metals. *Chem. Eng. J.* 118: 83–98.

LANGMUIR, I. 1981. The adsorption of gases on plane surfaces of glass, mica, and platinum. *J. Am. Chem. Soc,* 40:1361–1368.

LEE, H., DUK-WON, K., JUNHW, A.C. & DONG, H.L. 2003. Degradation kinetics of recalcitrant organic compounds in a decontamination process with UV/H_2O_2 and UV/H_2O_2/TiO_2 Processes. *Korean Journal of Chemcal Engineering* 20(3):503-508.

LI, D. & HANEDA, H. 2003. Morphologies of zinc oxide particles and their effects on photocatalysis. *Chemosphere,* 51:129–137.

LI, H.X., BIAN, Z.F., ZHU, J., ZHANG D.Q., LI G.S., HUO Y.N., LI, H. & LU, Y.F. 2007. Mesoporous Titania Spheres with Tunable Chamber Stucture and Enhanced Photocatalytic activity. *J. Am. Chem. Soc.* 129:8406-8407.

LI, Y., LU, G. & LI, S. 2001. Photocatalytic hydrogen generation and decomposition of oxalic acid over platinized TiO_2. *Applied Catalysis A*: *General*, 214:179-185.

LINIC, S., CHRISTOPHER, P. & INGRAM, D.B. 2011. Plasmonic-metal nanostructures for efficient conversion of solar to chemical energy. *Nature Materials,* 10:911–921.

LINSEBIGLER, A.L., LU, G. & YATES, J.T.1985. Photocatalysis on TiO_2 surfaces Principles, mechanisms, and selected results. *Chem. Rev,* 95:735–758.

LITTER, M.I. 1999. Heterogeneous photocatalysis of transition metal ions in photocatalytic systems. *Appl. Catal. B: Environ*, 23:89–114.

LIU, J. P., HUANG , X.T., LI, Y.Y., DUAN, J.X. & AI, H.H. 2006. Synthesis of flower-like ZnO microstructures via a simple solution route. *Materials Chemistry and Physics*, 98:523–527.

LIU, Y., HU, X., WANG, H., CHEN, A., LIU, S., GUO, Y., HE, Y., XI, H., LI, J., Shao-heng, L., Wang, Y. & Zhou, L. 2013. Photoreduction of Cr(VI) from acidic aqueous solution using TiO_2-impregnated glutaraldehyde-crosslinked alginate beads and the effects of Fe(III) ions. *Chemical Engineering Journal.* 226:131–138.

LYN, M.E & YING, D.Y. 2010. Drying model for calcium alginate beads. *Ind. Eng. Chem*, 49:1986-1990.

MA, C.M., SHEN, Y.S. & LIN, P.H. 2012. Photoreduction of Cr(VI) ions in aqueous solutions by UV/TiO_2 photocatalytic processes. *International journal of photoenergy,* 10: 1155-381971.

MAGRINI, K.A & WEBB J.D. 1990. Photocatalytic decomposition of aqueous organic compounds as a function of solar irradiation intensity. In *Solar Engineering 1990, presented at the 12th annual ASME International Solar Energy Conference, Miami, FL, April 1-4, Beard, J. T., Ebadian, M. A., Eds.; ASME: New York,* 1:159-162.

MALATO, S., FERNÁNDEZ-IBÁÑEZ, P., MALDONADO, M.I., BLANCO, J. & GERNJAK, W. 2009. Decontamination and disinfection of water by solar photocatalysis: recent overview and trends. *Catalysis Today,* 147:1–59.

MANOHAR, D.M., KRISHNAN, K.A. & ANIRUDHAN, T.S. 2002. Removal of mercury(II) from aqueous solutions and chlor-alkali industry wastewater using 2-mercaptobenzimidazole-clay. *Water Research,* 36:1609.

MANOJAR, A.L., SHAJI, V. & SANTHOSH, S.N. 2012. Photocatalytic water treatment by titanium dioxide: recent updates. *Catalysts,* 2:572-601.

MAZDIYASNI, K.S., LYNCH, C.T. & SMITH, J.S. 1965. Preparation of ultra-high-purity submicron refractory oxides. *J. Am. Ceram. Soc.* 48:372.

MEICHTRY, J.M., BRUSA, M., MAILHOT, G., GRELA, M.A., LITTER, M.I. 2007. Heterogeneous photocatalysis of Cr(VI) in the presence of citric acid over TiO_2 particles: relevance of Cr(V)-citrate complexes. *Appl Cat B: Env*, 71:101–107.

MEICHTRY, J.M., QUICI, N., MAILHOT, G., LITTER, M.2010. Heterogeneous photocatalysis degradation of citric acid over TiO_2 I: Mechanism of 3-oxoglutaric acid degradation. *Applied Catalysis B: Environmental*, 454-463.

MEKATEL, H., AMOKRAN, S., BELLAL, B., TRARI, M. & NI-BOU, D. 2012. Photocatalytic reduction of Cr(VI) on nanosized Fe_2O_3 supported on natural algerian clay: characteristics, kinetic and thermodynamic study. *Chemical Engineering Journal*, 200-202: 611-618.

MELTZER, A., BARRY, M. & YASKO G. 2006. pH dependence of iron photoreduction in a rocky mountain stream affected by acid mine drainage. *Environmental Science and Technology,* 34:254 – 258.

MILLS, A., ELLIOTT, S.N., PARKIN, I.P., O'NEILL, S.A. & CLARK R.J. 2002. Novel TiO_2 CVD films for semiconductor photocatalysis, *Journal of Photochemistry Photobiology A: Chemistry*, 151:171-179.

MOHAMMADI, T., MOHEBB, A., SADRZADEH, M. & RAZMI, A. 2005. Modeling of metal ion removal from wastewater by electrodialysis. *Sep. Purif. Technol.* 41:73–82.

MUNEER, M., PHILIP, R. & DAS, S. 1997. Photocatalytic degradation of waste water pollutants. Titanium dioxide-mediated oxidation of a textile dye, acid blue 40. *Res.Chem. Intermed,* 23:233–246.

MUNOZ, J. & DOMENECH, X. 1990. TiO_2 Catalysed reduction of Cr(VI) in aqueous solutions under ultraviolet illumination. *J. Appl. Electrochem*, 20:518.

MYTYCH , P., KAROCKI, A. & STASICKA, Z. 2003. Mechanism of photochemical reduction of Cr (VI) by alcohols & its environmental aspects. *J. Photochem. Photobiol. Chem*, 160:163-170.

NEZAMZADEH-EJHIEH, A. & SALIMI, Z. 2010. Decolorization of a binary azo dyes mixture using CuO incorporated nanozeolite-x as a heterogeneous catalyst and solar irradiation. *Appl. Catal. A: Gen,* 390:110–118.

NGAH W, S.W., ENDUD, C.S. & MAYANAR, R. 2002. Removal of copper (II) ions from aqueous solution onto chitosan and cross-linked Chitosan beads. *React Funct Polym,* 50:181-190.

NGUYEN, V. H. H., AMAL, R & BEYDOUN, D. 2006. Photodeposition of CdSe using Se-TiO_2 suspensions as photocatalysts, *J. Photochem. Photobiol. A: Chemistry*, 179(1-2): 57-65.

NILISHA, I. & YOGESH, P. 2014. Management of hexavalent chromium from industrial waste using low-cost waste biomass. *Procedia - Social and Behavioral Sciences*, 133:219-224.

NOMANBHAY, S.M. & PALANISAMY, K. 2005. Removal of heavy metal from industrial wastewater using chitosan coated oil palm shell charcoal. *Electron. J. Biotechnol*, 8:43–53.

OKAMOTO, K., YAMAMOTO, Y., TANAKA, H., TANAKA, M. & ITAYA, A.1985b. Photo oxidation of phenol hole oxidation of OH radical attack direct hole oxidation of the phenyl ring cation radical. *Itaya, Bull. Chem. Soc. Jpn.* 58:2023.

OKAMOTO, K., YAMAMOTO, Y., TANAKA, H., TANAKA, M. & ITAYA, A.1985a. Photocatalyst oxidation of OH versus hole oxidation intermediate Itaya A, *Bill. Chem. Soc. Jpn*, 58:2015.

PAPAGEORGIOU, S.K., KATSAROS, E.P., FAVVAS, G.E., ROMANOS, C.P., ATHANASEKOU, K.G., BELTSIOS, O.I., TZIALL, A. & FALARAS, P. 2012. Alginate fibers as photocatalyst immobilizing agents applied in hybrid photocatalytic/ultrafiltration water treatment processes, *Water Res*, 46:1858-1872.

PELAEZ, M., NOLAN, N.T., Pillai, S.C., Seery, M.K., Falaras, P., Kontos, A.G., Dunlop, P.S.M., Hamilton, J.W.J., Byrne, J.A., O'SHEA, K. 2012. A review on the visible light active titanium dioxide photocatalysts for environmental applications. *Appl. Catal*, 125:331-349.

PELIZZETTI, E. & MINERO, C. 1993. Mechanisms of the photo-oxidative degradation or organic pollutants over TiO_2 particles. *Electrochimica Acta*, 38: 47-55.

PETRUCCI R. H., HARWOOD, W.S. & HERRINGET, F.G. 2002.General chemistry: principles and modern applications. *Upper Saddle River, NJ: Prentice-Hall*, 8:749-762.

PINGFAN, D., LIXIN, S., JIE, X. & HOUBAO, C. 2013. Photocatalytic degradation of Rhodamine B using electrospun TiO2 and ZnO nanofibers: a comparative study. *J Mater Sci*, 48:8386–8392.

POPURI, S.R., JAMMALA, A., REDDY, K.V., NAGA, S. & ABBURI, K. 2007. Biosorption of hexavalent chromium using tamarind (Tamarindus indica) fruit shell-a comparative study. *Electronic Journal of Biotechnology*, 10:358-367.

PRAIRIE, M.R., EVANS, L.R., STANGE, B.M & MARTÌNEZ, S.L. 1993. An investigation of titanium dioxide photocatalysis for the treatment of water contaminated with metals and organic chemicals, *Environ. Sci. Technol,* 27:1776–1782.

PRAIRIE, M. R., EVANS, L. R., MARTINEZ, S. L.1994. Destruction of organics and removal of heavy metals in water via TiO_2, Photocatalysis. In Chemical Oxidation: Technology for the Nineties, 2nd International Symposium. *Technomic Publishing Company: Lancaster,* 1:428-441.

PRIMO, A., CORMA, A. & GARCIA, H. 2011. Titania supported gold nanoparticles as photocatalyst. *Physical Chemistry Chemical Physics*, 13:886–910.

QAMAR, M., GONDAL, M.A. &YAMANI, Z.H. 2011. Synthesis of nanostructured NiO and its application in laser-induced photocatalytic reduction of Cr(VI) from water. *J. Mol. Catal. A: Chem*, 341:83–88.

QAMAR, M., MUNEER, M. & BAHNEMANN, D. 2006. Heterogeneous photocatalysed degradation of two selected pesticide derivatives, triclopyr and daminozid in aqueous suspensions of titanium dioxide. *Journal of Environmental Management,* 80:99-106.

QIAN, Y., CHEN, Q., CHEN, Z., FAN, C. & ZHOU, G.1993. Preparation of ultrafine powders of TiO_2 by hydrothermal H_2O_2 oxidation starting from metallic Ti. *J. Mater. Chem,* 3:203.

QUICI, N., MORGADA, M.E., GETTAR, R.T., BOLTE, M. & LITTER M.I. 2007. Photocatalytic degradation of citric acid under different conditions: TiO_2 heterogeneous photocatalysis against homogeneous photolytic processes promoted by Fe(III) and H_2O_2. *Applied Catalysis B,* 71:117–124.

RAJ, K.J.A. & VISWANATHAN, B. 2004. Effect of surface area, pore volume and particle size of p25 titania on the phase transformation of anatase to rutile. *Indian Journal of Chemistry,* 48:1378–1382.

RINCO´ N, A.G. & PULGARIN, C. 2004. Effect of pH, inorganic ions, organic matter and H_2O_2 on E. coli K12 photocatalytic inactivation by TiO_2-implications in solar water disinfection. *Appl. Catal. B: Environ,* 51:283-302.

RODENAS, L. A.G, WEISZ, A.D, MAGAZ, G.E & BLESA, M.A. 2000. Effect of light on the electrokinetic behavior of TiO_2 particles in contact with Cr(VI) Aqueous Solutions. *Journal of colloid interface science*, 230:181-185.

RUPA, A.V., DIVAKAR, D. & SIVAKUMAR, T.2009. Titania and noble metals deposited titania catalysts in the photodegradation of tartrazine. *Catal Lett.* 132:259–267.

SAKTHIVEL, S., NEPPOLIAN, B., ARABINDOO, B., PALANICHAMY, M. & MURUGESAN, V. 2000. TiO_2 catalysed photodegradation of leather dye. *Indian J Sci Ind Res,* 59:556-62.

SAKTHIVEL, S., SHANKAR, M.V., PALANICHAMY, M., ARABINDOO, B., BAHNEMANN, D.W. & MURUGESAN, V. 2004. Enhancement of photocatalytic activity by metal deposition: characterization and photonic efficiency of Pt, Au and Pd deposited on TiO_2 catalyst. *Water Res,* 38:3001–8.

SAKTHIVEL, B., NEPPOLIAN, B., ARABINDOO, M., PALANICHAM, Y. & MURUGESAN V. 2000. ZnO/UV mediated photocatalytic degradation of acid green 16, a commonly used leather dye. *J. Sci. Ind. Res*. 59:556.

SAMUNEVA, B., KOZHUKHARQV, V., TRAPALIS, C. & KRANOLD, R. 1993. Sol-gel processing of titanium-containing thin coatings. *J. Mater. Sci*, 28:2353.

SAQUIB, M. & MUNEER, M. 2003. TiO_2-mediated photocatalytic degradation of a triphenylmethane dye (gentian violet), in aqueous suspensions. *Dyes Pigm,* 56:37-49.

SARKAR , D., GHOSH, C.K. & CHATTOPADHYAY, K.K. 2012. Morphology control of rutile TiO_2 hierarchical architectures and their excellent field emission properties. *Crystengcomm*, 14(8):2683-2690.

SCHRANK, S.G., JOSÉ H, J. & MOREIRA, R. F. P. 2002. Simultaneous photocatalytic Cr(VI) reduction and dye oxidation in a TiO_2 slurry reactor, *Journal of Photochemistry and Photobiology A*: *Chemistry*, 147:71-76.

SERPONE, N., AHYOU, Y.K., TRAN T.P., HARRIS, R., PELIZZETTI, E. & HIDAKA, H.1987. Simulated sunlight photoreduction and elimination of Hg(II) and Ch_3Hg(II) chloride salts from aqueous suspensions of Titanium-dioxide. *Sol. Energy*, 39:491-498.

SERPONE, N., BORGARELLOW, E., BARBENI, M. & PELIZZETTI, E.1984. Effect of cadmium sulphide preparation on the photo-catalysed decomposition of hydrogen sulphide in alkaline aqueous media. *Inorg Chim Acta, 90:191-4.*

SHABAN, Y. A. 2013. Effective photocatalytic reduction of Cr(VI) by carbon modified (CM)-n-TiO_2 nanoparticles under solar irradiation. *World Journal of nano science and engineering*, 3:154-160.

SHAO, D., WANG, X. & QIAOHUI, F.2009. Photocatalytic reduction of Cr(VI) to Cr(III) in solution containing ZnO or ZSM-5 zeolite using oxalate as model organic compound in environment. *Micropor. Mesopor. Mat*, 117:243.

SHARMA, J.C., GANDHI, J., SHARMA, A., GUPTA, N & BHARDWA, J.S.2008. Photocatalytic reduction of silver (I) to metallic silver over $SrWO_4$. *Int. J. Chem. Sci*, 6(2): 509-518.

SILVA, C.G., JUÁREZ, R., MARINO, T., MOLINARI, R. & GARCÍA, H.2011. Influence of excitation wavelength (UV or visible light) on the photocatalytic activity of titania containing gold nanoparticles for the generation of hydrogen or oxygen from water. *Journal of the American Chemical Society*, 133:595–602.

SING, K.S., EVERETT, D.H., HAUL R.A.W., MOSCOU, L., PIEROTTI, R., ROUQUEROL, J. & SIEMIENIEWSKA, T.1985. Reporting physisorption data for gas/solid systems with special reference to the determination of surface area and porosity. *Pure Appl. Chem,* 57:603–619.

SIRTORI, C., ADRIANE, M., FREITAS, D.E., SÉRGIO, T.F. & PATRICIO, P.Z. 2012. Photocatalytic Degradation of Camphor by Suspended and Immobilized Photocatalysts. *J. Braz. Chem. Soc.* 23:1563-1569.

SONG, L.M., ZHANG, S.J., WU, X.Q., ZHANG, S.N., TIAN, H.F., YE, J.Y. 2013. One-step synthesis of composite semiconductor AgBr/Ag5P3O10 heterojunctions and their photocatalytic activity, kinetic analysis, photocatalytic mechanism under visible light radiation, *Chem. Eng. J,* 214:336–342.

SRIWONG, C., WONGNAWA, S. & PATARAPAIBOOLCHAI, O.2012. Rubber sheet strewn with TiO_2 particles: Photocatalytic activity and recyclability. *Journal of Environmental Sciences,* 24(3):464-472.

SUBRAMANIAN, V., WOLF, E.E. & KAMAT, P.V.2004. Catalysis with TiO_2/Gold nanocomposites: Effect of metal particle size on the fermi level equilibration. *Journal of the American Chemical Society,* 126:4943–4950.

SUN, J., MAOB, J.D., GONGA, H. & LAN, Y. 2009. Fe(III) photocatalytic reduction of Cr(VI) by low-molecular-weight organic acids with –OH, *J. Hazard. Mater,* 168: 1569–1574.

TADA, H., KIYONAGA, T. & NAYA, S.I. 2009. Rational design and applications of highly efficient reaction systems photocatalyzed by noble metal nanoparticle-loaded titanium(iv) dioxide," *Chemical Society Reviews,* 38:1849–1858.

TEOH, W.Y., AMAL, R. & SCOTT, J.2012. Progress in heterogenours photocatalysis: From classical radical chemistry to engineering nanomaterials and solar reactors. *J. Phys. Chem. Lett.* 3, 629-639.

TESTA, J.J., GRELA, M. A. & LITTER, M. I. 2001. Experimental evidence in favor of an initial one-electron transfer process in the heterogeneous photocatalytic reduction of chromium(VI) over TiO_2. *Langmuir*, 17:3515-3517.

TESTA, J.J., GRELA, M.A. & LITTER M.I. 2004. Heterogeneous photocatalytic reduction of Chromium(VI) over TiO_2 particles in the presence of oxalate: involvement of Cr(V) species. *Environ. Sci. Technol,* 38:1589-1594.

TONG, H., OUYANG, S.X., BI, Y.P., UMEZAWA, N., OSHIKIRI, M. & YE, J.H. 2012. Nano-photocatalytic materials: possibilities and challenges. *Advanced Materials,* 24:229–251.

TRIVUNAC, K. & STEVANOVIC, S. 2006. Removal of heavy metal ions from water by complexation-assisted ultrafiltration. *Chemosphere,* 64:486-491.

TRYK, D.A., FUJISHIMA, A. & HONDA, K. 2000. Recent topics in photo electrochemistry: achievements and future prospects. *Electrochim. Acta,*45:2363.

TSAI, S.J. & CHENG, S. 1997. Effect of TiO_2 crystalline structure in photocatalytic degradation of phenolic contaminants. *Catal. Today,* 33:227-237.

TUPRAKAY, S. & LIENGCHARERNSI, T. 2005. Lifetime and regeneration of immobilized titania for photocatalytic removal of aqueous hexavalent chromium. *Journal of Hazardous Materials,* B:124,53–58.

VOHRA, M.S. &TANAKA, K. 2003. Photocatalytic Degradation of Aqueous Pollutants using Silica-Modified TiO_2. *Water Research,* 37:3992-2996.

WANG, C., WANG, M., XIE, K., WU, Q., SUN, L., LIN, Z. & LIN, C. 2011. Room temperature one-step synthesis of microarrays of N-doped flower-like anatase TiO_2 composed of well-defined multilayer nanoflakes by Ti anodization. *Nanotechnology,* 22:305-607.

WANG, L., WANG, N., ZHU, L., YU, H. & TANG, H. 2008. Photocatalytic reduction of Cr(VI) over different TiO_2 photocatalysts and the effects of dissolved organic species. *J. Hazard. Mater,* 152:93–99.

WANG, N., XU, Y., ZHU, L., SHEN, X. & TANG, H. 2009. Reconsideration to the deactivation of TiO_2 catalyst during simultaneous photocatalytic reduction of Cr(VI) and oxidation of salicylic acid, *J. Photochem. Photobiol,* 201:121–127.

WANG, N., ZHU, L.H., DENG, K.J., SHE, Y.B., YU, Y.M. & TANG H.Q. 2010. Visible light photocatalytic reduction of Cr(VI) on TiO_2 in situ modified with small molecular weight organic acids. *Appl. Catal,* 95:400.

WANG, X. & CARUSO, R.A. 2011. Enhancing photocatalytic activity of titania materials by using porous structures and the addition of gold nanoparticles. *Journal of Materials Chemistry,* 21:20–28.

WANG, X., BLACKFORD, M., PRINCE, K. & CARUSO, R. A. 2012. Preparation of boron-doped porous titania networks containing gold nanoparticles with enhanced visible-light photocatalytic activity. *ACS Applied Materials and Interfaces*, 4:476–482.

WANG, X., PEHKONEN, S.O. & RAY, A. K. 2004. Removal of aqueous Cr(VI) by a combination of photocatalytic reduction and coprecipitation, *Ind. Eng. Chem. Res,* 43:1665-1672.

WANG, Z.H. & ZHUANG, Q.X. 1993. Photocatalytic reduction of pollutant Hg(II) on WO_3 dispersion. *J Photochem Photobiol A Chem,* 75:105–111.

WATSON, S.S., BEYDOUN, D., SCOTT, J.A. & AMAL, R. 2003. The effect of preparation method on the photoactivity of crystalline titanium dioxide particles. *Chemical engineering journal,* 95:213–220.

WHO/UNEP. New and Emerging Environmental Threats to Human Health IMCHE/1/CP6 . /United Nations Environment Programme/Inter-Ministerial Conference on Health and Environment in Africa. Gabon: World Health Organization; 2008a. [accessed 20 April

2013].Availablehttp://www.afro.who.int/heag2008/docs_en/New%20and%20emerging%20threats.pdf.

WU, N.L. & LEE, M.S. 2004. Enhanced TiO_2 photocatalysis by Cu in hydrogen production from aqueous methanol solution. *J. Am. Ceram*. 29(15):1601-5.

XU, Y. & LANGFORD, C.H. 2000. Variation of Langmuir adsorption constant determined for TiO_2-photocatalyzed degradation if acetophenone under different light intensity. *J. Photochem. Photobiol. A: Chem.* 133:67-71.

XU, Y. & SCHOONEN, M.A.A. 2000. The absolute energy positions of conduction and valence bands of selected semiconducting minerals. *Mineral,* 85:543.

XU, Z., BAI, S., LIANG, J., ZHOU, L. & LAN, Y. 2013. Photocatalytic reduction of Cr(VI) by citric and oxilic acids over biogenetic jarosite. *Materials science and engineering,* 33:2192-2196.

YANG, L., XIAO, Y., LIU, S., LI, Y., CAI, Q., LUO, S. & ZENG, G. 2010. Photocatalytic reduction of Cr(VI) on WO_3 doped long TiO_2 nanotube arrays in the presence of citric acid. *Applied Catalysis B, Environmental*, 94: 142-149.

YIN, H.B., WADA, Y., KITAMURA, T., KAMBE, S., MURASAWA, S., MORI, H., SAKATA ,T. & YANAGIDA, S. 2001. Hydrothermal synthesis of nanosized anatase and rutile TiO_2 using amorphous phase TiO_2. *J. Mater. Chem*, 11:1694-703.

YU, J.G., LIU, W. & YU, H.G. 2008. A one-pot approach to hierarchically nanoporous titania hollow microspheres with high photocatalytic activity. *Crystal growth and design,* 8:930–934.

ZHANG, D., QI, L., MA, J. & CHENG, H. 2002. Formation of crystalline nanosized titania in reverse micelles at room temperature. *J. Mater.Chem*, 12:3677-3680.

ZHANG, F., NRIAGU, J.O. & ITOH, H. 2004. Photocatalytic removal and recovery of mercury from water using TiO_2-modified sewage sludge carbon, *J. Photochem. Photobiol. A: Chem*, 167:223–228.

ZHANG, J. & BISHOP, P.L. 2002. Stabilization/solidification (S/S) of mercury-containing wastes using reactivated carbon and Portland cement. *J. Hazard. Mater*, 92:199-212.

ZHAO, X., YU, J., CHENG, B. & ZHANG, Q. 2005. Synthesis and photocatalytic properties of TiO_2 nanostructures. *Physicochem. Eng. Aspects*, 78:268.

ZHOU, J., ZHAO, G., HAN, G. & SONG, B. 2013. Solvothermal growth of three-dimensional TiO_2 nanostructures and their optical and photocatalytic properties. *Ceramics International*, 39:8347-8354.

ZHOU, Y., HUANG, Y., LI, D. & HE, W. 2013. Three-dimensional sea-urchin-like hierarchical TiO_2 microspheres synthesized by a one-pot hydrothermal method and their enhanced photocatalytic activity. *Materials Research Bulletin*, 48:2420-2425.

ZHU, J., ZHENG, W., HE, B., ZHANG, J. & ANPO, M. 2004. Characterization of Fe–TiO_2 photocatalysts synthesized by hydrothermal method and their photocatalytic reactivity for photodegradation of XRG dye diluted in water. *Journal of Molecular Catalysis A: Chemical*, 216:35-43.

ZULKARNAIN, Z., LEE, K.H., MOHD, Z.H., ABDUL, H.A. & IMAD, R.H. 2009. Characterization of TiO_2–chitosan/glass photocatalyst for the removal of a monoazo dye via photodegradation-adsorption process. *Journal of Hazardous Materials*, 164:138-145.

APPENDICES

APPENDIX 1A: Sample Calculations

Preparation of 1000 mg/L Cr(VI) standard solution.

Molar mass of $K_2Cr_2O_7$ is 294.1846 g/mol

Table 1 A 1: Elemental composition of $K_2Cr_2O_7$

Symbol	Element	Atomic weight	Atoms	Mass percent
K	Potassium	39.0983	2	26.5808 %
Cr	Chromium	51.9961	2	35.3493 %
O	Oxygen	15.9994	7	38.0699 %

Proportion of Cr(VI) in $K_2Cr_2O_7 = \frac{\text{M}}{\text{Avg.M}} = \frac{103.9922}{294.1846} \times 100 = 35.35\%$

In every 100 mg of $K_2Cr_2O_7$ there is 35.35 mg of Cr(VI)

Therefore 2.835 g of $K_2Cr_2O_7$ is needed to produced 1000 mg/L of Cr(VI) standard solution.

Preparation of 20 mg/L of Cr(VI) from 1000 mg/L of Cr(VI) standard solution.

C_1 = 1000 mg/L, C_2 = 20 mg/L, 20 mL

$C_1V_1 = C_2V_2$

$V_1 = \frac{C2V2}{C1} = \frac{20 \times 20}{1000}$ = 0.4 mL

Therefore, to obtain 20 mg/L of Cr(VI) in 20 mL volume, 0.4 mL Cr(VI) standard was mixed in 19.6 mL high purity water.

Preparation of 1000 mg/L Hg(II) standard solution.

Molar mass of $HgCl_2$ is 271.4960 g/mol

Table 1 A 2: Elemental composition of $HgCl_2$

Symbol	Element	Atomic weight	Atoms	Mass percent
Hg	Mercury	200.59	1	73.8832 %
Cl	Chlorine	35.453	2	26.1168 %

% of Hg(II) in $HgCl_2$ $= \frac{M}{Avg.M} = \frac{200.59}{271.4960} = 73.88\%$

In every 100 mg of $HgCl_2$ there is 73.88 mg of Hg(II)

Therefore, 1.351 g of $HgCl_2$ is needed to produced 1000 mg/L of Hg(II) standard solution.

Preparation of 100 mg/L of Cr(VI) from 1000 mg/L of Cr(VI) standard solution.

C_1 = 1000 mg/L, C_2 = 100 mg/L, 20 mL

$C_1V_1 = C_2V_2$

$V_1 = \frac{C2V2}{C1} = \frac{100 \times 20}{1000} = 2$ mL

Therefore, to obtain 100 mg/L of Hg(II) in 20 mL volume, 2 mL Hg(II) standard was mixed in 98 mL high purity water.

APPENDIX 2A: Kinetics modeling of Cr(VI) and Hg(II) ions raw data.

Table 2A1: Pseudo-first order correlation coefficient, apparent constant values and reduction rate for Cr(VI) reduction.

pH	R^2	Rate constant (k, min^{-1})	Reduction rate ($mg.L^{-1}$ min^{-1})
2	0.999	0.075	1.33125
4	0.997	0.06	0.975
6	0.998	0.049	0.4116
8	0.996	0.038	0.2736
10	0.997	0.027	0.108
12	0.998	0.013	0.02275
Photocatalyst dosage (g/L)	R^2	Rate constant (k, min-1)	Reduction rate (mg.L-1 min-1)
0.5	0.964	0.005	0.052
1	0.955	0.01	0.12
1.5	0.988	0.013	0.2015
2	0.996	0.015	0.255
2.5	0.971	0.011	0.088
Concentration (mg/L)	R^2	Rate constant (k, min-1)	Reduction rate (mg.L-1 min-1)
10	0.998	0.101	1.79275
20	0.998	0.0849	1.422075
30	0.998	0.0548	0.7672
40	0.996	0.039	0.4095

50	0.992	0.03	0.255

Table 2A 2: Pseudo-first order correlation coefficient, apparent constant values and reduction rate for Hg(II) reduction.

pH	R^2	Rate constant (k, min^{-1})	Reduction rate ($mg.L^{-1}$ min^{-1})
2	0.997	0.015	0.28125
4	0.996	0.028	1.225
6	0.995	0.034	1.7425
8	0.997	0.05	3.75
10	0.997	0.061	4.59208
12	0.997	0.076	5.7532
Photocatalyst dosage (g/L)	R^2	Rate constant (k, min-1)	Reduction rate (mg.L-1 min-1)
0.5	0.981	0.007	0.2275
1	0.994	0.01	0.5125
1.5	0.988	0.014	1.015
2	0.996	0.017	1.4025
2.5	0.980	0.005	0.145
Concentration (mg/L)	R^2	Rate constant (k, min-1)	Reduction rate (mg.L-1 min-1)
20	0.966	0.017	0.765
40	0.981	0.025	1.3125

60	0.983	0.038	2.5745
80	0.995	0.058	4.35
100	0.997	0.071	5.76875
120	0.981	0.067	4.958

APPENDIX 3A: Influence of wavelength on the reduction of Cr(VI) and Hg(II).

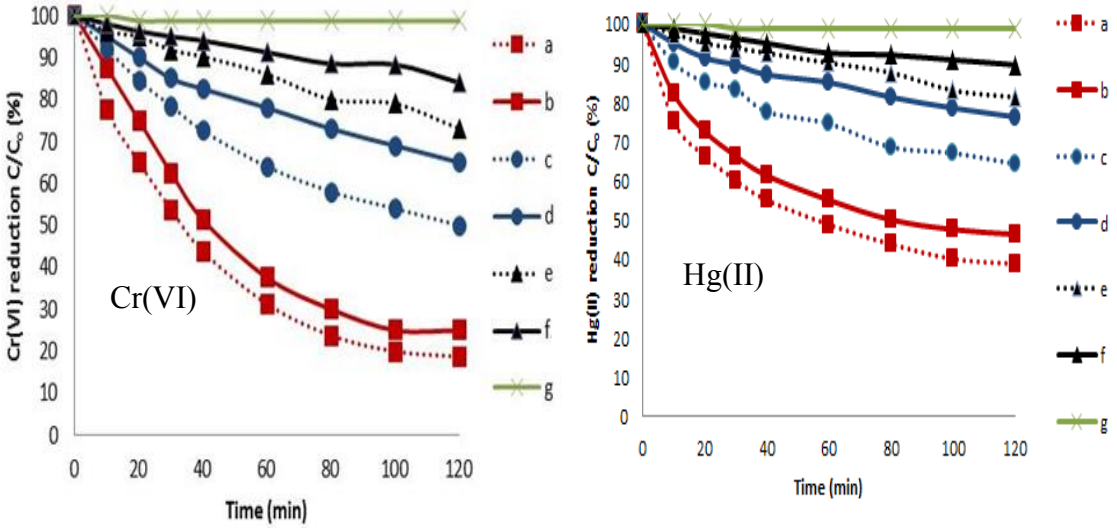

Fig 3A 1: Photoreduction of Cr(VI) and Hg(II); (a) UVC (Dandelion-like TiO_2), (b) UVC (P25-TiO_2), (c) Sunlight (Dandelion-like TiO_2), (d) Sunlight (P25-TiO_2), (e) UVLED (Dandelion-like TiO_2), (f) UVLED (P25-TiO_2) and (g) Photolysis. The initial composition of the solution were: Cr (VI), 20 mg/L; pH, 2 and Hg(II), 100 mg/L; catalyst dosage, 2 g/L; pH, 8.

APPENDIX 4A: Images and schematic diagrams of experimental set ups

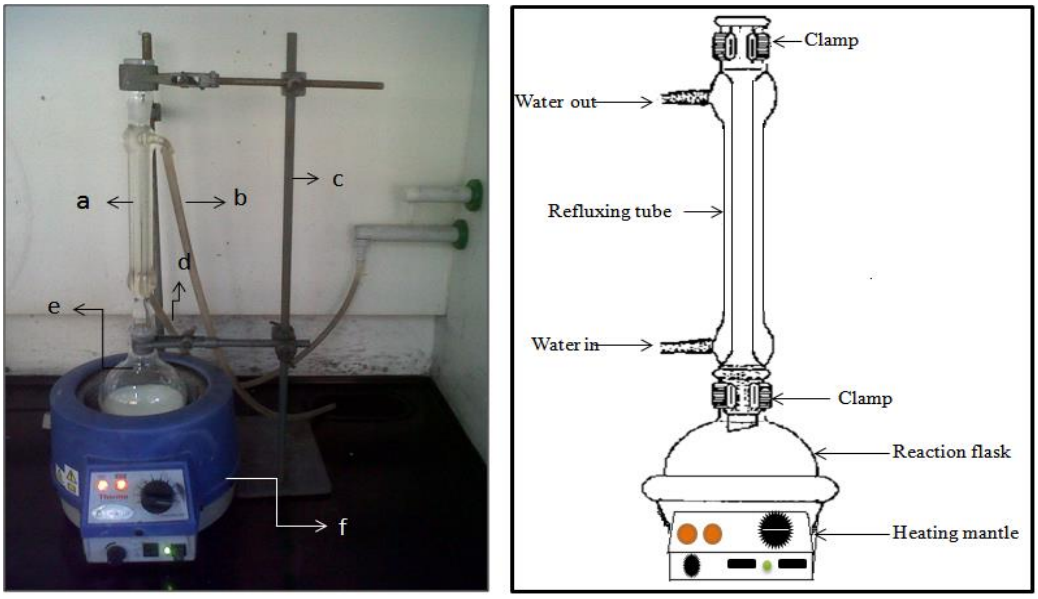

Fig A4 1: A digital image (left) and a diagrammatic representation (right) of experimental set-up for synthesis of the dandelions-like TiO_2 at Mintek catalyst preparation laboratory: a. refluxing tube; b. water out; c. stand; d. water in; e. reaction flask; f. heater mantle magnetic stirrer.

Fig A4 2: A digital image representation of labmax for preparation of gold nanoparticles catalyst at Mintek catalyst preparation laboratory.

Fig A4 3. A digital image representation for preparation of immobilized TiO_2 nanoparticles on calcium alginate at Mintek nanotechnology innovation centre (NIC) laboratory.

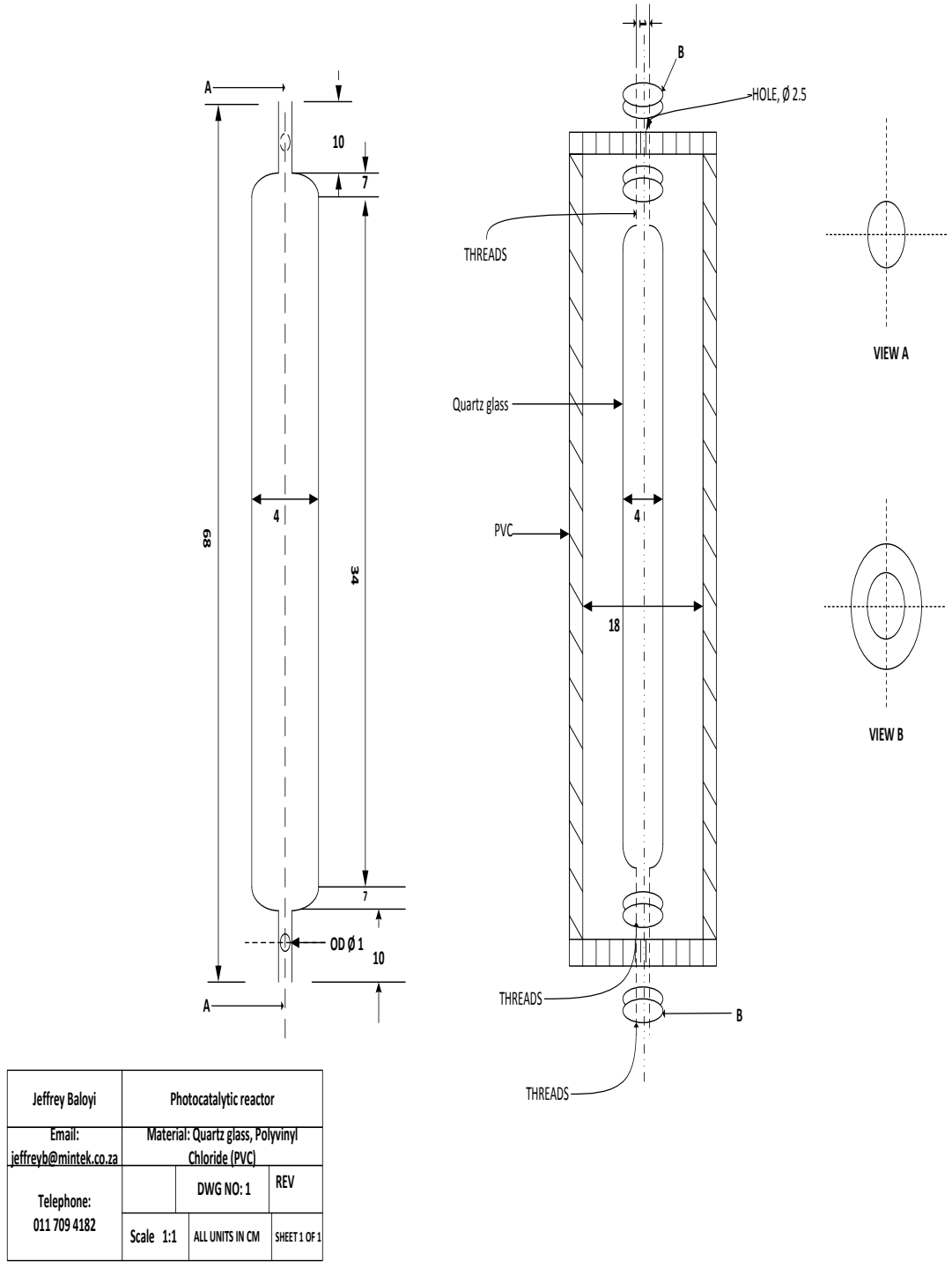

Fig A4 4: Structure of the photocatalytic reactor.